EVALUATION OF FUNCTIONAL CHANGES IN AKR1B1 AND AKR1B10 OVEREXPRESSING COLORECTAL CANCER CELL LINES

A THESIS SUBMITTED TO
THE GRADUATE SCHOOL OF NATURAL AND APPLIED SCIENCES
OF
MIDDLE EAST TECHNICAL UNIVERSITY

BY

İSMAİL GÜDERER

IN PARTIAL FULFILLMENT OF THE REQUIREMENTS
FOR
THE DEGREE OF MASTER OF SCIENCE
IN
BIOLOGY

FEBRUARY 2021

Approval of the thesis:

EVALUATION OF FUNCTIONAL CHANGES IN AKR1B1 AND AKR1B10 OVEREXPRESSING COLORECTAL CANCER CELL LINES

submitted by **İSMAİL GÜDERER** in partial fulfillment of the requirements for the degree of **Master of Science** i**n Biology, Middle East Technical University** by,

Prof. Dr. Halil Kalıpçılar
Dean, Graduate School of **Natural and Applied Sciences** _____

Prof. Dr. Ayşe Gül Gözen
Head of the Department, **Biological Sciences** _____

Prof. Dr. Sreeparna Banerjee
Supervisor, **Biological Sciences, METU** _____

Examining Committee Members:

Prof. Dr. Nülüfer Tülün Güray
Biological Sciences, METU _____

Prof. Dr. Sreeparna Banerjee
Biological Sciences, METU _____

Assist. Prof. Dr. Onur Çizmecioğlu
Molecular Biology and Genetics, Bilkent University _____

Date: 02.02.2021

I hereby declare that all information in this document has been obtained and presented in accordance with academic rules and ethical conduct. I also declare that, as required by these rules and conduct, I have fully cited and referenced all material and results that are not original to this work.

Name, Last name : Güderer, İsmail

Signature :

ABSTRACT

EVALUATION OF FUNCTIONAL CHANGES IN AKR1B1 AND AKR1B10 OVEREXPRESSING COLORECTAL CANCER CELL LINES

Güderer, İsmail
Master of Science, Biology
Supervisor: Prof. Dr. Sreeparna Banerjee

February 2021, 89 pages

Aldo-keto reductases (AKRs) are nicotinamide adenine dinucleotide phosphate (NADPH)-dependent enzymes with diverse cellular metabolism functions. AKR1B1 and AKR1B10 are two of the most studied enzymes in the AKR family. AKR1B1 reduces excess glucose into sorbitol using reducing electrons from NADPH, and the hyperactivation of the AKR1B1 pathways is associated with oxidative stress and cell death. AKR1B10 is a poor reductant of glucose but is a vital enzyme that can metabolize retinol and many other drugs and therefore is implicated in cancer development. Our previous research has shown that high expression of AKR1B1 and AKR1B10 in colorectal cancer can have divergent effects. Thus, while high expression of AKR1B1 was associated with a strong epithelial to mesenchymal (EMT) and pro-inflammatory phenotype, high expression of AKR1B10 showed activation of nutrient-sensing pathways. In order to better understand the functional effects and underlying cellular signaling pathways, we overexpressed both enzymes in cell lines RKO and SW480 that do not endogenously express AKR1B1 or AKR1B10.

Functional assays showed no significant alterations in cellular proliferation in 2D cell culture, which was also reflected in no alterations in colony formation capacity. AKR1B10 overexpressing cells had a greater vulnerability to serum starvation reflected by a high number of cells arrested in the G_1 phase of the cell cycle. AKR1B1 overexpressing cells compared to AKR1B10 overexpressing cells showed significantly higher motility, confirming our previous data. RNA sequencing of AKR1B1 and AKR1B10 overexpressing RKO cells indicated that gene ontology (GO) terms previously established in high AKR1B1 or AKR1B10 expressing tumor samples (that have an expression from both epithelial and stromal compartments) overlapped with the GO terms obtained in RKO cells. Thus, high AKR1B1 overexpressing cells were significantly associated with ROS-related processes, whereas AKR1B10 overexpressing cells were significantly associated with the inhibition of metabolic and biosynthetic processes.

Keywords: Aldo-keto reductases, colorectal cancer, functional analysis, transcriptomic analysis

ÖZ

AKR1B1 VE AKR1B10 AŞIRI İFADELENMESİNİN KOLOREKTAL KANSER HÜCRE HATLARI ÜZERİNDEKİ FONKSİYONEL ETKİLERİNİN DEĞERLENDİRİLMESİ

Güderer, İsmail
Yüksek Lisans, Biyoloji
Tez Yöneticisi: Prof. Dr. Sreeparna Banerjee

Şubat 2021, 89 sayfa

Aldo-keto redüktazlar (AKR'ler), çeşitli hücresel metabolizma fonksiyonlarına sahip nikotinamid adenin dinükleotid fosfat (NADPH) bağımlı enzimlerdir. AKR1B1 ve AKR1B10, AKR süperailesinde en çok çalışılan enzimlerden ikisidir. AKR1B1, hücredeki fazla glikozu, NADPH'den gelen indirgeyici elektronları kullanarak sorbitole indirger ve AKR1B1 yolaklarının hiperaktivasyonu, oksidatif stres ve hücre ölümü ile ilişkilidir. AKR1B10, glikozun zayıf bir indirgeyicisi olmasına karşın retinol ve diğer birçok ilacı metabolize edebilen ve bu nedenle kanser gelişiminde rol oynayan hayati bir enzimdir. Önceki araştırmamız, kolorektal kanserde yüksek AKR1B1 ve AKR1B10 ifadelenmesinin farklı etkilere sahip olabileceğini göstermiştir. Yüksek AKR1B1 ifadelenmesi, epitelyal-mezenkimal geçiş (EMT) ve güçlü bir proinflamatuar fenotip ile ilişkilendirilirken, AKR1B10'un yüksek ifadelenmesi, besin algılama yolaklarının aktivasyonunu göstermiştir. Fonksiyonel etkileri ve altta yatan hücresel sinyal yolaklarını daha iyi anlamak için, AKR1B1 veya AKR1B10'u endojen olarak ifade etmeyen RKO ve SW480 hücre hatlarında iki enzimin de aşırı ifadelenmesi sağlanmıştır.

Fonksiyonel analizler, 2D hücre kültüründe hücresel proliferasyonda önemli bir değişiklik göstermemiştir ve aynı zamanda koloni oluşturma kapasitesinde bir değişiklik gözlemlenmemesi de bunu doğrulamıştır. AKR1B10 aşırı ifade eden hücrelerde, hücre döngüsünün G1 fazında kalmış yüksek sayıda hücrenin olduğu gözlemlenmiştir, bu da hücrelerin serum açlığına karşı daha fazla savunmasızlığa sahip olduğunu göstermiştir. AKR1B10 aşırı ifade eden hücrelere kıyasla AKR1B1 aşırı ifade eden hücreler, önemli ölçüde daha yüksek hücresel hareketlilik göstermiş ve bu da önceki verilerimizi doğrulamıştır. RKO hücrelerinde AKR1B1 ve AKR1B10'u aşırı ifade eden hücrelerin RNA sekanslaması, daha önce yüksek AKR1B1 veya AKR1B10 ifade eden tümör numunelerinde (hem epitel hem de stromal bölmelerden ifadelenmeye sahip) oluşturulan gen ontolojisi (GO) terimlerinin RKO hücrelerinde elde edilen GO terimleriyle örtüştüğünü göstermiştir. Buna bağlı olarak, AKR1B1'i aşırı ifade eden hücreler, ROS ile ilgili süreçlerle önemli ölçüde ilişkilendirilirken, AKR1B10'u aşırı ifade eden hücreler, metabolik ve biyosentetik süreçlerin inhibisyonu ile önemli ölçüde ilişkilendirildi.

Anahtar Kelimeler: Aldo-keto redüktaz, kolorektal kanser, fonksiyonel analiz, transkriptomik analiz

This thesis is dedicated to my family.

For their endless love, support, and encouragement

ACKNOWLEDGMENTS

The author wishes to express his deepest gratitude to his supervisor Prof. Dr. Sreeparna Banerjee, for the guidance, advice, criticism, encouragement, insight, and support throughout the research. The author is very grateful for her time devoted to this study and sincerely appreciate her careful revision.

The author would like to thank the jury members, Prof. Dr. Nülüfer Tülün Güray and Assist. Prof. Dr. Onur Çizmecioğlu for their valuable time and contributions.

The author would also like to thank Prof. Dr. Mesut Muyan for his suggestions and comments for the experiments carried out in this study.

The technical assistance of Dr. Sinem Tunçer, Betül Taşkoparan, Müge Sak, and Ege Solel in the earlier days of my laboratory experience and the technical assistance of Dr. Menekşe Ermiş Şen for confocal imaging is gratefully acknowledged.

The author wishes to express his sincere gratitude to all the former and present members of Banerjee Laboratory. The author deeply appreciates and thanks Melis Çolakoğlu, Sinem Ulusan, Burak Kızıl, Güniz Sırt, Aydan Torun, Hepşen Hazal Hüsnügil, Aliye Ezgi Güleç, and Göksu Oral for their friendship and support through all these years. The author would also like to thank his team members in this study, Esin Gülce Seza, Çağdaş Ermiş, and Hoşnaz Tuğral. Their technical assistance, emotional support, and friendship throughout the research were immeasurable.

The author would also like to thank Dilara Koç for her enduring love and kindness, sharing the author's wish to complete this study, and for her patience and assistance.

Finally, the author wishes to express his deepest love and gratitude to his family for their constant support, encouragement, and immeasurable sacrifices.

This work is partially funded by the Scientific and Technological Research Council of Turkey under grant number TUBİTAK 118Z688.

TABLE OF CONTENTS

LIST OF TABLES

TABLES

LIST OF FIGURES

FIGURES

LIST OF ABBREVIATIONS

ABBREVIATIONS

AKR Aldo-keto reductases

CMS Consensus molecular subtypes

CRC Colorectal cancer

EMT Epithelial-Mesenchymal transition

NADPH Nicotinamide adenine dinucleotide phosphate, reduced form

$NADP^+$ Nicotinamide adenine dinucleotide phosphate, oxidized form

NADH Nicotinamide adenine dinucleotide, reduced form

NAD^+ Nicotinamide adenine dinucleotide, oxidized form

PAGE Polyacrylamide gel electrophoresis

PBS Phosphate-buffered saline

PEI Polyethylenimine

PI Propidium iodide

PPP Pentose phosphate pathway

PVDF Polyvinylidene flüoride

ROS Reactive oxygen species

SDS Sodium dodecyl sulfate

TBS-T Tris-buffered saline and Tween-20

CHAPTER 1

INTRODUCTION

Carcinogenesis is an evolving process rooted in both genetic and epigenetic alterations. These alterations accumulate over time, leading to malignant transformation of normal cells. Six essential alterations were initially suggested as essential for malignant growth: evading apoptosis, self-sufficiency in growth signals, insensitivity to anti-growth signals, sustaining angiogenesis, limitless replicative potential, and tissue invasion and metastasis (Hanahan & Weinberg, 2000). Later on, two additional hallmarks were added: evasion of immune destruction and reprogramming energy metabolism (Hanahan & Weinberg, 2011).

1.1 Reprogramming Energy Metabolism

Uncontrolled growth of abnormal cells defines cancer. This type of growth comes with a high metabolic burden because these cells need to replicate all of their internal components as they divide. Normal cells under aerobic conditions prefer to generate ATP through the breakdown of glucose to pyruvate via glycolysis followed by transport of pyruvate to the mitochondria and further breakdown to carbon dioxide, which generates ~32 ATP molecules. However, even under aerobic conditions, cancer cells mostly rely on the glycolysis pathway to generate ATP. This switch from oxidative phosphorylation to aerobic glycolysis is also known as the Warburg effect (see below for further details).

This switch to aerobic glycolysis brings in another problem: cancer cells have to find a way to compensate for around 16-fold lower ATP generation efficiency. The solution is to increase the glycolytic flux and glucose uptake. Typically, decreased oxygen availability (hypoxia) pushes cells to consume glucose and produce lactate,

and this response is controlled by the hypoxia-inducible factor 1 (HIF-1) transcription factor (Gordan & Simon, 2007). HIF-1 activity requires the protein HIF-1α (Cramer et al., 2003), which is regulated by the PI3K/Akt/mTOR pathway (Majumder et al., 2004). HIF-1α gets stabilized post-translationally under hypoxic conditions, leading to the upregulation of transcriptional targets of HIF-1α such as glycolytic enzymes and lactate dehydrogenase A (LDH-A) (Semenza et al., 1994). Constitutive expression of HIF-1α in tumors due to mutations and loss of tumor suppressors may lead to an increase in the glycolytic flux even under normoxic conditions.

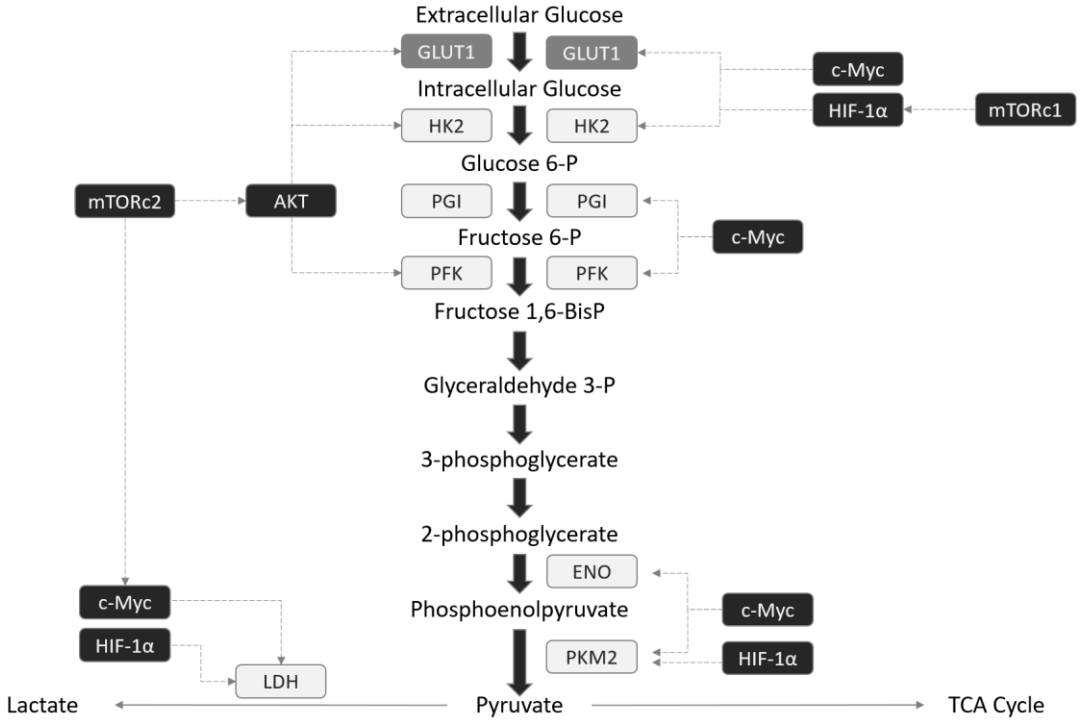

Figure 1.1 The effect of HIF-1α and c-Myc on glycolytic enzymes

HIF-1α and c-Myc transcriptionally regulate the expression of several enzymes of the glycolytic cascade and LDH. Thus, the transcriptional activity of HIF-1α and c-Myc can initiate the switch to oxidative glycolysis, also known as the Warburg Effect. Several other proteins of nutrient-sensing pathways such as mTORc1/2 and AKT are also known to regulate glycolytic enzymes (Redrawn from Magaway et al., 2019). *Abbreviations: GLUT1, Glucose transporter 1; HK2, Hexokinase 2; PGI,*

Phosphoglucoisomerase; PFK, Phosphofructokinase; ENO, Enolase; PKM2, Pyruvate Kinase M2; mTORc1/2, mechanistic target of rapamycin complex 1/2; HIF-1α, Hypoxia-inducible factor 1-alpha.

The *myc* family of genes responsible for cellular growth and cell cycle entry is generally amplified in human cancers. From this gene family, c-Myc regulates the expression of glycolytic enzymes and LDH-A (Osthus et al., 2000). Both HIF-1 and c-Myc also regulates the expression of glucose transporter GLUT1 (B. L. Ebert et al., 1995; Osthus et al., 2000), which provides the necessary glucose uptake for increased glycolytic flux needed by the cancer cells. On the other hand, c-Myc enhances the expression of enzymes required for nucleotide and one-carbon metabolism (DeBerardinis et al., 2008). These findings show that c-Myc controls both catabolic and anabolic pathways needed for cells to proliferate.

1.2 Warburg Effect

Warburg reported that even in the presence of adequate oxygen, cancer cells prefer to utilize glucose and generate lactate (Warburg, 1956). In cancer cells, the high glycolytic flux causes a decrease in the cytoplasmic ratio of NAD^+/NADH. Nicotinamide adenine dinucleotide (NAD) is a major coenzyme that functions with oxidoreductases. Its oxidized form, NAD^+, is required for the continuation of glycolysis. The enzyme LDH-A converts pyruvate, the end product of glycolysis, to lactate, which regenerates NAD^+ from NADH and allows glycolysis to persist. Apart from the advantage of the Warburg effect on energy generation, commitment to glycolysis alters the tumor microenvironment, promotes carbon flux into synthetic pathways, and may modulate various signaling pathways (Liberti & Locasale, 2016).

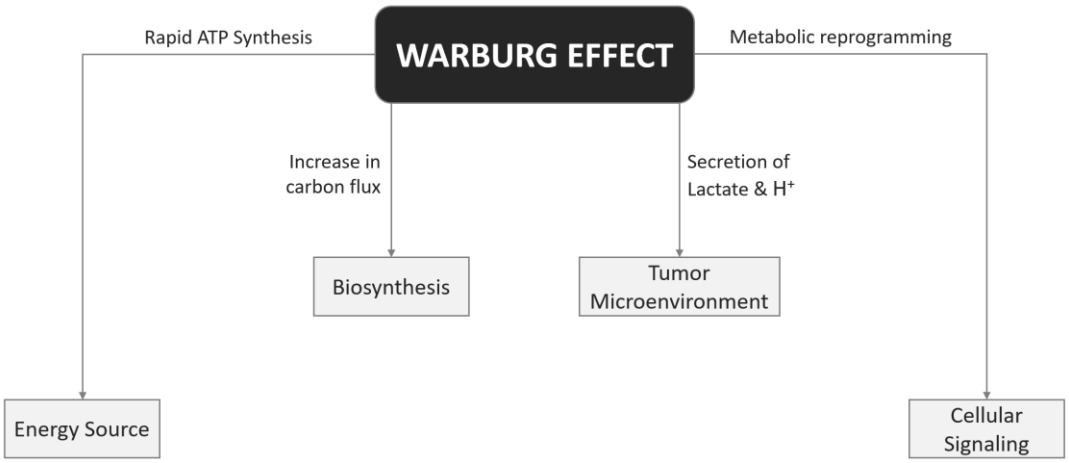

Figure 1.2 Alterations seen with the Warburg Effect

The preference for glycolysis and lactate production in normoxic conditions instead of aerobic respiration [Tricarboxylic acid cycle (TCA) followed by oxidative phosphorylation (OXPHOS)] is known as the Warburg Effect. The alterations seen in the energy source, biosynthesis, tumor microenvironment, and cellular signaling in many cancer types are thought to result from the Warburg Effect.

In normal conditions, the accumulation of lactate and H^+ within the cells would be detrimental. The rate-limiting enzyme of glycolysis, phosphofructokinase, gets inhibited by protons (Trivedi & Danforth, 1966), promoting efflux of lactate and H^+ to the environment in cancer cells. However, lactate cannot readily pass through the plasma membrane. Proton-linked monocarboxylate transporters (MCTs) carry out the co-transportation of lactate and H^+ through the membrane (Poole & Halestrap, 1993). The excreted lactate and H^+ increase the acidity of the tumor microenvironment, leading to immune suppression via inhibition of T cells (Fischer et al., 2007) and increased invasiveness via peritumoral acidosis (Estrella et al., 2013). Lactate can also be used as an energy source by the tumor, which may provide therapy resistance against metabolic inhibitors. (de la Cruz-López et al., 2019).

Maintaining the Warburg effect requires upregulation of glycolytic enzymes. The enzymes needed for glycolysis can take up to 10% of the total proteome in cancer cells (Madhukar et al., 2015). Hence, the glycolysis intermediates in cancer cells will be more abundant compared to a normal cell. The last step in glycolysis is catalyzed by pyruvate kinase, and in cancer cells, the M2 isoform (PKM2) is more abundant. This isoform has a tyrosine residue, which can be phosphorylated via the tyrosine kinase signaling pathway. Although PKM2 is in a feed-forward loop with the glycolysis intermediate fructose 1,6-bisphosphate, phosphotyrosine peptides can inhibit this positive signaling (Christofk et al., 2008). The resulting increase in glycolysis intermediates may provide an opportunity for the activation of anabolic pathways branching from glycolysis. These include serine-glycine-one-carbon metabolism that feeds glutathione, glycerol synthesis for the generation of complex lipids, the hexosamine pathway that is essential for protein glycosylation, and the pentose-phosphate pathway, which generates ribose for nucleotide synthesis as well as nicotinamide adenine dinucleotide phosphate (NADPH) for reductive biosynthesis (DeBerardinis & Chandel, 2020).

1.3 Pentose Phosphate Pathway

The pentose phosphate pathway (PPP), also known as the pentose phosphate shunt, is a metabolic pathway that occurs in the cytosol parallel to glycolysis. It is divided into two biochemical branches: an oxidative branch and a non-oxidative branch. PPP branches after the first step of glycolysis that generates the intermediate glucose 6-phosphate (G6P) and produces ribulose-5-phosphate (Ru5P), CO_2, and NADPH via the oxidative branch (Kruger & Von Schaewen, 2003). The non-oxidative branch generates ribose-5-phosphate (R5P), which is a building block of nucleic acids.

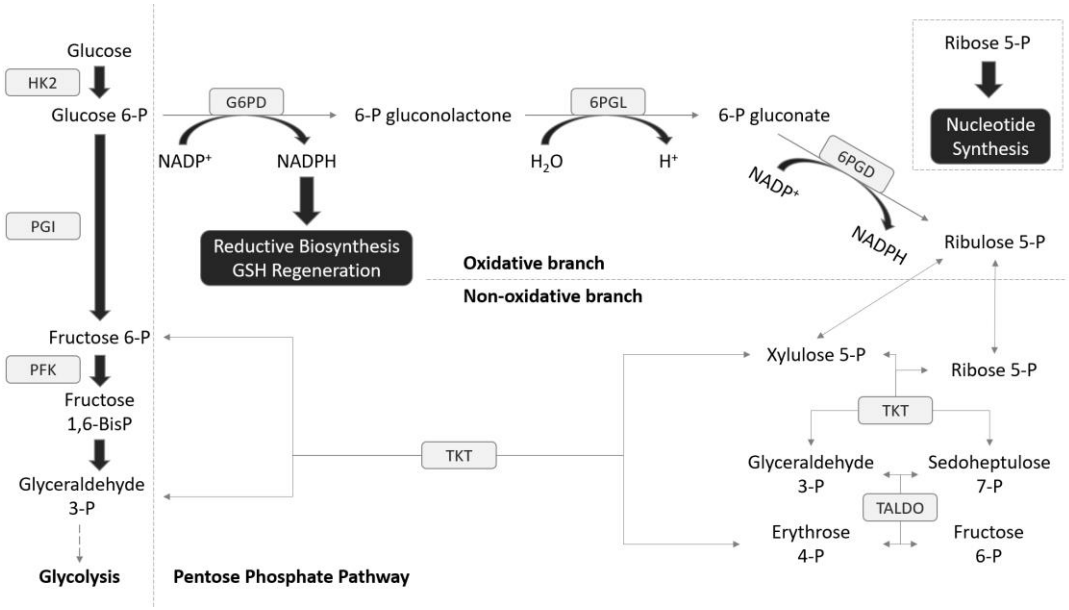

Figure 1.3 The pentose phosphate shunt

The pentose phosphate pathway (PPP) diverts carbon from glycolysis to generate NADPH and nucleotide precursors. TKT and TALDO enzymes catalyze intermediate conversions, which connect PPP and glycolysis. The NADPH generated in this pathway is used to maintain reduced glutathione (GSH) levels in the cells, mitigating oxidative stress. Abbreviations: HK2, Hexokinase 2; PGI, Phosphoglucoisomerase; PFK, Phosphofructokinase; G6PD, Glucose-6-phosphate dehydrogenase; 6PGL, 6-phosphogluconolactonase; 6PGD, phosphogluconate dehydrogenase; TKT, transketolase; TALDO, transaldolase.

The first step in the oxidative branch is catalyzed by glucose-6-phosphate dehydrogenase (G6PD) enzyme, which converts G6P to 6-phosphogluconolactone and generates NADPH. The second step converts phosphogluconolactone to 6-phosphogluconate (6PG) with the 6-phosphogluconolactonase (6PGL) enzyme. The last step in the oxidative branch also generates another NADPH via decarboxylation of 6PG to Ru5P, catalyzed by phosphogluconate dehydrogenase (6PGD) enzyme (Alfarouk et al., 2020). The overall reaction of the oxidative branch is:

$$G6P + 2\ NADP^+ + H_2O \rightarrow Ru5P + 2\ NADPH + 2\ H^+ + CO_2$$

Conversion of Ru5P to R5P by the ribose-5-phosphate isomerase (RPI) enzyme is the first step of the non-oxidative branch. Other steps of this branch involve transketolase (TKT) and transaldolase (TALDO) enzymes. TKT catalyzes a reversible transfer of two-carbon units (Mitschke et al., 2010), and TALDO catalyzes the reversible transfer of three-carbon units (Perl, 2007), which both link glycolysis and PPP via the generated intermediates.

1.4 Functions of NADPH

NADP is a structural analog of NAD, and it is generated by NAD kinases that transfer a phosphate group to adenosine ribose moiety of NAD (Agledal et al., 2010). The presence of NAD and NADP is universal among prokaryotes and eukaryotes. They both function as cofactors with dehydrogenase enzymes. However, their primary roles are different. Under normal conditions, NAD is predominantly present in its oxidized form (NAD^+), and NADP is in its reduced form (NADPH). NAD functions in catabolic activities such as glycolysis and the TCA cycle, whereas NADPH fuels antioxidant systems and serves as an electron donor for reductive biosynthesis (VanLinden et al., 2015).

Several pathways regenerate NADPH in the cells with enzymes such as malic enzyme 1 (ME1), cytosolic 10-formyltetrahydrofolate dehydrogenase (ALDH1L1), and previously described members of the oxidative PPP shunt. ME1 is a cytosolic enzyme that converts malate to pyruvate while generating NADPH from $NADP^+$. The malic enzyme is a major source of NADPH as it can produce NADPH almost at the same level as G6PD from the PPP shunt (DeBerardinis et al., 2007). ALDH1L1 catalyzes the conversion of 10-formyltetrahydrofolate to tetrahydrofolate and CO_2 while generating NADPH from $NADP^+$ (Hong et al., 1999). The enzymes G6PD and 6PGD from the oxidative PPP shunt also generate NADPH, as discussed in the previous section.

Reductive biosynthesis pathways require NADPH to serve as an electron donor. Fatty acid synthesis, one of the primary biosynthetic reactions, is a reductive process. For example, the most abundant fatty acid, palmitate, is synthesized by fatty acid synthase (FAS) via the utilization of acetyl-CoA, malonyl-CoA, and NADPH (Wakil, 1989). Other than fatty acid synthesis, cholesterol and steroid hormone synthesis also require NADPH.

The maintenance of reactive oxygen species (ROS) within the cell is essential for mitigating oxidative stress. Glutathione is an important antioxidant that is widely distributed in biological fluids and tissues. Free glutathione in the cells exists in its reduced form, GSH. Glutathione reductase (GR) is the enzyme that converts GSSG (the oxidized form) to GSH by utilizing reducing electrons from NADPH (Pai & Schulz, 1983). GSH is used by the glutathione peroxidase (GPx) enzyme system to reduce reactive oxygen species (Flohe et al., 1973). Like GSSG/GSH, the thioredoxin (Trx) system also uses NADPH as a source of electrons to reduce ROS (Luthman & Holmgren, 1982). Both GSH and Trx systems are known to be hyperactivated in cancer cells in order to mitigate oxidative stress and maintain cell survival (Liou & Storz, 2010).

1.4.1 Role of NADPH in cancer

In cancer cells, ROS can activate pathways involved in protein synthesis, glucose metabolism, cell growth and survival, contributing to tumor progression (Storz, 2005). Elevated ROS levels increase the demand for NADPH for anti-oxidative reactions. Also, the continuous proliferation of cancer cells creates a demand for NADPH in reductive biosynthesis pathways. Taken together, this elevated demand for NADPH can be exploited to kill cancer cells selectively (Ju et al., 2020).

1.5 The Aldo-Keto Reductase Protein Superfamily

The aldo-keto reductases (AKRs) are NADPH-dependent oxidoreductases, whose primary function is to reduce aldehydes and ketones to primary and secondary alcohols. AKRs generally consist of the same number of residues with a conserved three-dimensional fold, and variations around the active site provide substrate specificity (Jez et al., 1997).

The naming of AKR enzymes begins with the root symbol of AKR, followed by the family's Arabic number (>40% sequence identity), the subfamily's letter (>60% sequence identity), and the representative protein sequence's Arabic number (Mindnich & Penning, 2009). There are currently ~190 known AKR members that fall into 15 different families (Hyndman et al., 2003). Comprehensive information about all AKRs can be found on a website (https://www.med.upenn.edu/akr/). There are 15 human AKR members identified by the Human Genome Organisation (HUGO), as shown in Table 1.1.

Table 1.1 List of human aldo-keto reductases

Gene	Protein (Alias name)	Symbols	Chromosomal Location
AKR1A1	Aldehyde reductase	ALR	1p34.1
AKR1B1	Aldose reductase	AR, ALDR1	7q33
AKR1B10	Small intestine aldose reductase	ARL1, HIS	7q33
AKR1B15	Farnesol dehydrogenase		7q33
AKR1C1	Dihydrodiol dehydrogenase 1	DDH, DD1	10p15.1
AKR1C2	Dihydrodiol dehydrogenase 2	DDH2, DD2	10p15.1
AKR1C3	Dihydrodiol dehydrogenase X	DDX	10p15.1
AKR1C4	Dihydrodiol dehydrogenase 4	DD4, CDR	10p15.1
AKR1D1	Δ^4-3-ketosteroid-5-beta-reductase		7q33

Table 1.2 (continued) List of human aldo-keto reductases

AKR1E2	Human testis aldo-keto reductase	htAKR	10p15.1
AKR6A3	Potassium voltage-gated channel subfamily A member regulatory beta subunit 1	KCNA1B	3q25.31
AKR6A5	Potassium voltage-gated channel subfamily A member regulatory beta subunit 2	KCNA2B	1p36.31
AKR6A9	Potassium voltage-gated channel subfamily A member regulatory beta subunit 3	KCNA3B	17p13.1
AKR7A2	Aflatoxin aldehyde reductase	AFAR1	1p36.13
AKR7A3	Aflatoxin aldehyde reductase	AFAR2	1p36.13

The molecular weight of AKRs is in the region of 34-37 kDa, and they prefer to utilize NADPH instead of NADH. As described in earlier sections, cells maintain their $NADP^+$ pool in its reduced form, and cancer cells upregulate their NADPH-generating pathways to cope with ROS levels and carry out reductive biosynthesis. Thus, AKRs generally can function without being affected by the fluctuations in the cofactor ratios and carry out their metabolic activities and detoxification (Barski et al., 2008). However, it has been shown that reduction reactions carried out by AKR1Bs can deplete their cofactor NADPH, which results in cell death via disruption of the GSSG/GSH system (Zhang et al., 2018).

AKRs have diverse functions in metabolic oxidation-reduction reactions. These reactions include reduction of glucose, glucocorticoids, and small carbonyl metabolites to glutathione conjugates and phospholipid aldehydes (Barski et al., 2008). AKRs also function in anti-oxidative response, xenobiotic metabolism,

transcriptional regulation (Penning, 2015), as well as drug metabolism, xylose metabolism, and steroid metabolism.

1.5.1 AKR1B1

Aldo-keto reductase family 1 member B1 (AKR1B1), also known as aldose reductase (AR), is the first and rate-limiting enzyme in the polyol pathway. It converts glucose to sorbitol, which consumes NADPH during the process. It also reduces steroids and their derivatives and prostaglandins. Besides these reductions, AKR1B1 can reduce lipid aldehydes that may regulate cell growth and death (Dixit et al., 2000). AKR1B1, especially under hyperglycemic conditions, plays a role in the development of secondary diabetic complications (Donaghue et al., 2005). In cancer, AKR1B1 is associated with epithelial-to-mesenchymal transition (EMT) phenotype, tumor aggressiveness and invasiveness, and ZEB1 expression (Schwab et al., 2018). ZEB1 is a transcription factor that is involved in EMT and stemness (Krebs et al., 2017).

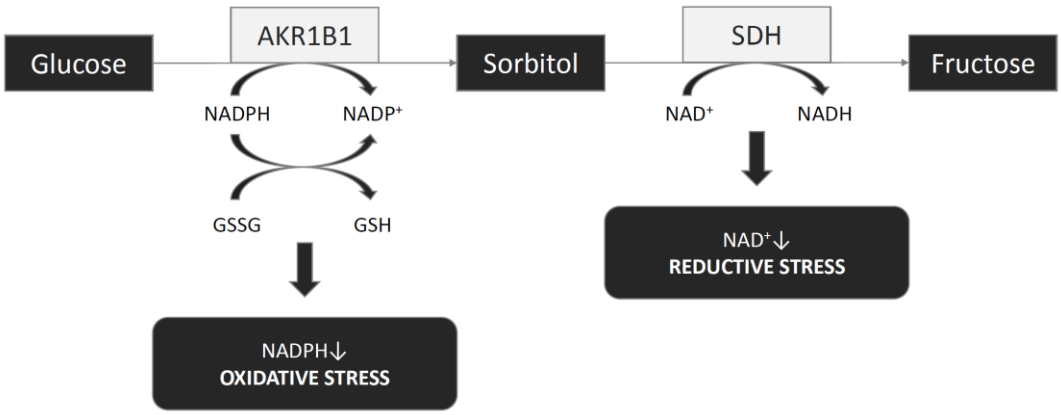

Figure 1.4 The polyol pathway

In the polyol pathway, AKR1B1 catalyzes the conversion of glucose to sorbitol while consuming NADPH. The reduction in NADPH levels may lead to oxidative stress

due to disruption in the GSSG/GSH antioxidant system. Abbreviations: AKR1B1, Aldo keto reductase family 1 member B1; SDH, Sorbitol dehydrogenase.

AKR1B1 is detected in all human tissues, with high expression in adrenal glands. The AKR1B1 gene is located on chromosome 7q33, and its expression is regulated by several transcription factors, including the cAMP-responsive element-binding protein (CREB; Lefrançois-Martinez et al., 2004), nuclear factor of activated T-cells 5 (NFAT5; Yang et al., 2006), and nuclear factor-erythroid 2 related factor 2 (Nrf2; Ebert et al., 2011). The promoter of AKR1B1 also contains binding sites for AP-1 and NF-κB, which may imply that AKR1B1 is a component of antioxidant and inflammatory responses (Srivastava et al., 2011).

1.5.2 AKR1B10

Aldo-keto reductase family 1 member B10 (AKR1B1), also known as small intestine aldose reductase/aldose reductase-like 1 (ARL1), is an enzyme that is primarily expressed in the small intestine, colon, liver, and thymus. AKR1B10 has the same size as AKR1B1; both consist of 316 amino acids. They have similar substrate specificity, and their amino acid sequence is 71% identical to each other (Cao et al., 1998). AKR1B10 shares the same chromosomal location as AKR1B1, 7q33. Besides the common features between the two enzymes, AKR1B10 differs from AKR1B1 in its inability to reduce glucose and its high catalytic efficiency for the reduction of retinals (Crosas et al., 2003).

Retinoids are signaling molecules involved in cell proliferation, cell differentiation, and morphogenesis of cell types (Tang & Gudas, 2011). By decreasing the cellular levels of retinoic acids, AKR1B10 controls retinoic acid homeostasis in the cells. AKR1B10 reduces retinals to retinols, which may deprive receptors of retinoids via diversion of retinals from the retinoic acid conversion step and interfere with the signaling pathway (Penning, 2005). In cancer, upregulation of AKR1B10 may be

linked to loss of retinoic acids resulting in loss of cell differentiation and cancer development (Penning & Lerman, 2008).

Our laboratory has shown divergent effects related to the high expression of AKR1B1 and AKR1B10. The high expression of AKR1B10 in colorectal cancer (CRC) cell lines was associated with tumor-suppressive characteristics such as slower cell cycle progression, reduced motility, and reduced proliferation. High expression of AKR1B10 combined with a low expression of the enzyme AKR1B1 ($AKR1B1^{LOW}$ / $AKR1B10^{HIGH}$) in CRC showed longer disease-free survival (DFS; Taskoparan et al., 2017). Additionally, our laboratory has shown that patient samples with $AKR1B1^{HIGH}$ / $AKR1B10^{LOW}$ gene signature were classified as consensus molecular subtype 4 (CMS4) with mesenchymal characteristics. In contrast, patients with $AKR1B1^{LOW}$ / $AKR1B10^{HIGH}$ gene signature were classified as CMS3, which is associated with dysregulation of metabolism (Demirkol Canlı et al., 2020). It is worth noting that AKR1B10 expression is associated with poor and good outcomes within different tumor types, and the root of this difference is currently unknown.

1.6 Aims of the study

An ongoing study in our laboratory has established two different gene signatures based on expression levels of AKR1B1 and AKR1B10, classified under different consensus molecular subtypes (CMS). The gene signatures $AKR1B1^{HIGH}$ / $AKR1B10^{LOW}$ and $AKR1B1^{LOW}$ / $AKR1B10^{HIGH}$ could be a prognostic factor for DFS and recurrence-free survival (RFS; Demirkol Canlı et al., 2020). This thesis was designed as a part of that ongoing study to mechanistically investigate why the increased expression of AKR1B1 or AKR1B10 was associated with the distinct and specific CMS categories.

In my thesis, I aimed to generate AKR1B1 and AKR1B10 overexpressing models in the cell lines RKO and SW480 that do not endogenously express these enzymes. Additionally, we aimed to better understand the functional effects and underlying

cellular signaling pathways related to the expression and activity of AKR1B1 and AKR1B10, particularly in the context of their association with CMS4 and CMS3 classifications, respectively.

CHAPTER 2

MATERIALS AND METHODS

2.1 Cell Line Characteristics

RKO is a poorly differentiated colon carcinoma cell line. According to the Catalogue of Somatic Mutations in Cancer (COSMIC) database, RKO cells carry heterozygous mutations in BRAF, neurofibromin 1 (NF1), phosphatidylinositol-4,5-bisphosphate 3-kinase catalytic subunit alpha (PI3KCA), and a deletion mutation in NADPH-generating enzyme ALDH1L1 (Bamford et al., 2004; Mouradov et al., 2014). SW480 cells were isolated from a moderately differentiated colon adenocarcinoma (Dukes' type B). Although RKO cells are microsatellite unstable, SW480 cells are classified as microsatellite stable, and SW480 cells carry homozygous mutations in KRAS and p53 (Ahmed et al., 2013). Additionally, neither cell line belongs to the CMS3 or CMS4 categories (Linnekamp et al., 2018), providing us the opportunity to determine whether AKR1B1 or AKR1B10 overexpression can alter their expression profile to match the CMS4 or CMS3 classification better.

The culture media of RKO and SW480 differ in their primary source of energy. RKO cells are grown with glucose, whereas SW480 cells are grown with galactose. This difference in carbohydrates provides us opportunities to study AKRs under different energetic conditions. Our laboratory's previous research also has shown that RKO and SW480 cells do not express either of the enzymes AKR1B1 and AKR1B10 (Taskoparan et al., 2017). Therefore, we have selected these cell lines to generate overexpression models.

2.2 Cell Culture

The colon cancer cell lines SW480 and RKO were purchased from ATCC (Middlesex, UK). Human embryonic kidney cell line HEK293FT was a kind gift from Dr. Mayda Gürsel (Middle East Technical University). SW480 cells were grown in Leibovitz's L-15 Medium supplemented with 10% FBS, 4mM L-glutamine, and 1% Penicillin-Streptomycin solution. RKO cells were grown in EMEM supplemented with 10% FBS, 2 mM L-glutamine, 1% Non-Essential Amino Acids Solution, 1 mM Sodium Pyruvate, and 1% Penicillin-Streptomycin solution. HEK293FT cells were grown in DMEM (high glucose) supplemented with 10% FBS, 6 mM L-glutamine, 1% Non-Essential Amino Acids Solution, 1 mM Sodium Pyruvate, and 1% Penicillin-Streptomycin solution. RKO and HEK293FT cells were grown in a humidified incubator with 5% CO_2 at 37°C, whereas SW480 cells were grown with 100% air at 37°C. All cell culture consumables were purchased from Biological Industries (Israel).

2.3 Cloning and Transfection

pLenti-puro (a gift from Dr. Ie-Ming Shih, Addgene plasmid # 39481) was digested with restriction enzymes *EcoRI* and *XbaI*. AKR1B1 (NM_001628) and AKR1B10 (NM_020299) cDNA sequences were cloned into the pLenti-puro vector (cloning was carried out by Esin Gülce Seza). The cloning was confirmed by sequencing (BMLabosis, Ankara). All transfections were carried out with the transfection reagent polyethylenimine (PEI) at a ratio of 1:3 w/v [DNA in μg to PEI (1 mg/ml) in μl].

2.4 Generation of Lentiviruses

HEK293FT cells were co-transfected with the packaging plasmid psPax2, envelope plasmid p-CMV-VSV-G (gifts from Dr. Tolga Emre, Boğaziçi University) along with the transfer plasmid pLenti-puro containing either the AKR1B1 or AKR1B10 cDNA. The cells were seeded in 10 cm cell culture dishes and allowed to attach for 24 hours. When the cells were at ~70% confluency, they were co-transfected with the three lentiviral plasmids at a ratio of 2.5:2.5:5 (packaging plasmid to envelope plasmid to transfer plasmid). The generated viruses were collected at 48 and 72 hours post-transfection in individual harvests, snap-frozen in liquid nitrogen, and stored at -80 ℃.

2.5 Transduction

Transduction experiments were carried out by seeding 50,000 cells of both RKO and SW480 cell lines in two separate 12-well plates. The cells were allowed to attach for 24 hours. Virus dilutions were prepared at a ratio of 1:1, volume of lentivirus (µL) to volume of respective complete medium + 10 µg/mL polybrene (µL). Polybrene (Merck Millipore, Germany) was used to enhance transduction efficiency. The cells were incubated for 72 hours with their respective virus-containing media.

2.6 Generation of Stable Polyclonal and Monoclonal Cells

After transduction, cells were directly taken into their respective selection medium containing puromycin (Invivogen, USA). The selection was continued until the wild type RKO and SW480 cells were dead. The primary stocks of the polyclonal cells were taken at this time and stored in the vapor phase of liquid nitrogen.

Monoclonal cells were generated by using the serial dilution method. Previously generated polyclonal cells were counted, and several dilutions were prepared. The

final cell dilution had 100 cells in 15 ml of their respective selective medium. From this dilution, 100 μL was pipetted to each well of a 96-well plate. This process was repeated for each group of RKO and SW480 cell lines. After seeding, 96-well plates were screened under a light microscope for single cells. At least five colonies for each transduction group were selected, passaged, and expanded from those that formed single colonies. The expanded cells were stored in the vapor phase of liquid nitrogen, and their respective expression was confirmed with the western blot technique.

2.7 Protein Isolation and Quantification

A protein isolation mixture was prepared by mixing M-PER Mammalian Protein Extraction Reagent (Thermo Fisher Scientific, USA) with phosphatase inhibitor and protease inhibitor cocktail (Roche, Germany) according to the manufacturer's instructions. Samples collected from cell culture were washed with PBS and centrifugated at 2000 x g for 2 minutes. The pellet was resuspended in the prepared protein isolation mixture and kept on ice for 30 minutes. Then, the samples were centrifuged at 14000 x g for 15 minutes, the supernatant containing the total protein extract was transferred to pre-chilled Eppendorf tubes and stored at -80 ℃.

The protein content of the isolated samples was quantified by the Bradford assay. Coomassie Protein Assay Reagent (Thermo Fisher Scientific, USA) was used with a standard curve generated by bovine serum albumin for quantification.

2.8 Western Blot

Western blot technique was used in order to determine expression levels of our proteins of interest. Total proteins were separated by SDS-PAGE at 100 V for ~2 hours, and 10-to-50 μg of proteins were loaded to 10-12% gels. PageRuler Plus Prestained Protein Ladder (Thermo Fisher Scientific, USA) was used as a molecular weight marker in the 10-250 kDa range.

Western blot transfer was carried out with the traditional wet transfer method. The proteins in SDS-PAGE gel were transferred to a polyvinylidene fluoride (PVDF) membrane at 115 V and 4 ℃ for 75 minutes. After transfer, the membrane was blocked with either 5% skimmed milk in TBS-T or 5% BSA in TBS-T at room temperature for 1 hour-or-overnight at 4 ℃.

Primary antibody (Table 2.1) incubation was carried out overnight at 4 ℃. The membrane was washed three times with TBS-T, and secondary antibody incubation was carried out at room temperature for 1 hour. Visualization of the membrane was carried out with Chemi-Doc MP Imaging System (BioRad, USA) using Clarity ECL Substrate (BioRad, USA). Where required, the membranes were stripped with a mild stripping buffer and reprobed with other antibodies. The mild stripping buffer was heated to 60 ℃ and applied on the membranes for 5 minutes, followed by washing with TBS-T three times.

In this study, the α-Tubulin antibody was used as a loading control to confirm equal protein loading in western blots.

Table 2.1 List of antibodies used in this study

Name of antibody	Company (Catalog #)	Host	Molecular Weight (kDa)	Dilution	Blocking Agent
AKR1B1	Thermo Fisher (PA5-29718)	Rabbit	36	1:500	Skim milk
AKR1B10	Thermo Fisher (PA5-23017)	Rabbit	36	1:500	Skim milk
α-Tubulin	Protein Tech (HRP-60031)	Mouse	52	1:4000	BSA

2.9 RNA Isolation

According to the manufacturer's instructions, total RNA isolation was carried out using the Nucleospin RNA Kit (Macherey-Nagel, Germany). The isolated RNA content was measured with BioDrop (Biochrom, UK) and stored at -80 ℃. A260/280 ratio of ~2 and A260/230 ratio between 2.0 – 2.2 was accepted as pure RNA.

2.9.1 RNA Isolation of RNA-seq Samples

Total RNA for RNA-seq was isolated with two different protocols: one set was isolated as described in Section 2.9. The remaining two sets were isolated with TRIzol (Thermo Fisher Scientific, USA) according to the manufacturer's instructions. RNA sequencing from three biological replicates was carried out by Beijing Genome Institute (BGI, Hong Kong).

2.10 cDNA Synthesis

Total RNA was treated with DNase I enzyme (Thermo Fisher Scientific, USA). cDNA synthesis was performed using RevertAid First Strand cDNA Synthesis Kit (Thermo Fisher Scientific, USA) with 1 µg RNA and random hexamer primers according to the manufacturer's instructions, and cDNA was stored at -20 ℃.

2.11 RT-PCR and qRT-PCR

Reverse Transcriptase – Polymerase Chain Reaction (RT-PCR) was carried out in a total volume of 20 µl containing 2 µl of cDNA (1:10 dilution), 4 µl of 5X FIREPol Master Mix Ready to Load (Solis BioDyne, Estonia), 0.5 µM forward and reverse primers and molecular biology grade water. The reaction was performed in a thermal cycler (Applied Biosystems, USA) with an initial denaturation of 3 minutes and denaturation of 30 seconds at 95 ℃, annealing of 30 seconds at a primer-specific

temperature (54 to 66 ℃), and an elongation of 30 seconds and final elongation of 7 minutes at 72 ℃. β-actin was used as an internal control for all reactions. For visualization, 20 µl of the reaction product was mixed with 4 µl of 6X loading dye and loaded to 2% agarose gel. The gels were run at 100 V, incubated in 10 mg/ml ethidium bromide solution (Applichem, Germany), and imaged under UV light with Quantum ST4 Imaging System (Vilber Lourmat, France).

Quantitative RT-PCR (qRT-PCR) was carried out in a total volume of 10 µl containing 1 µl of cDNA (1:10 dilution) and 9 µl of the reaction mix. The mix had 0.5 µM forward and reverse primers, 5 µl of GoTaq qPCR Master Mix (Promega, USA), and molecular biology grade water. For each primer pair (Table 2.2), standard curves were generated. β-actin was used as an internal control for all reactions. The reactions were performed in the Rotor-Gene Q 6000 System (Qiagen, Germany). Please see the appendix for NCBI accession numbers for each target of the primers used in this study (Table C.1).

Table 2.2 List of primers used in this study

Gene	Primer Type	Primer Sequence	T_M (℃)
AKR1B1	Forward	AAGCCGTCTCCTGCTCA	55
	Reverse	TTGCTGACGATGAAGAGC	55
AKR1B10	Forward	CAGAATGAACATGAAGTGGGG	55
	Reverse	GCTTTTCCACCGATGGC	55
G6PD	Forward	TGACCTGGCCAAGAAGAAGA	57
	Reverse	CAAAGAAGTCCTCCAGCTTG	57
β-actin	Forward	CAGCCATGTACGTTGCTATCCAGG	60
	Reverse	AGGTCCAGACGCAGGATGGCATG	60
TALDO	Forward	GTCATCAACCTGGGAAGGAA	60
	Reverse	CAACAAATGGGGAGATGAGG	60
TKT	Forward	GAAGATCAGCTCCGACTTGG	60
	Reverse	GTCGAAGTATTTGCCGGTGT	60

2.12 Proliferation Assay

We determined whether overexpression of AKR1B1 or AKR1B10 in the RKO cell line affected their proliferation. For this, an MTT [3-(4, 5-dimethylthiazol-2-yl)-2, 5-diphenyltetrazolium bromide] assay was used according to the manufacturer's instructions (Thermo Fisher Scientific, USA). 10,000 cells per well were seeded on three different 96-well plates and incubated for 24, 48, and 72 hours, respectively. At the end of each incubation period, the medium was replaced, and the MTT solution dissolved in PBS was added to the wells. After 4 hours of incubation with MTT, 1% SDS – 0.01M HCl solution was added to each well. Plates were incubated for 16 hours, and absorbance of the samples was measured using a Multiskan-GO microplate spectrophotometer (Thermo Fisher Scientific, USA) at 570 nm.

The effect of overexpression of AKR1B1 or AKR1B10 in the RKO cells were also investigated in 3D cell culture. For this, 10,000 cells per well were seeded on an ultra-low attachment 96-well plate (Corning, USA) and incubated for 5 days in a humidified incubator with 5% CO2 at 37°C. The spheroid images were taken, and the area of the spheroids was calculated with ImageJ. According to the manufacturer's instructions, a LIVE/DEAD^{TM} Viability/Cytotoxicity assay (Thermo Fisher Scientific, USA) was used to determine whether the cells in the spheroids were alive or dead. For this, spheroids were stained either calcein AM (which stains live cells) and ethidium homodimer (which stains dead cells). Stained spheroids were imaged with ZEISS LSM 800 confocal microscope. The signal intensity of the fluorescent dyes was calculated with ImageJ.

2.13 Colony Formation Assay

We assessed whether overexpression of AKR1B1 or AKR1B10 in the RKO cell line affected the ability of a single cell to grow into a colony. For this, cells were counted and plated as 1000 cells per well in a 6-well plate and incubated at 37 ℃ for 8 days. Colonies were fixed with a 4% Paraformaldehyde (PFA) fixative solution (Sigma

Aldrich, USA) for 15 minutes at room temperature. The PFA was washed with PBS, and 1 ml of staining solution [0.5% crystal violet (Sigma Aldrich, USA) in 80% dH_2O and 20% methanol] was applied. The plate was incubated for 20 minutes on a platform rocker at room temperature following a previously published protocol (Feoktistova et al., 2016). The excess crystal violet stain on the plate was washed in a stream of tap water four times. Following washing, the lid of the plate was removed to air-dry overnight. The next day, the plate was imaged by using the white sample tray of the Chemi-Doc MP Imaging System (BioRad, USA).

2.14 Cell Cycle Assay

RKO cells overexpressing AKR1B1, AKR1B10, or transduced with the empty vector were counted, and 500,000 cells per well of a 6-well plate were seeded. The plate was incubated for 24 hours, and the complete medium was replaced with a medium containing 1% FBS to serum starve and synchronize the cells. After 16 hours of incubation, half of the cells were collected as the synchronized control; the starvation medium in the remaining cells was replaced with a complete medium incubated for 8 hours to release the synchronized cells. The cells were collected, washed with PBS, and fixed by dropwise addition of 1 ml of ice-cold 70% ethanol on the cells while vortexing gently. After overnight incubation at -20 ℃, the samples were centrifugated at 2000 x g for 2 minutes, and ethanol was removed from the cells. The cells were rewashed with PBS and centrifugated at 2000 x g for 2 minutes. PBS was removed, and a staining solution containing 0.1% Triton X-100, 2 mg/ml RNase A and 20 μg/ml Propidium Iodide (PI; Sigma Aldrich, USA) was applied to the cells. After incubation at room temperature for 30 minutes, cell cycle analysis was carried out on Accuri C6 Flow Cytometer (BD Biosciences, USA). SSC (side scatter), FSC (forward scatter), and FL-2 channels with staining controls were used for the PI cell cycle analysis.

2.15 Motility Assay

Scratch wound healing assay was carried out to determine the effect of AKR1B1 and AKR1B10 overexpression on the motility of RKO cells. According to the established protocol in our laboratory (Tunçer et al., 2016), cells were seeded at 80% confluency. The next day, scratch wounds were made with a 100 µl sterile pipette tip. Cell debris was removed by washing the cells twice with cell culture grade PBS. Cells were incubated for 72 hours in a complete medium containing 0.5 µM mitomycin C to prevent cell division. At 0, 24, 48, and 72 hours, the medium containing 0.5 µM mitomycin C was refreshed, and the scratch wound images were taken. The area of the scratch was calculated with ImageJ.

2.16 Statistical Analysis

All experiments were carried out with at least two or three different biological replicates; each had at least three technical replicates. GraphPad Prism 6.1 (GraphPad Software Inc., USA) was used for data analysis. One-way ANOVA, Student's t-test, or Mann Whitney U test was carried out to determine significance. *p-value* < 0.05 was considered as statistically significant.

2.16.1 Analysis of RNA-seq Results

Analysis of raw RNA-seq data was carried out by Genoks (Ankara, Turkey). The analysis pipeline is shown in Appendix G. Raw read counts of the transcripts provided by Genoks were re-analyzed in our laboratory to confirm the differential gene expression results. For this, the *DEBrowser* package from Bioconductor was used in the R environment. The raw read counts were filtered and corrected for batch effect. Differentially expressed genes were analyzed with the *DESeq2* package. Gene Ontology Enrichment Analysis was carried out with ShinyGO v0.61.

CHAPTER 3

RESULTS

Although aldo-keto reductases AKR1B1 and AKR1B10 share a high similarity in their structures and functions, previous research from our laboratory has shown that the effects of expression of AKR1B1 and AKR1B10 in colorectal cancer (CRC) were fairly divergent (Taskoparan et al., 2017). Briefly, high AKR1B1 expression was associated with cell motility, cell cycle progression, and pro-inflammatory gene expression, whereas high AKR1B10 expression was associated with a weak inflammatory but more metabolic phenotype with the activation of nutrient-sensing pathways. Moreover, a recent study from our laboratory associated $AKR1B1^{HIGH}/AKR1B10^{LOW}$ gene signature in colon cancer patients with enhanced mesenchymal characteristics with significantly poor prognosis; meanwhile, $AKR1B1^{LOW}/AKR1B10^{HIGH}$ gene signature was associated with epithelial characteristics and better prognosis (Demirkol Canlı et al., 2020). In the context of these differences, we hypothesized that these different effects of AKR1B1 and AKR1B10 expression might result from altered signaling pathways. Two different cell lines that do not endogenously express either enzyme, RKO and SW480, were selected to identify the signaling pathways involved. AKR1B1 and AKR1B10 were overexpressed in these cell lines with the lentiviral transduction method and evaluated for functional alterations and differential gene expression using RNA sequencing.

3.1 Overexpression of AKR1B1 and AKR1B10 genes in RKO and SW480

Lentiviruses carrying either AKR1B1 or AKR1B10 cDNA sequences were generated in HEK293FT cells. The lentiviral particles were transduced to both RKO and SW480 cells. Cells were selected with a predetermined dose of puromycin

according to the respective kill curves (RKO, Figure D.1; SW480, Figure D.2) to generate stable overexpression models. The selection was continued until the wild-type non-transduced control cells were all dead (approximately 10 days). The cells were expanded, stored, and the overexpression of AKR1B1 or AKR1B10 in the generated polyclonal cells was confirmed for both RKO (Figure 3.1A) and SW480 (Figure 3.1B) cells with western blot.

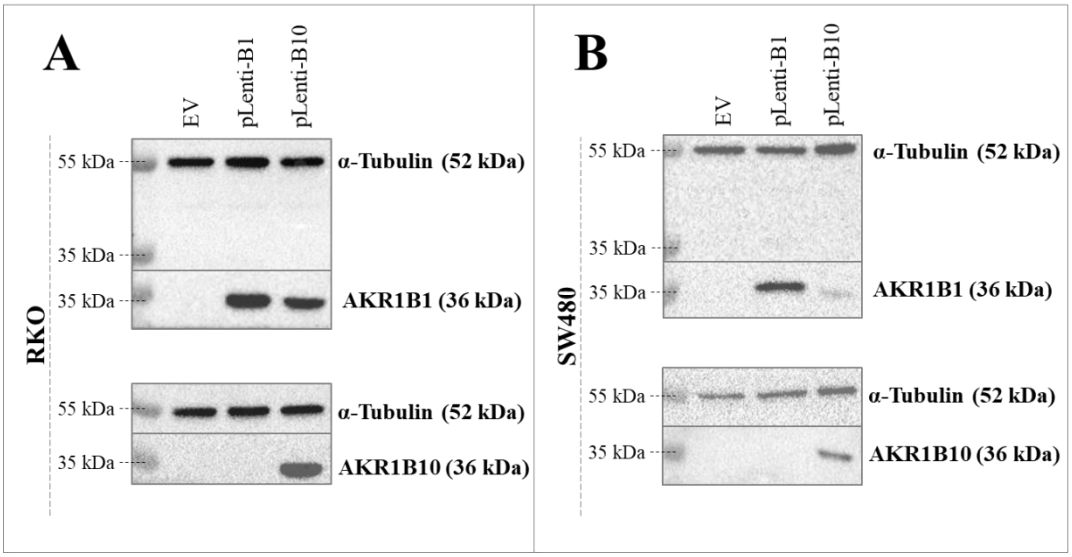

Figure 3.1 Confirmation of overexpression of AKR1B1 and AKR1B10 in RKO and SW480 cell lines with western blot

Overexpression of AKR1B1 and AKR1B10 in RKO and SW480 cell lines was confirmed with western blot. 15 µg of total protein was loaded to a 10% SDS-PAGE gel and wet-transferred to a PVDF membrane. The membrane was then processed for western blot according to standard techniques. AKR1B1 and AKR1B10 antibodies were blotted in two separate membranes for each cell line; (A) Expression of AKR1B1 and AKR1B10 in the RKO cells, (B) Expression of AKR1B1 and AKR1B10 in the SW480 cells. A representative image from 3 independent biological replicates is shown with α-Tubulin as the loading control. Abbreviations: EV, Empty Vector; pLenti-B1, cells transduced with AKR1B1-carrying viruses; pLenti-B10, cells transduced with AKR1B10-carrying viruses.

According to the manufacturer's specifications, the AKR1B1 polyclonal antibody (Thermo Fisher, #PA5-29718) used in this thesis was generated by challenging rabbit host against a recombinant fragment corresponding to a region within amino acids 1 and 316 of human AKR1B1. Since AKR1B1 and AKR1B10 share 71% similarity in their amino acid sequence (Cao et al., 1998), we speculated that the bands we observed in AKR1B10 lanes when blotted with AKR1B1 antibody were a non-specific interaction. A qRT-PCR was also performed to confirm that there is no cross-contamination between AKR1B1 and AKR1B10-overexpressing polyclonal cells (RKO, Figure 3.2A; SW480, Figure 3.2B).

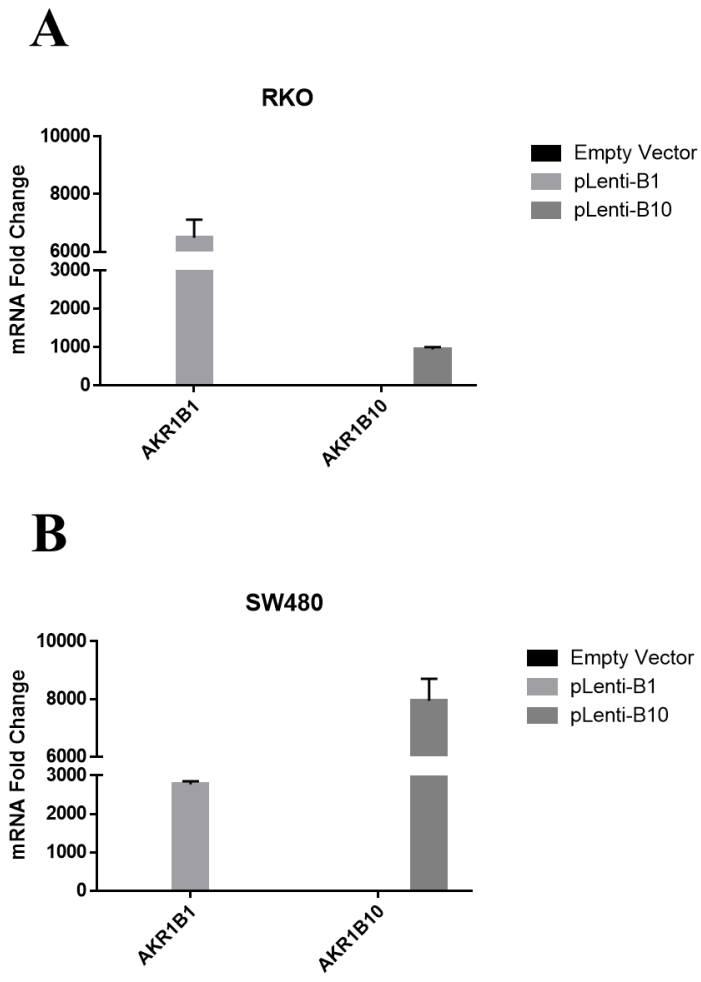

Figure 3.2 Confirmation of overexpression of AKR1B1 and AKR1B10 in RKO and SW480 cell lines with qRT-PCR

Overexpression of AKR1B1 and AKR1B10 in RKO and SW480 cell lines was confirmed with the qRT-PCR technique. The reaction was carried out in 40 cycles by using 1:10 diluted 1 µg of cDNA with 3 technical replicates for each group. β-actin was used as an internal control. C_t values of endogenous expression of both genes were beyond the detection limit (N/A), and C_t value of Empty Vector (EV) transduced cells were considered as 40 to carry out the analysis. Abbreviations: pLenti-B1, cells transduced with AKR1B1-carrying viruses; pLenti-B10, cells transduced with AKR1B10-carrying viruses.

The qRT-PCR results have shown that there was indeed no cross-contamination between AKR1B1 and AKR1B10-overexpressing cells. After generating stable polyclonal cells in both cell lines, the functional assays were carried out on generated RKO cells. Analysis and functional assays of stable polyclonal SW480 cells were carried out by our laboratory member, Çağdaş Ermiş.

3.2 Effects of AKR1B1 and AKR1B10 on cellular proliferation

An MTT Assay was conducted to determine whether the overexpression of AKR1B1 or AKR1B10 affected cellular proliferation in RKO cells. Wild-type (WT) and empty vector (EV) groups were used as controls to assess the effect of the lentiviral transduction on cell proliferation. There were no significant changes between WT, EV, and AKR1B1 or AKR1B10 overexpressing cells, which indicates that the overexpression of AKR1B1 or AKR1B10 did not influence proliferative signaling pathways (Figure 3.3).

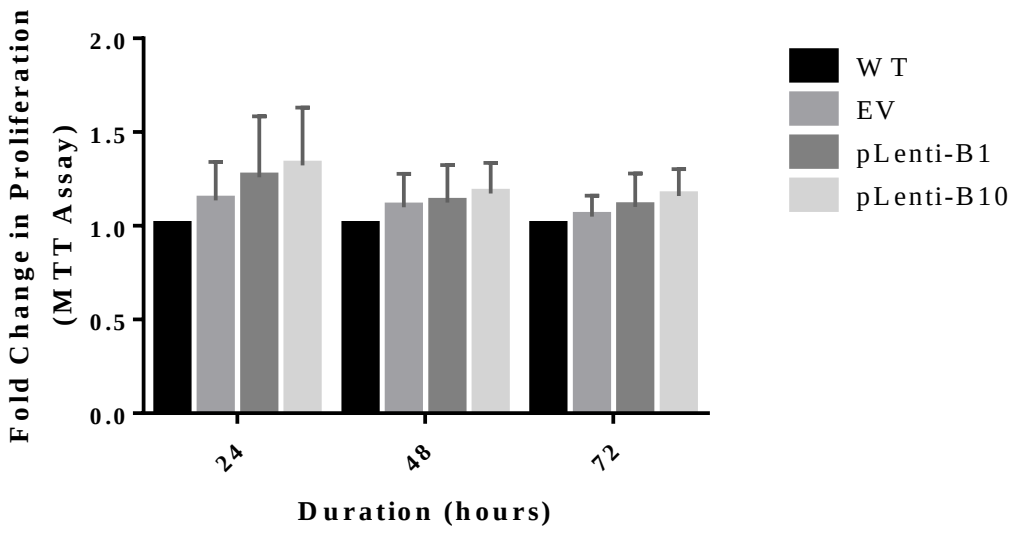

Figure 3.3 The effects of AKR1B1 and AKR1B10 overexpression on cellular proliferation of RKO cells in 2D cell culture

RKO wild-type, empty vector, AKR1B1 and AKR1B10 overexpressing cells were plated at a density of 10,000 cells per well in a 96-well plate. The cells were allowed to attach for 24 hours. The medium was replaced, and MTT was added 24, 48, and 72 hours post-attachment and incubated for 4 hours. Then, 1% SDS – 0.01M HCl solution was added and incubated overnight. The absorbance at 570 nm was measured using a microplate reader. Two independent biological replicates were carried out. No significant changes in cellular proliferation were observed ($^{n.s.}p > 0.05$, ANOVA). Abbreviations: WT, wild-type; EV, empty vector; pLenti-B1, cells transduced with AKR1B1-carrying viruses; pLenti-B10, cells transduced with AKR1B10-carrying viruses.

Although RKO cells did not show any significant changes *in vitro* 2D cell culture, we wanted to examine the effects of overexpression on proliferation in a 3D cell culture environment. For this, we have generated RKO spheroids in ultra-low attachment 96-well plates. We have observed that AKR1B1 and AKR1B10 overexpressing cells formed consistently larger spheroids compared to EV (Figure 3.4).

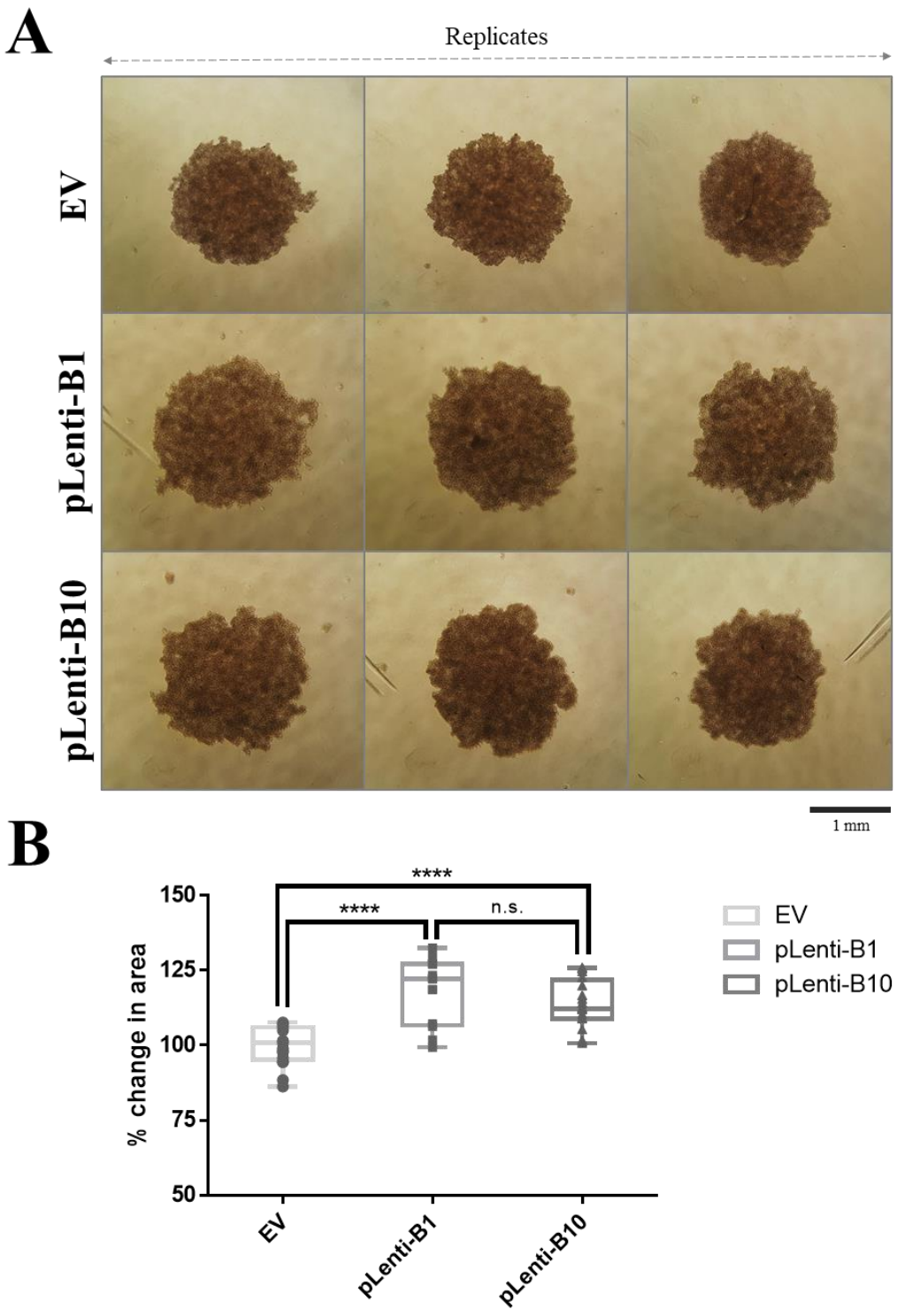

Figure 3.4 The effects of AKR1B1 and AKR1B10 overexpression on cellular proliferation of RKO cells in 3D cell culture

RKO empty vector, AKR1B1 and AKR1B10 overexpressing cells were plated at a density of 10,000 cells per well in an ultra-low attachment 96-well plate. The cells were allowed to form colonies and grow for 5 days in a humidified incubator with 5% CO_2 at 37°C. Cells were imaged under a light microscope at the end of the incubation period. (A) Three technical replicates from each group are shown, (B) % change in spheroid area normalized to mean of EV with statistical significance. Two independent replicates were carried out. Significant changes in the spheroid area between EV vs. pLenti-B1 and EV vs. pLenti-B10 groups were observed ($n \approx 18$ for each group, $^{****}p < 0.0001$, unpaired t-test). pLenti-B1 vs. pLenti-B10 spheroid area comparison was not significant ($^{n.s.}p > 0.05$, unpaired t-test). Abbreviations: EV, empty vector; pLenti-B1, cells transduced with AKR1B1-carrying viruses; pLenti-B10, cells transduced with AKR1B10-carrying viruses.

To determine whether the cells in the spheroids are alive or dead, we stained the same spheroids with calcein and ethidium homodimer. Following staining, 10 spheroids from each group were imaged (Figure 3.5A). We observed that spheroids formed by AKR1B1 overexpressing cells had a greater number of viable cells (measured by calcein fluorescence intensity; Figure 3.5B). Meanwhile, both AKR1B1 and AKR1B10 overexpressing cells had a significantly lesser amount of dead cells compared to the control group (Figure 3.5C).

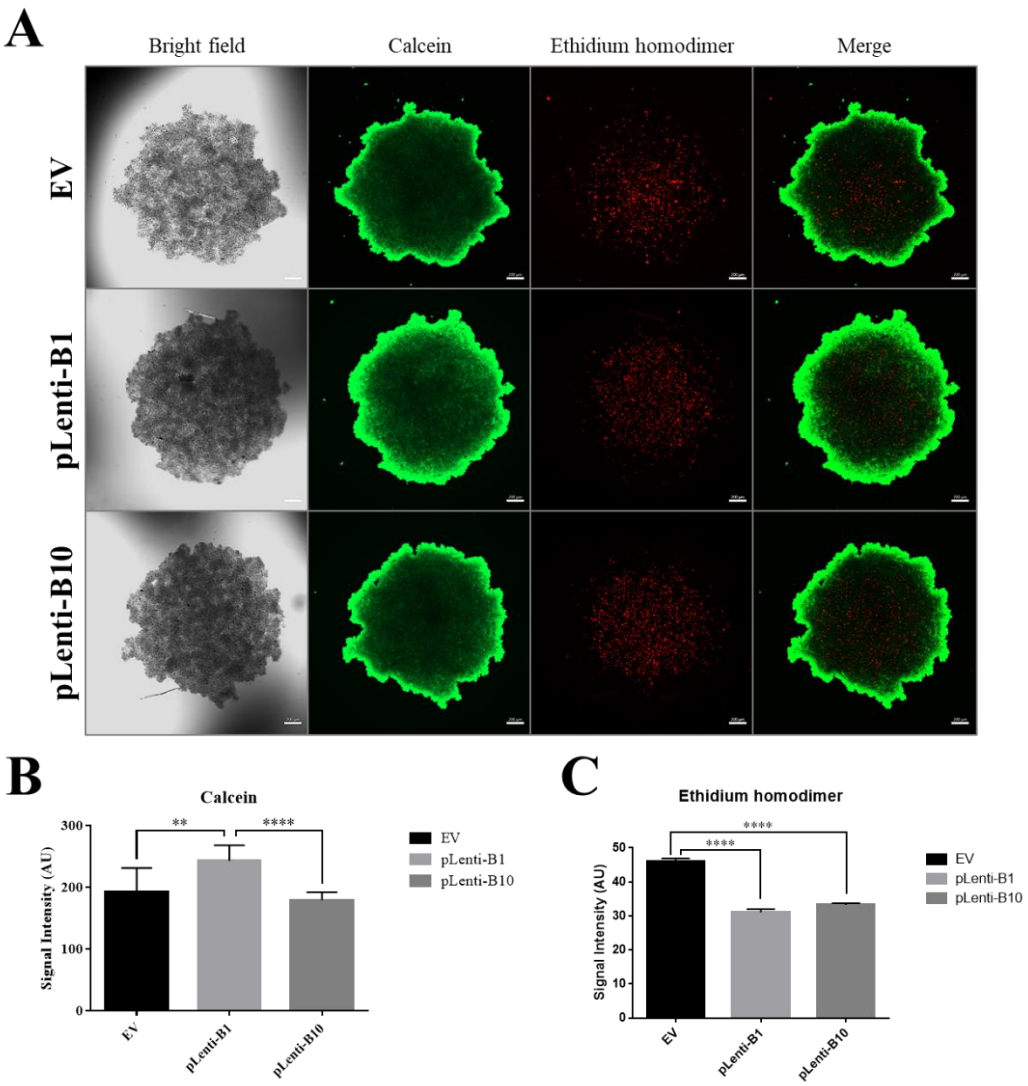

Figure 3.5 The effects of AKR1B1 and AKR1B10 overexpression on the viability of RKO cells in 3D cell culture

RKO empty vector, AKR1B1 and AKR1B10 overexpressing cells were plated at a density of 10,000 cells per well in an ultra-low attachment 96-well plate. The cells were allowed to form colonies and grow for 5 days in a humidified incubator with 5% CO_2 at 37°C. Cells were stained with calcein and ethidium homodimer at the end of the incubation period, and images were taken under a confocal microscope. (A) A representative image from each group is shown, (B) bar graph of calcein signal intensity, (C) bar graph of ethidium homodimer signal intensity. Ten technical

replicates for each group were carried out. Significant changes in calcein signal intensity in the EV vs. pLenti-B1($^{**}p < 0.01$, unpaired t-test) and pLenti-B1 vs. pLenti-B10 groups were observed ($^{****}p < 0.0001$, unpaired t-test). EV vs. pLenti-B10 calcein intensity were not significantly different ($^{n.s.}p > 0.05$, unpaired t-test). Significant changes in ethidium homodimer signal intensity were observed in the EV vs. pLenti-B1 and EV vs. pLenti-B10 cells ($^{****}p < 0.0001$, unpaired t-test). Abbreviations: EV, empty vector; pLenti-B1, cells transduced with AKR1B1-carrying viruses; pLenti-B10, cells transduced with AKR1B10-carrying viruses.

3.3 Effect of AKR1B1 and AKR1B10 on the clonogenic capability

A colony formation assay was performed to assess the effects of AKR1B1 and AKR1B10 on RKO cell survival and growth. There were no significant changes in colony numbers between EV and AKR1B1 or AKR1B10 overexpressing cells, which indicates that the overexpression of AKR1B1 or AKR1B10 did not affect their capability to form a colony (Figure 3.6).

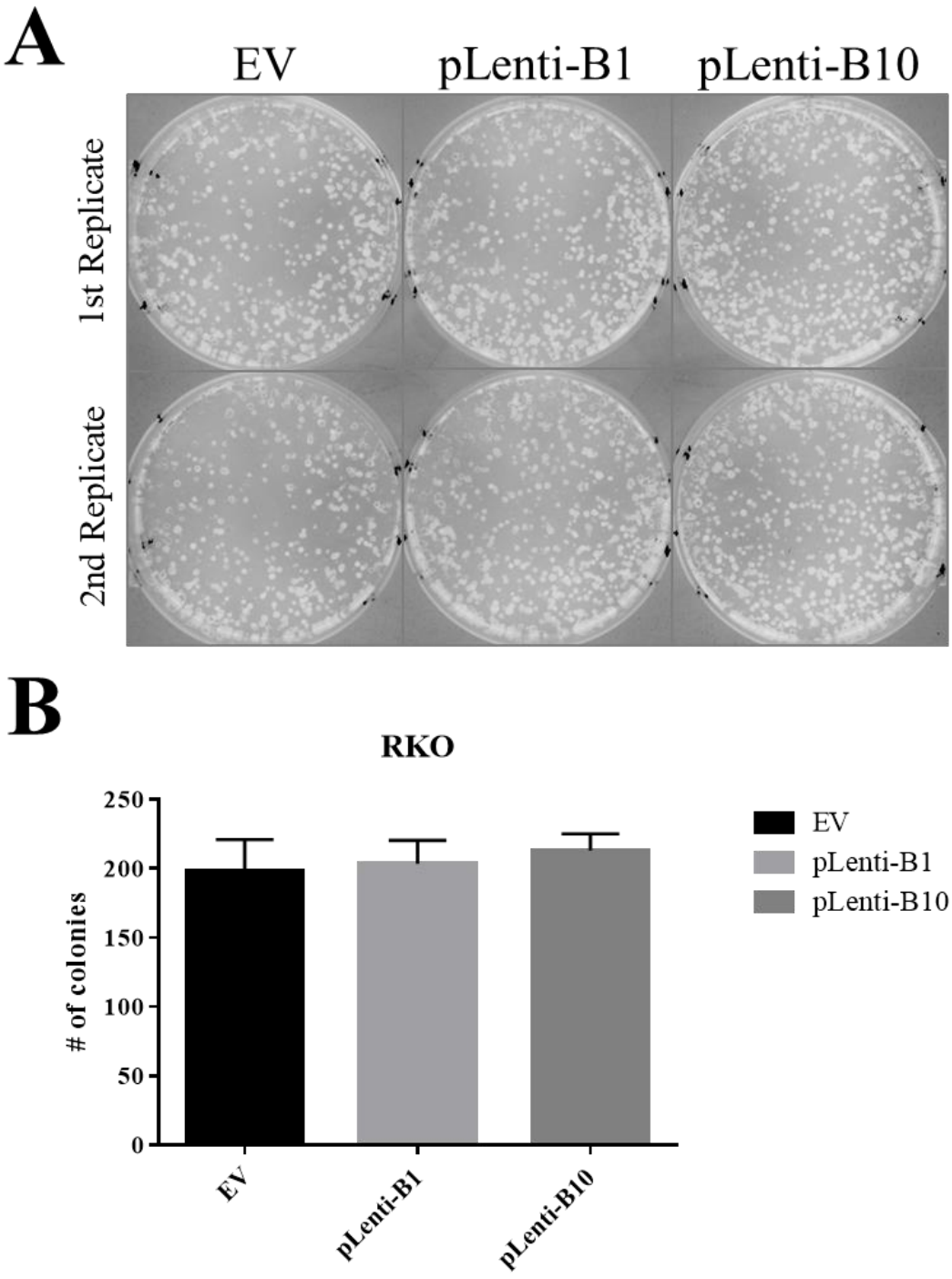

Figure 3.6 The effects of AKR1B1 and AKR1B10 overexpression on clonogenic capacity in RKO cells

RKO empty vector, AKR1B1 and AKR1B10 overexpressing cells were plated at a density of 1,000 cells per well in a 6-well plate. Cells were incubated for 8 days in a humidified incubator with 5% CO_2 at 37°C. Colonies were fixed, stained with crystal violet to make them visible, then imaged and counted with an ImageJ macro (Figure E.2). (A) Two technical replicates from each group are shown, (B) bar graph of the number of observed colonies. Two independent biological replicates were carried out. No significant changes in colony numbers were found ($^{n.s.}p > 0.05$, unpaired t-test). Abbreviations: EV, empty vector; pLenti-B1, cells transduced with AKR1B1-carrying viruses; pLenti-B10, cells transduced with AKR1B10-carrying viruses.

3.4 Effects of AKR1B1 and AKR1B10 on cell cycle progression

In order to investigate the effect of AKR1B1 and AKR1B10 overexpression in RKO cell cycle progression, we carried out PI staining, then examined cell cycle distribution with flow cytometry. The histograms for the cell cycle distribution were generated with BD Accuri C6 Software (BD Biosciences, USA), and proper gatings were set to distinguish cell populations and eliminate doublet cells (Figure 3.7).

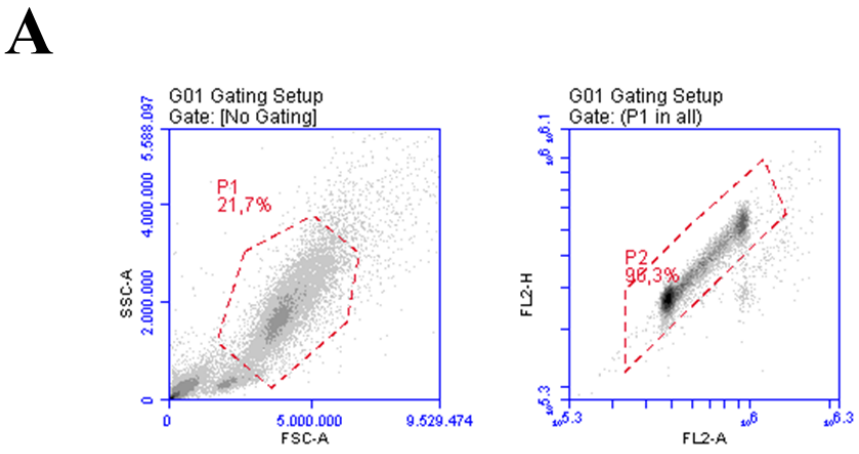

Figure 3.7 The effects of AKR1B1 and AKR1B10 overexpression on cell cycle progression in RKO cells

B

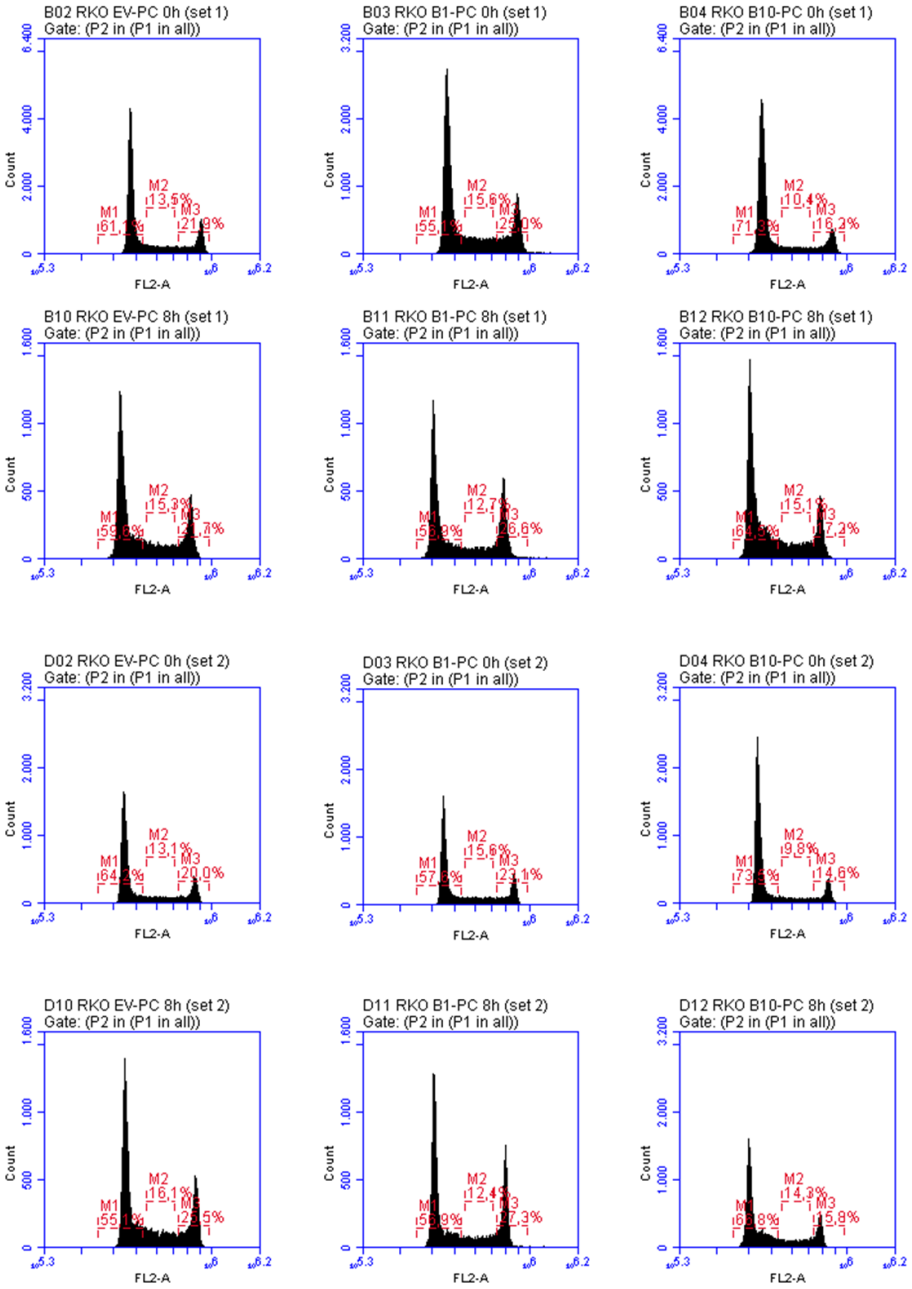

Figure 3.8 (continued) The effects of AKR1B1 and AKR1B10 overexpression on cell cycle progression in RKO cells

Synchronized by serum starvation and cycling RKO cells (AKR1B1, AKR1B10, and EV) were stained with PI for 30 minutes and analyzed with BD Accuri C6 flow cytometer. Gatings were set to eliminate cell debris (FSC-A vs. SSC-A) and discriminate cell doublets (FL2-A vs. FL2-H). 50,000 cells were analyzed for each group in the gated sample with flow cytometry. Two independent biological replicates were carried out. (A) Gating setup of the flow cytometry readings, (B) cell cycle distribution of the experimental groups. Abbreviations: EV-PC, polyclonal empty vector cells; B1-PC, polyclonal AKR1B1 overexpressing cells; B10-PC, polyclonal AKR1B10 overexpressing cells.

None of the cells showed significant alterations in the cell cycle progression at all cell cycle phases, except the AKR1B10-overexpressing group compared to AKR1B1-overexpressing cells in synchronized cells. The percentage of cells at different cell cycle stages (G_1, S, and G_2/M) are shown in a bar diagram (Figure 3.8).

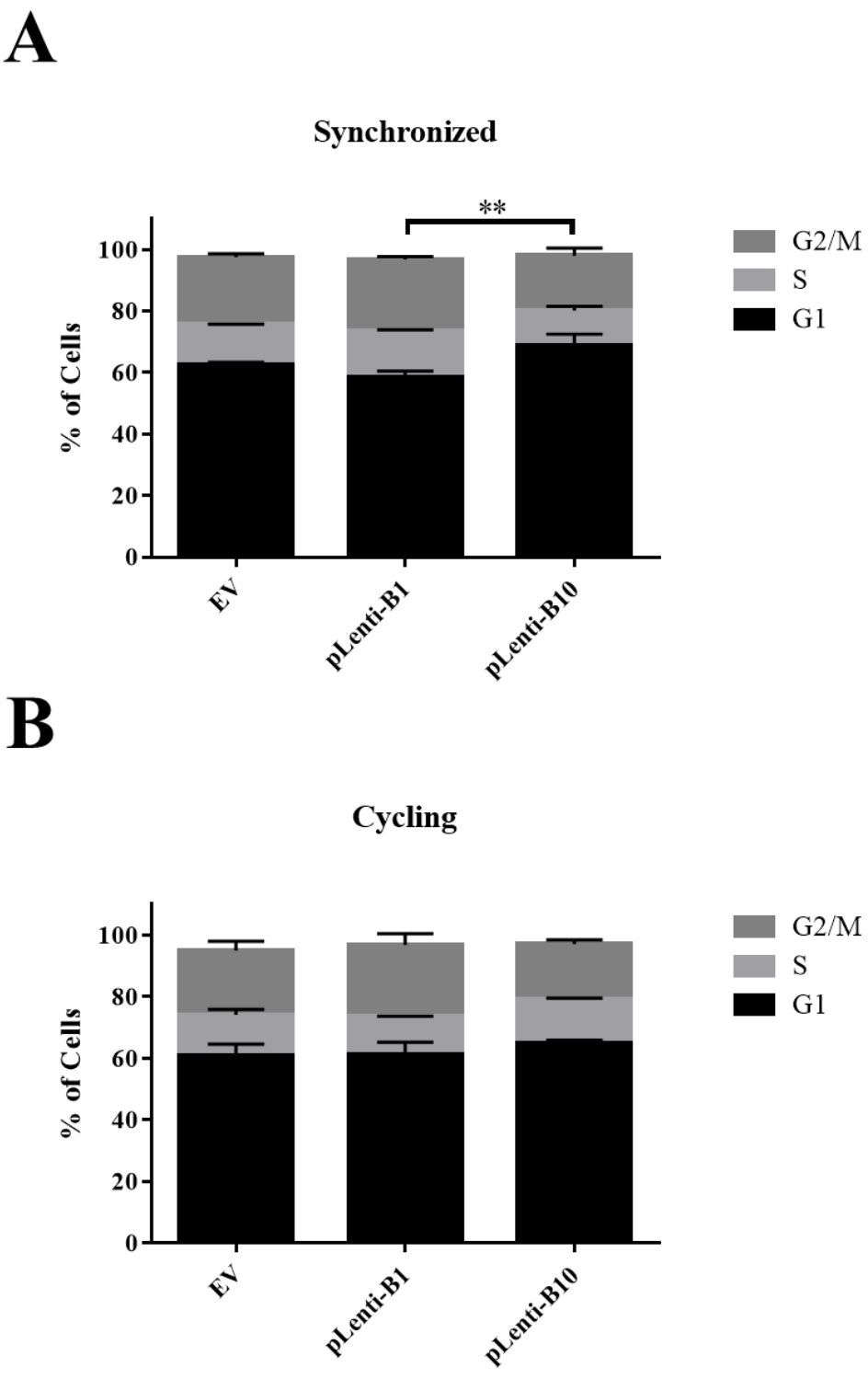

Figure 3.9 Cell cycle distribution in EV, pLenti-B1, and pLenti-B1 groups of RKO cells

RKO empty vector, AKR1B1 and AKR1B10 overexpressing cells were plated at a density of 500,000 cells per well in a 6-well plate. The cells were allowed to attach for 24 hours. The medium was replaced, and a starvation medium with 1% FBS was added. Cells were incubated (synchronized) overnight (~16 hours), and half of the cells were collected as the synchronized group, and the remaining cells were given a complete medium for 8 hours (cycling group). Cell cycle distribution was calculated with PI staining and flow cytometry. No significant cell cycle progression changes were found between synchronized and cycling groups ($^{n.s.}p > 0.05$, ANOVA) Except for pLenti-B1 vs. pLenti-B10 groups in synchronized cells, the pLenti-B10 group had a greater number of cells in G_1 compared to the pLenti-B1 group ($^{**}p < 0.01$, ANOVA). Abbreviations: EV, empty vector; pLenti-B1, cells transduced with AKR1B1-carrying viruses; pLenti-B10, cells transduced with AKR1B10-carrying viruses.

3.5 Effects of AKR1B1 and AKR1B10 on cellular motility

Our previous studies have shown that high expression of AKR1B1 was correlated with increased cellular motility and mesenchymal characteristics, whereas AKR1B10 expression was shown to reduce cellular motility in HCT-116 cells (Taskoparan et al., 2017). A scratch wound healing assay was performed to confirm these changes in the RKO model. The scratch wound area was imaged daily for three days (Figure 3.9A), and images were analyzed with ImageJ. No significant changes were found between EV and AKR1B1 or AKR1B10 overexpressing cells at all time points, except for the EV vs. pLenti-B10 cells at 48 hours. In this case, the AKR1B10 overexpressing cells showed a small decrease in wound area closure. Between the AKR1B1 and AKR1B10 overexpressing cells, we found that overexpression of AKR1B10 resulted in lower motility by a slower closure of the wound area compared to the AKR1B1 overexpressing group at all time points (Figure 3.9B).

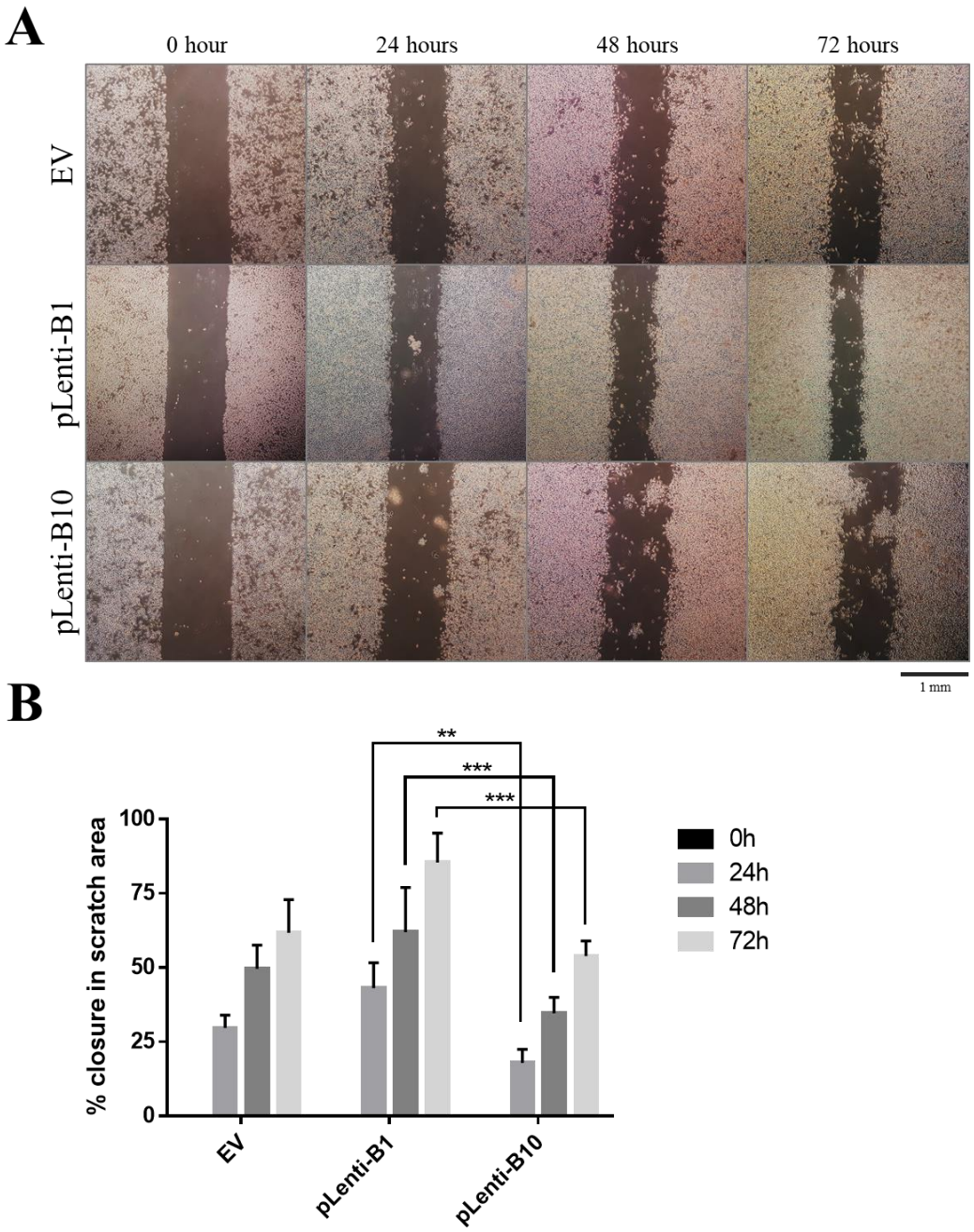

Figure 3.10 Effect of AKR1B1 and AKR1B10 overexpression in the motility of RKO cells

RKO empty vector (EV), AKR1B1 and AKR1B10 overexpressing cells were seeded in a 6-well plate at a density of 1,000,000 cells per well. Cells were allowed to attach and reach ~95% confluency. Then, scratch wounds were generated with 100 µl pipette tips, and cells were washed extensively with PBS. A complete medium containing 0.5 µM Mitomycin C was given to the cells in order to inhibit proliferation. Cells were incubated for 72 hours, and at every 24 hours, their medium was refreshed, and pictures of the wells were taken. Pictures were analyzed with an ImageJ macro (Figure E.3). Three independent biological replicates were carried out. No significant changes were found between EV vs. pLenti-B1 or pLenti-B10 groups ($^{n.s.}p > 0.05$, ANOVA), except for EV vs. pLenti-B10 at 48 hours, AKR1B10 overexpressing cells showed a small decrease in wound area closure ($^{*}p < 0.05$, ANOVA). pLenti-B1 vs. pLenti-B10 groups showed significant differences in all of the time points ($^{**}p < 0.01$ for 24 hours, $^{***}p < 0.001$ for 48 and 72 hours, ANOVA). Abbreviations: EV, empty vector; pLenti-B1, cells transduced with AKR1B1-carrying viruses; pLenti-B10, cells transduced with AKR1B10-carrying viruses.

3.6 Effects of AKR1B1 and AKR1B10 on the pentose phosphate pathway

Since AKRs prefer to use NADPH as their primary reducing electron donor, we investigated one of the major pathways for the NADPH generation, the pentose phosphate pathway (PPP). We analyzed TKT, TALDO, and G6PD enzymes of the PPP with qRT-PCR. Compared to empty vector control, TKT expression was modestly elevated in both AKR1B1 and AKR1B10 overexpressing cells (Figure 3.10A), whereas TALDO expression was modestly elevated only in AKR1B1 overexpressing cells (Figure 3.10B). G6PD expression was not affected by the expression of either enzyme (Figure 3.11).

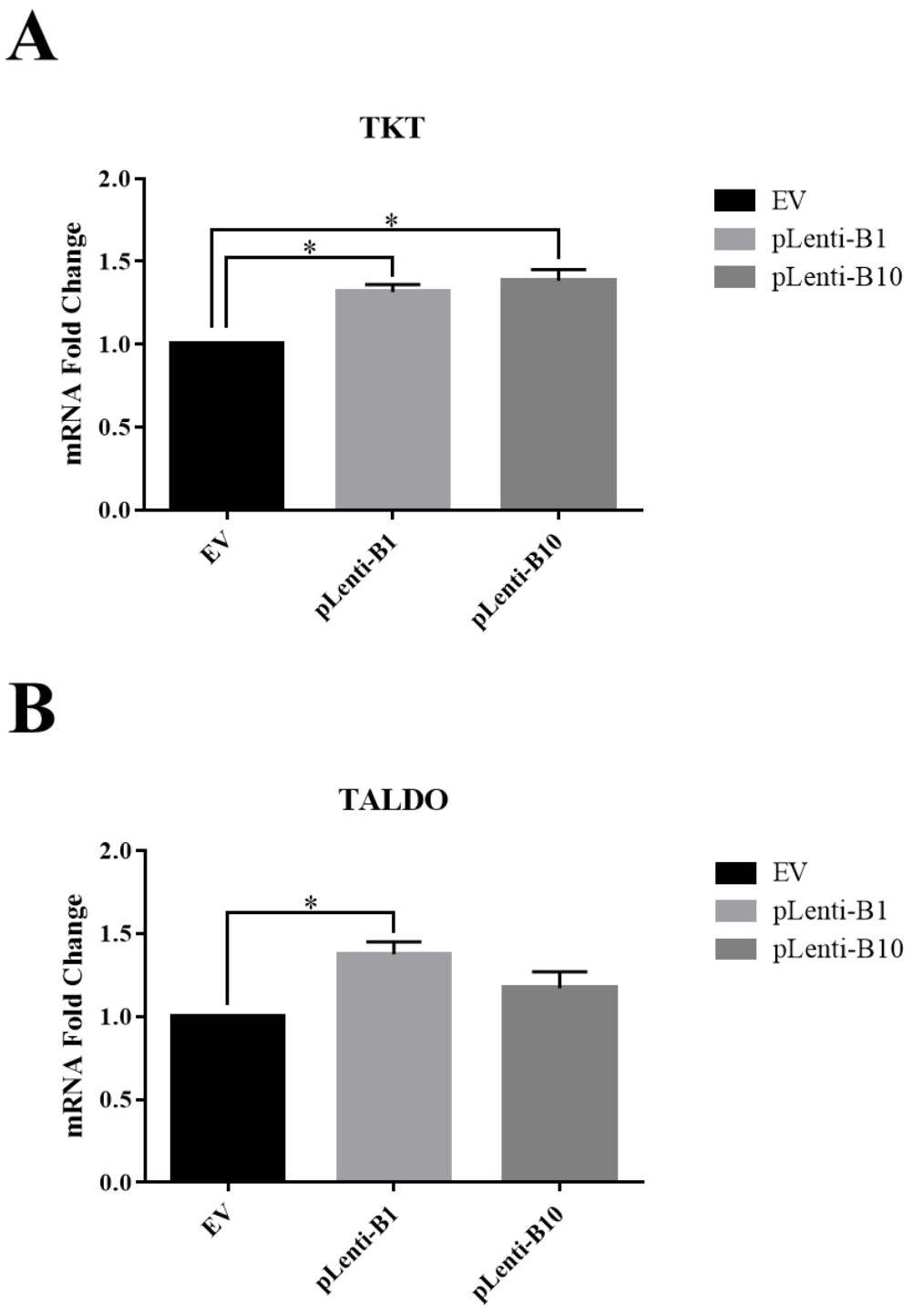

Figure 3.11 Effect of AKR1B1 and AKR1B10 overexpression in the expression of PPP enzymes, TKT and TALDO, functional in the non-oxidative branch.

Total RNA was isolated from RKO cells grown in a complete medium. 1 µg of cDNA was synthesized, and 1:10 diluted for the qRT-PCR. The diluted cDNA of EV, AKR1B1 and AKR1B10-overexpressing was used in qRT-PCR with three technical replicates for each group. β-actin was used as an internal control. (A) Expression of TKT enzyme in experimental groups, (B) expression of TALDO enzyme in experimental groups. The reaction was carried out on two different biological replicates. EV vs. pLenti-B1 and EV vs. pLenti-B10 groups shown a significant but modest increase in TKT expression ($^{*}p < 0.05$, unpaired t-test). Similarly, compared to EV, a significant but modest increase was seen in TALDO expression in the AKR1B1-overexpressing group ($^{*}p < 0.05$, unpaired t-test) but not with the AKR1B10-overexpressing group ($^{n.s.}p > 0.05$, unpaired t-test). Abbreviations: EV, empty vector; pLenti-B1, cells transduced with AKR1B1-carrying viruses; pLenti-B10, cells transduced with AKR1B10-carrying viruses.

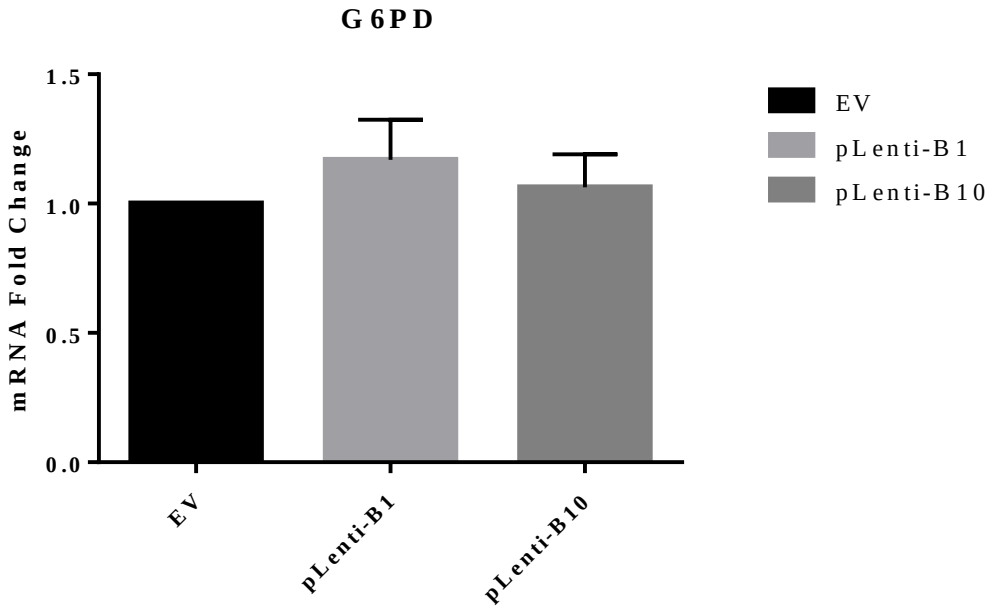

Figure 3.12 Effect of AKR1B1 and AKR1B10 overexpression in the expression of NADPH-generating PPP enzyme, G6PD, functional in the oxidative branch.

Total RNA was isolated from RKO cells grown in a complete medium. 1 µg of cDNA was synthesized, and 1:10 diluted for the qRT-PCR. The diluted cDNA of EV,

AKR1B1 and AKR1B10-overexpressing was used in qRT-PCR with three technical replicates for each group. β-actin was used as an internal control. Neither of the AKR1B1 and AKR1B10-overexpressing cells shows any significant difference in G6PD enzyme expression ($^{n.s.}p > 0.05$, unpaired t-test). Abbreviations: EV, empty vector; pLenti-B1, cells transduced with AKR1B1-carrying viruses; pLenti-B10, cells transduced with AKR1B10-carrying viruses.

3.7 Effects of AKR1B1 and AKR1B10 on cellular signaling pathways

In order to have a more comprehensive overview of the signaling pathways that are activated upon overexpression of AKR1B1 and AKR1B10, RNA sequencing (RNA-seq) was carried with the AKR1B1 and AKR1B10 overexpressing RKO cells. RNA-seq was carried out by BGI (Hong Kong, China), and initial processing of the raw data was carried out by Genoks (Ankara, Turkey) following a pipeline shown in Figure G.1 in the Appendix. I analyzed the differentially expressed genes by using the raw read counts of transcripts provided by Genoks. I have filtered features where counts per million reads mapped (CPM), were lower than 1, and the Combat batch-effect correction method was applied to the data before differential gene expression (DEG) analysis (Figure G.2 and Figure G.3).

Comparisons were carried out between EV vs. AKR1B1 and AKR1B10-overexpressing groups as well as AKR1B1 overexpression vs. AKR1B10 overexpression groups for DEG analysis with the *DeSeq2* package from Bioconductor 3.12 in R (Love et al., 2014). DEG were filtered with cutoffs of logFC < 1 and logFC > 1 along with $p < 0.01$. Interquartile range (IQR), volcano, principal component analysis (PCA), density and MA plots, and a heatmap were generated for each group. These steps were carried out in Interactive Differential Expression Analysis Browser (DEBrowser) from Bioconductor 3.12 in R (Kucukural et al., 2019). Gene ontology (GO) term analysis was carried out with ShinyGO v0.61 (Ge et al., 2020).

3.7.1 Comparison of EV vs. AKR1B1-overexpressing RKO cells

Differential gene expression (DGE) analysis was carried out between control (EV) cells with AKR1B1 overexpressing RKO cells to determine the differentially expressed genes upon AKR1B1 overexpression. Our analysis identified 83 significant differentially expressed genes between EV and AKR1B1 overexpressing cells; 37 of the identified genes were upregulated, and 46 genes were downregulated in the AKR1B1 overexpressing cells (Figure 3.12).

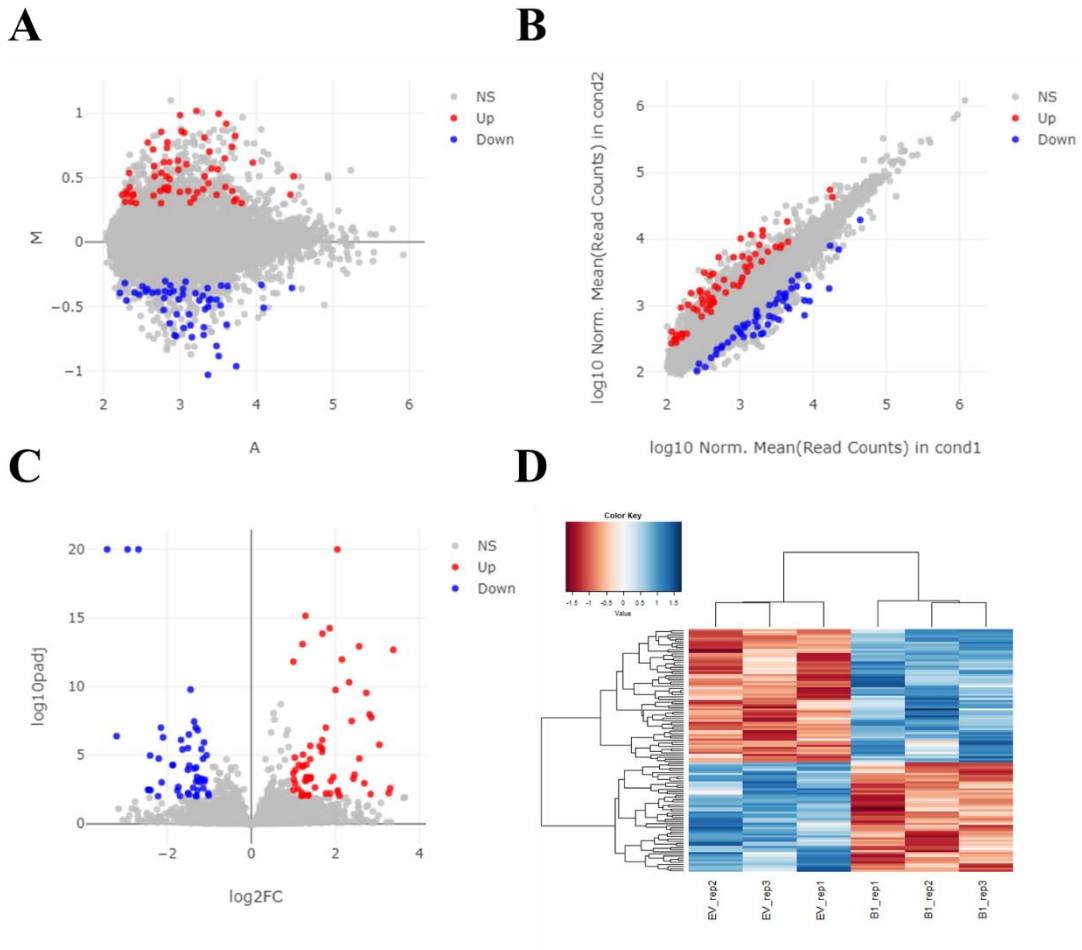

Figure 3.13 Effect of AKR1B1 overexpression in RKO compared to control cells

The RAW read-counts of transcripts were filtered where CPM was less than 1 and corrected for batch-effect with the Combat method. DeSeq2 was used to identify

differentially expressed genes with cutoffs of p-value < 0.01 and logFC < -1 or logFC > 1. A total of 37 genes were upregulated, and 46 genes were downregulated with AKR1B1 overexpression. Please see Appendix G for quality control (QC) plots (Figure G.4). (A) MA-plot of differentially expressed genes, (B) scatter plot of differentially expressed genes, (C) Volcano plot of differentially expressed genes, (D) heatmap of the upregulated and downregulated genes. Abbreviations: NS, Not significant; Up, upregulated genes; Down, downregulated genes; EV_rep1/2/3 (cond1), empty vector control cells with three replicates; B1_rep1/2/3 (cond2), AKR1B1 overexpressing cells with three replicates.

In order to understand the biological importance of the identified differentially expressed genes, gene ontology enrichment analysis was carried out with ShinyGO v.0.61. The differentially expressed genes list was uploaded and analyzed under the "GO Biological Process" geneset. Our analysis identified that several different GO terms related to the regulation of cellular response to reactive oxygen species (ROS) were enriched with AKR1B1 overexpression, along with negative regulation of cellular response to drug, histone acetylation, and chromosome and chromatin organization GO terms (Figure 3.13).

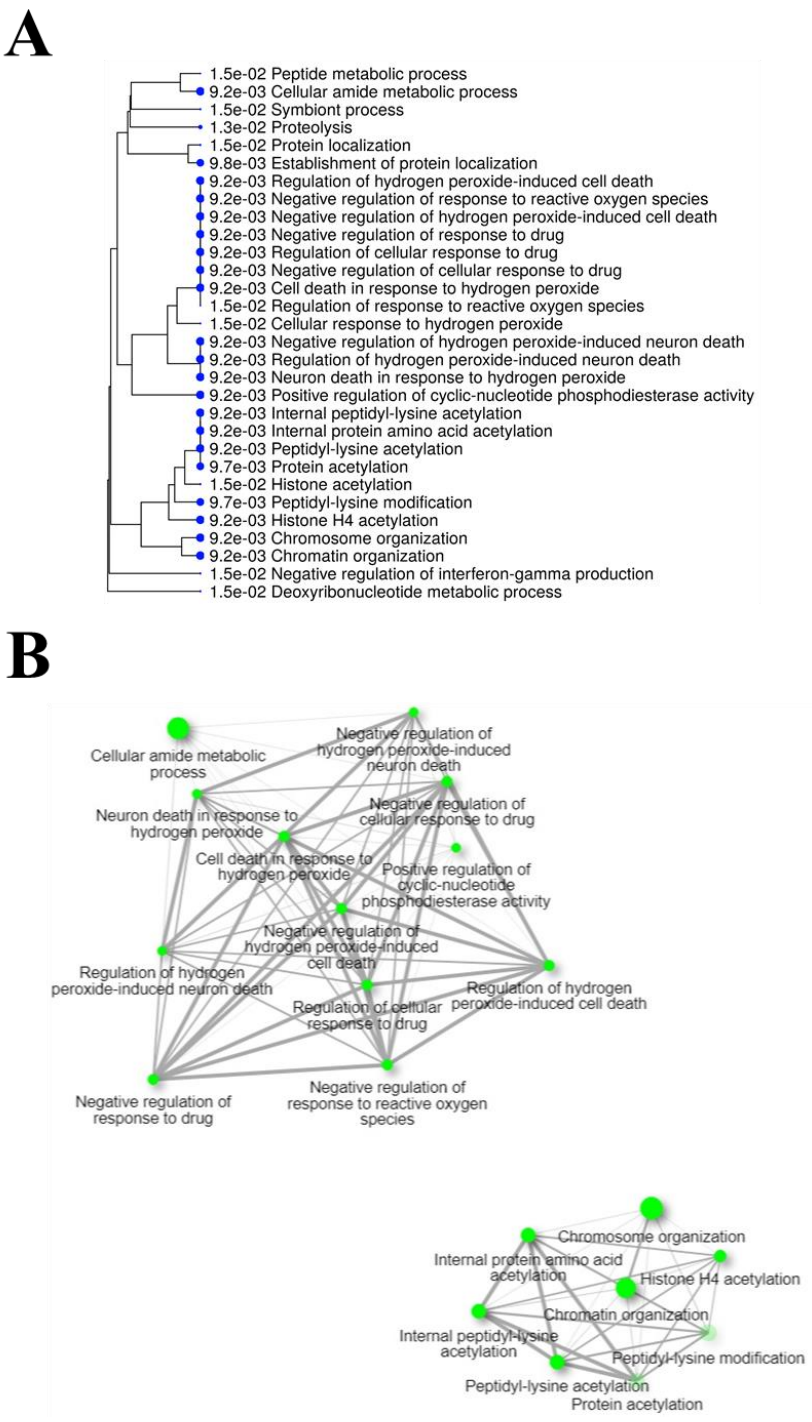

Figure 3.14 Gene ontology enrichment analysis of AKR1B1 overexpression

The differentially expressed genes were uploaded to ShinyGO v0.61 and analyzed in the "GO Biological Process" geneset with a p-value cutoff (FDR) of 0.05. (A) 30 of

the most significant GO terms shown in a hierarchical clustering tree, (B) 20 of the most significant GO terms shown with a network representation where bigger nodes represent larger gene sets, and thicker edges represent more overlapped genes.

3.7.2 Comparison of EV vs. AKR1B10-overexpressing RKO cells

Next, we analyzed the effect of overexpression of AKR1B10 in differential gene expression compared to control (EV) RKO cells. Our analysis identified 84 differentially expressed genes between EV and AKR1B10 overexpressing cells; 44 of the identified genes were upregulated, and 40 genes were downregulated in AKR1B10 overexpressing cells (Figure 3.14).

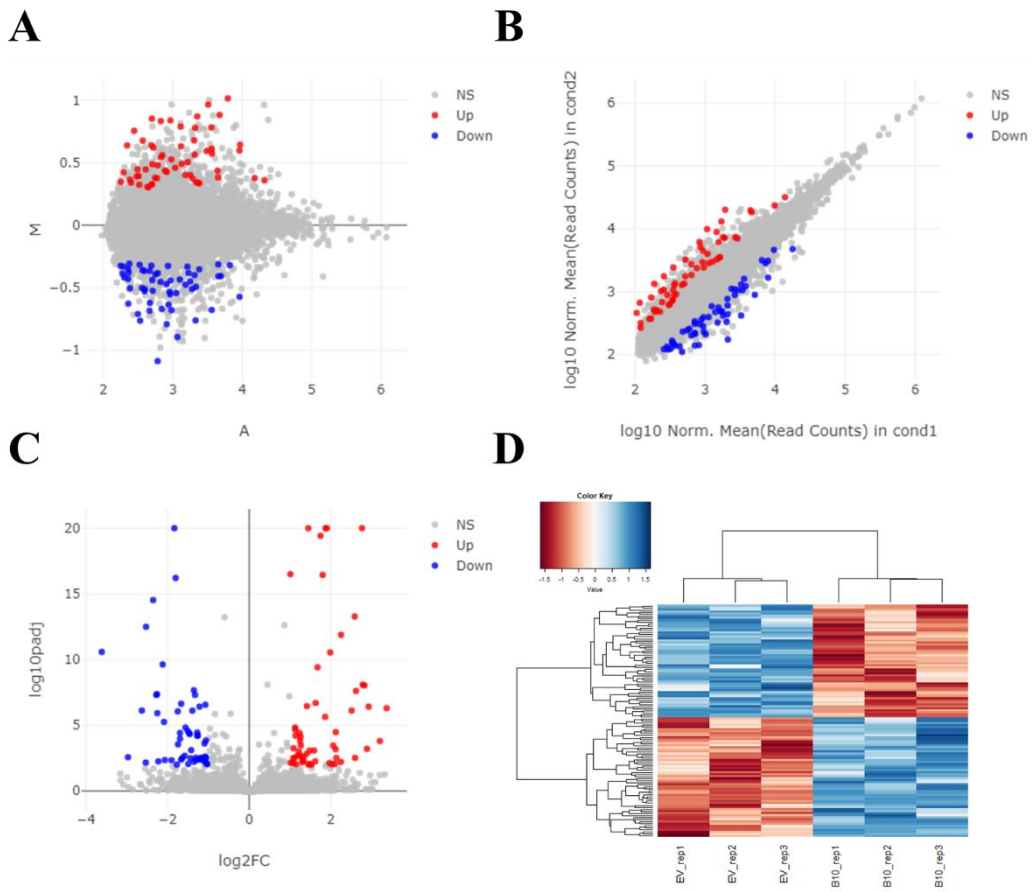

Figure 3.15 Effect of AKR1B10 overexpression in RKO compared to control cells

The RAW read-counts of transcripts were filtered where CPM was less than 1 and corrected for batch-effect with the Combat method. DeSeq2 was used to identify differentially expressed genes with cutoffs of p-value < 0.01 and logFC < -1 or logFC > 1. A total of 44 genes were upregulated, and 40 genes were downregulated with AKR1B10 overexpression. Please see Appendix G for quality control (QC) plots (Figure G.5). (A) MA-plot of differentially expressed genes, (B) scatter plot of differentially expressed genes, (C) Volcano plot of differentially expressed genes, (D) heatmap of the upregulated and downregulated genes. Abbreviations: NS, Not significant; Up, upregulated genes; Down, downregulated genes; EV_rep1/2/3 (cond1), empty vector control cells with three replicates; B10_rep1/2/3 (cond2), AKR1B10 overexpressing cells with three replicates.

Gene ontology enrichment analysis was carried out with ShinyGO v.0.61 to understand the biological importance of the identified differentially expressed genes as described above using the "GO Biological Process" geneset. Our analysis identified several different GO terms related to the regulation of metabolic/biosynthetic process that was enriched with AKR1B10 overexpression, along with the GO terms mitotic cell cycle progress, mRNA and RNA processing (Figure 3.15).

A

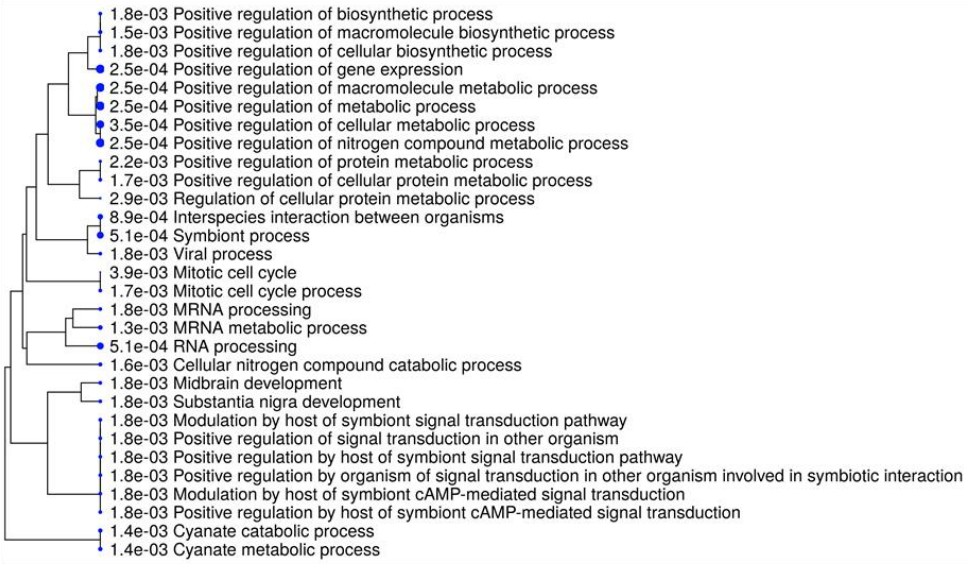

B

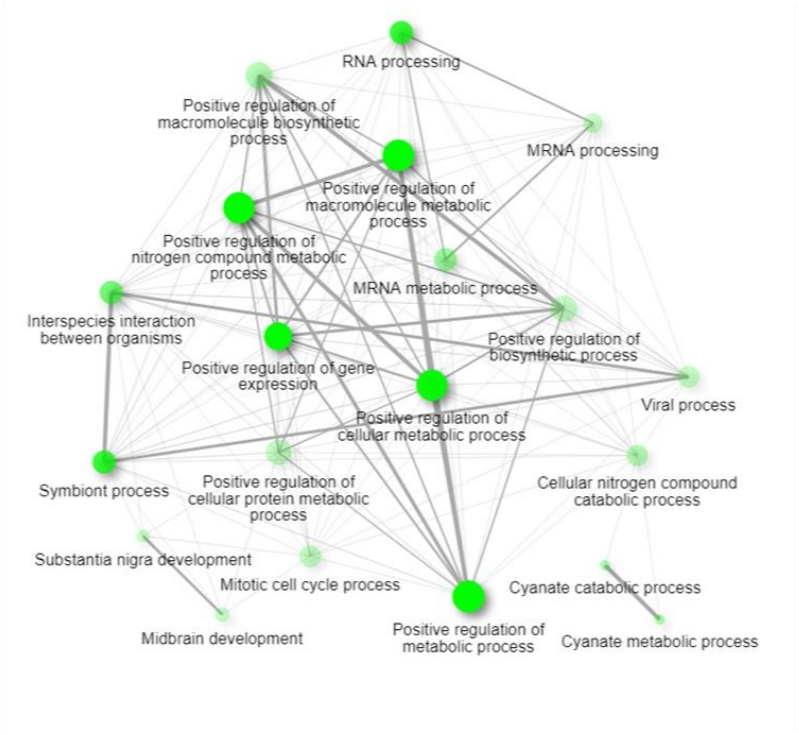

Figure 3.16 Gene ontology enrichment analysis of AKR1B10 overexpression

The differentially expressed genes were uploaded to ShinyGO v0.61 and analyzed in the "GO Biological Process" geneset with a p-value cutoff (FDR) of 0.05. (A) 30 of the most significant GO terms shown in a hierarchical clustering tree, (B) 20 of the most significant GO terms shown with a network representation where bigger nodes represent larger gene sets, and thicker edges represent more overlapped genes.

CHAPTER 4

DISCUSSION

Aldo-keto reductases (AKRs) are enzymes that preferably use NADPH as their source of reducing electrons. These enzymes have been shown to reduce aldehydes and ketones to primary and secondary alcohols. There are many catalytic roles of AKRs in cells, such as the conversion of glucose to sorbitol, reduction of glucocorticoids and small carbonyl metabolites to glutathione conjugates and phospholipid aldehydes (Barski et al., 2008). The targets of AKRs include pharmaceuticals such as anticancer and antidiabetic drugs. Several members of the AKRs are also implicated in cancer cell proliferation (Yan et al., 2007), cancer development (Byrns et al., 2008), and chemotherapy resistance (Wsol et al., 2007). Two members of the AKR superfamily, AKR1B1 and AKR1B10, are known for their catalytic roles in the polyol pathway and retinol metabolism, respectively.

AKR1B1 catalyzes the conversion of glucose to sorbitol in the polyol pathway, using NADPH as a cofactor. Under hyperglycemic conditions, this sorbitol can accumulate in the cells, leading to diabetic complications due to increased osmotic stress (Ramana, 2011). Since the promotor region of AKR1B1 contains AP-1 and NF-κB (Srivastava et al., 2011), AKR1B1 is implicated in oxidative stress and inflammatory signaling. Previous studies have shown that inhibition of AKR1B1 can prevent tumor necrosis factor-alpha (TNF-α) mediated activation of NF-κB (Tammali et al., 2007). It is also shown that high activity of AKR1B1 can lead to depletion of its cofactor, NADPH, subsequent cell death related to disruption in the GSSG/GSH antioxidant system of the cells (Zhang et al., 2018).

Unlike AKR1B1, AKR1B10 is an insufficient reductant enzyme of glucose but with higher catalytic efficiency for retinals (Crosas et al., 2003). AKR1B10 catalyzes the reduction of retinals to retinols. High expression of AKR1B10 is indicated in cancer

development due to loss of retinoic acids (Penning & Lerman, 2008). In lung cancer cells, it has been shown that AKR1B10 inhibition was associated with decreased cell proliferation, cell adhesion and migration, and inhibition of cell cycle progression (Zhou et al., 2018). However, recent studies have shown that AKR1B10 has tumor-suppressive properties associated with a good CRC prognosis. It was found that AKR1B10 was a direct transcriptional target of p53, and expression of AKR1B10 was related to the tumor-suppressive function of p53 (Ohashi et al., 2013).

A previous study from our laboratory has shown that high AKR1B1 expression was associated with a faster progression through the cell cycle, increased cellular motility and inflammation, whereas high AKR1B10 expression was associated with a weak inflammatory phenotype and lower motility (Taskoparan et al., 2017). Another recent study published from our laboratory showed that AKR1B1 expression in patient tumor specimens was strongly positively correlated with mesenchymal markers such as vimentin, ZEB1, ZEB2, TWIST1, and TWIST2 while being negatively correlated with epithelial marker E-cadherin. On the other hand, AKR1B10 expression was weakly but significantly negatively correlated with mesenchymal markers and positively correlated with epithelial markers (Demirkol Canlı et al., 2020).

Consensus molecular subtypes (CMS) is a classification system for CRC generated by an international consortium (Guinney et al., 2015). CMS classifications (Table 4.1) are important for biological interpretability and clinical stratification in CRC.

Table 4.1 List of CMS classifications and their distinguishing features

Classification	Distinguishing Features
CMS1	hypermutated, microsatellite unstable, and strong immune activation
CMS2	epithelial, marked WNT and MYC signaling activation
CMS3	epithelial and evident metabolic dysregulation
CMS4	prominent transforming growth factor-β activation, stromal invasion, and angiogenesis

Our recent study also established two gene signatures related to differential DFS and RFS. AKR1B1^{HIGH} / AKR1B10^{LOW} gene signature was classified as CMS4 with mesenchymal characteristics, while AKR1B1^{LOW} / AKR1B10^{HIGH} gene signature was classified as CMS3 with epithelial characteristics and metabolic dysregulation (Demirkol Canlı et al., 2020).

In this study, we wanted to confirm our previous findings in different cell line models and better understand the functional effects and underlying differences in cell signaling related to the expression of AKR1B1 and AKR1B10. For this purpose, we have generated an overexpression model with lentiviral transduction of both enzymes in two CRC cell lines, RKO and SW480, that do not endogenously express either of the enzymes. Cell lines (monoclones and polyclones) with stable overexpression of the enzymes were generated and confirmed with western blot (Figure 3.1) and qRT-PCR (Figure 3.2). These data reconfirmed our previous findings of no endogenous expression of AKR1B1 and AKR1B10 enzymes in the wild-type cells.

Since neither of the cell lines used for the generation of stable polyclonal cells endogenously expresses AKR1B1 and AKR1B10, we thought that overexpression of AKR1B1 or AKR1B10 in these cells would correspond respectively to the

previously established gene signatures: AKR1B1^{HIGH} / AKR1B10^{LOW} and AKR1B1^{LOW} / AKR1B10^{HIGH}. We have investigated cell proliferation, cell cycle progression, cell motility, and expression of PPP enzymes by conducting several functional assays.

Although AKR1B1^{LOW} / AKR1B10^{HIGH} signature was associated with inhibition of pathways related to cell proliferation (Demirkol Canlı et al., 2020), we did not observe any significant alterations in cellular proliferation in 2D cell culture (Figure 3.3). We have also analyzed the clonogenic capacity of AKR1B1 and AKR1B10 overexpressing cells, and we have found no significant changes between the groups matching our 2D proliferation results (Figure 3.6). However, in 3D cell culture, both AKR1B1 and AKR1B10 overexpressing RKO cells showed a significantly increased spheroid area than control cells (Figure 3.4), suggesting a higher proliferative rate for with the overexpression of both enzymes. Moreover, staining of the spheroids revealed that AKR1B1 overexpressing cells had a higher number of viable cells in spheroids than control cells and AKR1B10 overexpressing cells (Figure 3.5B), whereas both AKR1B1 and AKR1B10 overexpression reduced the cell death (Figure 3.5C). The 3D culture was carried out in an ultra-low attachment plate, which provides different outside-in survival signals than 2D growth in cell culture plates. The 3D culture conditions are more superior to 2D culture as it mimics several aspects of the tumor microenvironment (Pinto et al., 2020), including:

1. Heterogeneous supply of oxygen and nutrients to the out versus inner layers of cells,

2. Presence of different layers of cells, including proliferating, quiescent and necrotic zones, which resemble in vivo tumors more closely,

3. Enhanced interactions between cells and between cells and ECM.

AKR1B1 or AKR1B10 overexpression has likely enabled the adaptation of the cells to some or all of these factors, which may have contributed to the increase in the size

and survival of the spheroids. Our future studies will focus on better understanding the signaling pathways in 3D cultured cells, particularly in the context of low availability of nutrients and/or oxygen.

The $AKR1B1^{LOW}$ / $AKR1B10^{HIGH}$ gene signature in colorectal tumors predicted a better prognosis. Therefore, we hypothesized that this effect might be reflected by slower cell proliferation and/or slower cell cycle progression. We did not observe any dramatic differences in the proliferation of AKR1B10 overexpressing in either short term (MTT) or long term (clonogenic) assays. Evaluation of cell cycle distribution showed a significantly increased number of cells arrested at G_1 in the AKR1B10 overexpressing cells that are synchronized (Figure 3.8A); however, this was not reflected in cycling cells (Figure 3.8B). The cells were synchronized at G_1/S by serum withdrawal, a protocol that is widely used in the literature (Langan & Chou, 2011). The arrest of a greater percentage of AKR1B10 but not the AKR1B1 overexpressing cells or the EV cells at the G_1 stage of the cell cycle upon serum withdrawal suggests a greater vulnerability of these cells to lack of nutrients. AKR1B10 overexpressing tumors are already known to have a high expression of metabolism-related genes (Demirkol Canlı et al., 2020). Therefore, we can speculate that withdrawal of nutrients could have led to altered signaling events in the AKR1B10 overexpressing cells, enabling them to arrest at greater numbers upon serum starvation. The metabolic vulnerability of these cells is further emphasized in their ability to re-enter the cell cycle and progress through it when the serum-free medium was replaced with a complete medium.

Epithelial to mesenchymal transition (EMT) involves a functional transition from an epithelial cell that interacts with the basement membrane to a mesenchymal cell with enhanced migratory capacity and invasiveness (Kalluri & Weinberg, 2009). Since our previous studies have shown a positive correlation between AKR1B1 and mesenchymal characteristics (Demirkol Canlı et al., 2020) and cellular motility (Taskoparan et al., 2017), we have conducted a scratch wound healing assay in our RKO stable overexpression model (Figure 3.9A). Although there were no significant

differences compared to control cells, AKR1B1 overexpressing RKO cells had significantly higher closure in the scratch wound area than the AKR1B10 overexpressing RKO cells. This difference shows that, although small, AKR1B1 and AKR1B10 have opposite effects in cellular motility in the RKO overexpression model, confirming earlier findings of our laboratory.

The $AKR1B1^{LOW}$ / $AKR1B10^{HIGH}$ gene signature, classified as CMS3, was also associated with the inhibition of metabolic pathways that produce biomass (Demirkol Canlı et al., 2020). The Pentose Phosphate Pathway (PPP) is known to be highly active in cancer cells as an alternative route for the utilization of glucose for the generation of cytosolic NADPH and ribose that can be used for nucleotide biosynthesis (Jin & Zhou, 2019). Since the AKR pathways utilize NADPH and previous *in silico* observations from our laboratory (unpublished data) suggest a very strong correlation between the expression of AKRs and NADPH producing enzymes, we have determined the expression of the major PPP enzymes G6PD, TKT, and TALDO. The expression of TKT was significantly increased, albeit modestly, in both AKR1B1 and AKR1B10 overexpressing RKO cells (Figure 3.10A). TALDO enzyme expression was significantly increased, again modestly, in AKR1B1 overexpressing cells, but not in the AKR1B10 overexpressing cells (Figure 3.10B). On the other hand, the NADPH-producing enzyme of PPP, G6PD, did not show a significant expression change in either of AKR1B1 and AKR1B10 overexpressing groups (Figure 3.11). We speculate that the expression of the non-oxidative branch of the PPP may have been preferentially activated in the AKR1B1 overexpressing cells, which may lead to more synthesis of ribose for the generation of nucleotides (Figure 1.3). This would also aid in rapid cell division and may have contributed to the higher proliferation observed in the AKR1B1 overexpression spheroids. It also needs to be kept in mind that enzyme expression may not correlate with enzyme activity as the level of substrates and cofactors determines the latter in addition to the enzyme expression. We will evaluate the NADP/NADPH ratio in the AKR1B1 and AKR1B10 overexpressing cells as a better metric to evaluate the activation of PPP or other NADPH generating pathways in these cells.

In order to comprehensively evaluate differentially expressed genes in AKR1B1 and AKR1B10 overexpressing cells compared to controls, we have carried out RNA-seq. Previous studies have associated the expression of AKR1B1 with a ROS-induced inflammatory response (Srivastava et al., 2011). Our group has previously shown that silencing AKR1B1 in HCT-116 cells resulted in a significantly lower amount of ROS formation and lower NF-κB transcriptional activity (Taskoparan et al., 2017). GO analysis of the RNA-seq data indicated that ROS related GO terms were highly enriched in AKR1B1 overexpressing cells (Figure 3.13), confirming the previous findings in this model. Also, functional enrichment in the GO Molecular Function geneset showed that NF-κB binding was significantly enriched with AKR1B1 overexpression (data not shown). Hyperactivation of the polyol pathway in AKR1B1 overexpressing cells may lead to a depletion of NADPH, which in turn, may decrease the cytosolic GSH/GSSG ratio and lead to oxidative stress. Although cancer cells are known to be vulnerable to a high amount of oxidative stress, submaximal and/or transient activation of oxidative stress may lead to the activation of inflammatory pathways, leading to the secretion of various mitogenic cytokines and growth factors in intestinal epithelial cells (Reuter et al., 2010). Measurement of intracellular ROS and GSH/GSSG levels will provide a better understanding of how endogenous antioxidant and ROS levels are altered in AKR1B1 overexpressing RKO cells. Our *in silico* analysis also showed enrichment in the GO terms histone acetylation and chromosome and chromatin organization. These enrichments indicate that apart from its enzymatic activity, AKR1B1 might be affecting the transcriptional regulation of genes via epigenetic mechanisms.

AKR1B10 overexpression showed significant enrichment in the regulation of metabolic and biosynthetic pathways (Figure 3.15). This enrichment was also expected; our group has previously shown that tumor samples with high expression of AKR1B10 were associated with an inhibition of metabolic pathways that produce biomass (Demirkol Canlı et al., 2020). Analysis of RKO cells overexpressing AKR1B10 showed a remarkable corroboration of tumor data. Thus, AKR1B10 overexpression led to inhibition of pathways related to positive regulation of

metabolic and biosynthetic pathways. We have also seen enrichment in the mitotic cell cycle and its process, which may be related to our *in vitro* results, which showed the vulnerability of AKR1B10 overexpressing cells to serum starvation.

This study describes the first high throughput transcriptomic data analysis of a colon cancer cell line overexpressing AKR1B1 or AKR1B10. Transcriptomic analyses carried out on tumor samples entail the use of both epithelial and stromal compartments. In fact, using *in silico* tools such as the ESTIMATE algorithm (https://bioinformatics.mdanderson.org/public-software/estimate/), a previous study from our lab has shown that a considerable proportion of AKR1B1 expression in CRC tumors is contributed by the stromal compartment (Demirkol Canlı et al., 2020). Nonetheless, many of the gene ontology terms appear to be remarkably conserved between the AKR1B1 or AKR1B10 high expressing CRC samples and the AKR1B1 or AKR1B10 overexpressing colon cancer cell line suggesting that epithelial expression of these genes also contribute to the gene expression profiles observed in tumors.

CHAPTER 5

CONCLUSION AND FUTURE STUDIES

The primary findings of this study are as follows:

1. The overexpression of AKR1B1 and AKR1B10 in RKO cells did not influence their proliferative rates and colony formation in 2D cell culture. However, both AKR1B1 and AKR1B10 expressing cells developed larger spheroids, which correspond to higher proliferative rates of these cells compared to control cells. Moreover, AKR1B1 overexpressing spheroids had a higher number of viable cells within their structure, whereas both AKR1B1 and AKR1B10 overexpressing spheroids had a lesser amount of dead cells compared to the control group. In the future, spheroids can be harvested and further analyzed for markers of cellular proliferation and cell cycle progression to shed light on these differences between control cells and AKR expressing cells in 3D cell culture.

2. Overexpression of AKR1B10 led to a high number of cells were arrested in the G_1 phase following serum starvation. AKR1B10 overexpressing cells and tumors are known to be highly enriched in metabolic pathways, which makes this finding not surprising. This finding may also, in part, provide a mechanistic understanding of why AKR1B10 overexpressing tumors show a better prognosis, as cells in the tumor core that have limited access to nutrients may be more susceptible to death. Future studies on how serum and/or glucose starvation can alter nutrient-sensing pathways such as the PI3K/AKT/mTOR signaling axis in RKO cells will be carried out. In conjunction with the transcriptomic data, these data will provide a comprehensive analysis of how AKR1B10 expression may alter metabolism relevant to mitogenic signaling in cancer cells.

3. No significant change in motility with the overexpression of either enzyme was observed compared to control cells; however, there was a significant decrease in motility of the AKR1B10 cells compared to the AKR1B1 cells, indicating their opposing roles in motility. The role of glucose/serum starvation on the motility of AKR1B1 or AKR1B10 expressing RKO cells will be carried out in the future to provide us a better understanding of whether nutrient restriction can exacerbate the differences in the motility of these cells.

4. mRNA expression of three PPP enzymes, G6PD, TKT, and TALDO, showed no change to very modest changes between control and AKR1B1 or AKR1B10 overexpressing cells. In our future efforts, we will further evaluate the cytosolic NADP/NADPH ratio as the enzyme expression may not reflect the effect of AKRs on the functions of PPP enzymes.

5. RNA sequencing results have shown that AKR1B1 and AKR1B10 overexpression show highly divergent gene expression patterns in RKO cells. AKR1B1 was associated with response to the regulation of ROS levels, whereas AKR1B10 was associated with the regulation of metabolic and biosynthetic processes. In our future studies, we will analyze the endogenous antioxidant system (cytosolic ROS levels, GSH/GSSG ratio) in these cells along with the altered GO terms on a gene by gene basis to identify the regulators of ROS related signaling pathways.

Taken together, although AKR1B1 and AKR1B10 shares a high similarity in their structure, their functions in the cells are different. Our study has shown that AKR1B1 and AKR1B10 overexpression in the RKO model significantly pushes cells into differing states in motility and viability *in vitro* and in regulating ROS and metabolic processes *in silico*. Our future studies will elaborate on the *in silico* results and elucidate signaling pathways related to AKR1B1 and AKR1B10 enzymes.

REFERENCES

Agledal, L., Niere, M., & Ziegler, M. (2010). The phosphate makes a difference: Cellular functions of NADP. In *Redox Report*. https://doi.org/10.1179/174329210X12650506623122

Ahmed, D., Eide, P. W., Eilertsen, I. A., Danielsen, S. A., Eknæs, M., Hektoen, M., Lind, G. E., & Lothe, R. A. (2013). Epigenetic and genetic features of 24 colon cancer cell lines. *Oncogenesis*. https://doi.org/10.1038/oncsis.2013.35

Alfarouk, K. O., Ahmed, S. B. M., Elliott, R. L., Benoit, A., Alqahtani, S. S., Ibrahim, M. E., Bashir, A. H. H., Alhoufie, S. T. S., Elhassan, G. O., Wales, C. C., Schwartz, L. H., Ali, H. S., Ahmed, A., Forde, P. F., Devesa, J., Cardone, R. A., Fais, S., Harguindey, S., & Reshkin, S. J. (2020). The pentose phosphate pathway dynamics in cancer and its dependency on intracellular pH. In *Metabolites*. https://doi.org/10.3390/metabo10070285

Bamford, S., Dawson, E., Forbes, S., Clements, J., Pettett, R., Dogan, A., Flanagan, A., Teague, J., Futreal, P. A., Stratton, M. R., & Wooster, R. (2004). The COSMIC (Catalogue of Somatic Mutations in Cancer) database and website. *British Journal of Cancer*. https://doi.org/10.1038/sj.bjc.6601894

Barski, O. A., Tipparaju, S. M., & Bhatnagar, A. (2008). The aldo-keto reductase superfamily and its role in drug metabolism and detoxification. In *Drug Metabolism Reviews*. https://doi.org/10.1080/03602530802431439

Byrns, M. C., Steckelbroeck, S., & Penning, T. M. (2008). An indomethacin analogue, N-(4-chlorobenzoyl)-melatonin, is a selective inhibitor of aldo-keto reductase 1C3 (type 2 3α-HSD, type 5 17β-HSD, and prostaglandin F synthase), a potential target for the treatment of hormone dependent and hormone independent m. *Biochemical Pharmacology*. https://doi.org/10.1016/j.bcp.2007.09.008

Cao, D., Fan, S. T., & Chung, S. S. M. (1998). Identification and characterization of a novel human aldose reductase- like gene. *Journal of Biological Chemistry*.

https://doi.org/10.1074/jbc.273.19.11429

Christofk, H. R., Vander Heiden, M. G., Wu, N., Asara, J. M., & Cantley, L. C. (2008). Pyruvate kinase M2 is a phosphotyrosine-binding protein. *Nature*. https://doi.org/10.1038/nature06667

Cramer, T., Yamanishi, Y., Clausen, B. E., Förster, I., Pawlinski, R., Mackman, N., Haase, V. H., Jaenisch, R., Corr, M., Nizet, V., Firestein, G. S., Gerber, H. P., Ferrara, N., & Johnson, R. S. (2003). HIF-1α is essential for myeloid cell-mediated inflammation. *Cell*. https://doi.org/10.1016/S0092-8674(03)00154-5

Crosas, B., Hyndman, D. J., Gallego, O., Martras, S., Parés, X., Flynn, T. G., & Farrés, J. (2003). Human aldose reductase and human small intestine aldose reductase are efficient retinal reductases: Consequences for retinoid metabolism. *Biochemical Journal*. https://doi.org/10.1042/BJ20021818

de la Cruz-López, K. G., Castro-Muñoz, L. J., Reyes-Hernández, D. O., García-Carrancá, A., & Manzo-Merino, J. (2019). Lactate in the Regulation of Tumor Microenvironment and Therapeutic Approaches. In *Frontiers in Oncology*. https://doi.org/10.3389/fonc.2019.01143

DeBerardinis, R. J., & Chandel, N. S. (2020). We need to talk about the Warburg effect. In *Nature Metabolism*. https://doi.org/10.1038/s42255-020-0172-2

DeBerardinis, R. J., Lum, J. J., Hatzivassiliou, G., & Thompson, C. B. (2008). The Biology of Cancer: Metabolic Reprogramming Fuels Cell Growth and Proliferation. In *Cell Metabolism*. https://doi.org/10.1016/j.cmet.2007.10.002

DeBerardinis, R. J., Mancuso, A., Daikhin, E., Nissim, I., Yudkoff, M., Wehrli, S., & Thompson, C. B. (2007). Beyond aerobic glycolysis: Transformed cells can engage in glutamine metabolism that exceeds the requirement for protein and nucleotide synthesis. *Proceedings of the National Academy of Sciences of the United States of America*. https://doi.org/10.1073/pnas.0709747104

Demirkol Canll, S., Seza, E. G., Sheraj, I., Gömçeli, I., Turhan, N., Carberry, S., Prehn, J. H. M., Güre, A. O., & Banerjee, S. (2020). Evaluation of an aldo-keto

reductase gene signature with prognostic significance in colon cancer via activation of epithelial to mesenchymal transition and the p70S6K pathway. *Carcinogenesis*. https://doi.org/10.1093/carcin/bgaa072

Dixit, B. L., Balendiran, G. K., Watowich, S. J., Srivastava, S., Ramana, K. V., Petrash, J. M., Bhatnagar, A., & Srivastava, S. K. (2000). Kinetic and structural characterization of the glutathione-binding site of aldose reductase. *Journal of Biological Chemistry*. https://doi.org/10.1074/jbc.M909235199

Donaghue, K. C., Margan, S. H., Chan, A. K. F., Holloway, B., Silink, M., Rangel, T., & Bennetts, B. (2005). The association of aldose reductase gene (AKR1B1) polymorphisms with diabetic neuropathy in adolescents. *Diabetic Medicine*. https://doi.org/10.1111/j.1464-5491.2005.01631.x

Ebert, B., Kisiela, M., Wsól, V., & Maser, E. (2011). Proteasome inhibitors MG-132 and bortezomib induce AKR1C1, AKR1C3, AKR1B1, and AKR1B10 in human colon cancer cell lines SW-480 and HT-29. *Chemico-Biological Interactions*. https://doi.org/10.1016/j.cbi.2010.12.026

Ebert, B. L., Firth, J. D., & Ratcliffe, P. J. (1995). Hypoxia and mitochondrial inhibitors regulate expression of glucose transporter-1 via distinct cis-acting sequences. *Journal of Biological Chemistry*. https://doi.org/10.1074/jbc.270.49.29083

Estrella, V., Chen, T., Lloyd, M., Wojtkowiak, J., Cornnell, H. H., Ibrahim-Hashim, A., Bailey, K., Balagurunathan, Y., Rothberg, J. M., Sloane, B. F., Johnson, J., Gatenby, R. A., & Gillies, R. J. (2013). Acidity generated by the tumor microenvironment drives local invasion. *Cancer Research*. https://doi.org/10.1158/0008-5472.CAN-12-2796

Feoktistova, M., Geserick, P., & Leverkus, M. (2016). Crystal violet assay for determining viability of cultured cells. *Cold Spring Harbor Protocols*. https://doi.org/10.1101/pdb.prot087379

Flohe, L., Günzler, W. A., & Schock, H. H. (1973). Glutathione peroxidase: A selfnoenzyme. *FEBS Letters*. https://doi.org/10.1016/0014-5793(73)80755-0

Ge, S. X., Jung, D., Jung, D., & Yao, R. (2020). ShinyGO: A graphical gene-set enrichment tool for animals and plants. *Bioinformatics*. https://doi.org/10.1093/bioinformatics/btz931

Gordan, J. D., & Simon, M. C. (2007). Hypoxia-inducible factors: central regulators of the tumor phenotype. In *Current Opinion in Genetics and Development*. https://doi.org/10.1016/j.gde.2006.12.006

Guan, B., Wang, T. L., & Shih, I. M. (2011). ARID1A, a factor that promotes formation of SWI/SNF-mediated chromatin remodeling, is a tumor suppressor in gynecologic cancers. *Cancer Research*. https://doi.org/10.1158/0008-5472.CAN-11-1562

Guinney, J., Dienstmann, R., Wang, X., De Reyniès, A., Schlicker, A., Soneson, C., Marisa, L., Roepman, P., Nyamundanda, G., Angelino, P., Bot, B. M., Morris, J. S., Simon, I. M., Gerster, S., Fessler, E., De Sousa .E Melo, F., Missiaglia, E., Ramay, H., Barras, D., … Tejpar, S. (2015). The consensus molecular subtypes of colorectal cancer. *Nature Medicine*. https://doi.org/10.1038/nm.3967

Hanahan, D., & Weinberg, R. A. (2000). The hallmarks of cancer. In *Cell*. https://doi.org/10.1016/S0092-8674(00)81683-9

Hanahan, D., & Weinberg, R. A. (2011). Hallmarks of cancer: The next generation. In *Cell*. https://doi.org/10.1016/j.cell.2011.02.013

Hong, M., Lee, Y., Kim, J. W., Lim, J. S., Chang, S. Y., Lee, K. S., Paik, S. G., & Choe, I. S. (1999). Isolation and characterization of cDNA clone for human liver 10-formyltetrahydrofolate dehydrogenase. *Biochemistry and Molecular Biology International*. https://doi.org/10.1080/15216549900201433

Hyndman, D., Bauman, D. R., Heredia, V. V., & Penning, T. M. (2003). The aldo-keto reductase superfamily homepage. *Chemico-Biological Interactions*. https://doi.org/10.1016/S0009-2797(02)00193-X

Jez, J. M., Bennett, M. J., Schlegel, B. P., Lewis, M., & Penning, T. M. (1997).

Comparative anatomy of the aldo-keto reductase superfamily. In *Biochemical Journal*. https://doi.org/10.1042/bj3260625

Jin, L., & Zhou, Y. (2019). Crucial role of the pentose phosphate pathway in malignant tumors (review). *Oncology Letters*. https://doi.org/10.3892/ol.2019.10112

Ju, H. Q., Lin, J. F., Tian, T., Xie, D., & Xu, R. H. (2020). NADPH homeostasis in cancer: functions, mechanisms and therapeutic implications. In *Signal Transduction and Targeted Therapy*. https://doi.org/10.1038/s41392-020-00326-0

Kalluri, R., & Weinberg, R. A. (2009). The basics of epithelial-mesenchymal transition. In *Journal of Clinical Investigation*. https://doi.org/10.1172/JCI39104

Krebs, A. M., Mitschke, J., Losada, M. L., Schmalhofer, O., Boerries, M., Busch, H., Boettcher, M., Mougiakakos, Di., Reichardt, W., Bronsert, P., Brunton, V. G., Pilarsky, C., Winkler, T. H., Brabletz, S., Stemmler, M. P., & Brabletz, T. (2017). The EMT-activator Zeb1 is a key factor for cell plasticity and promotes metastasis in pancreatic cancer. *Nature Cell Biology*. https://doi.org/10.1038/ncb3513

Kruger, N. J., & Von Schaewen, A. (2003). The oxidative pentose phosphate pathway: Structure and organisation. In *Current Opinion in Plant Biology*. https://doi.org/10.1016/S1369-5266(03)00039-6

Kucukural, A., Yukselen, O., Ozata, D. M., Moore, M. J., & Garber, M. (2019). DEBrowser: interactive differential expression analysis and visualization tool for count data. *BMC Genomics*. https://doi.org/10.1186/s12864-018-5362-x

Langan, T. J., & Chou, R. C. (2011). Synchronization of mammalian cell cultures by serum deprivation. *Methods in Molecular Biology*. https://doi.org/10.1007/978-1-61779-182-6_5

Lefrançois-Martinez, A. M., Bertherat, J., Val, P., Tournaire, C., Gallo-Payet, N.,

Hyndman, D., Veyssière, G., Bertagna, X., Jean, C., & Martinez, A. (2004). Decreased expression of cyclic adenosine monophosphate-regulated aldose reductase (AKR1B1) is associated with malignancy in human sporadic adrenocortical tumors. *Journal of Clinical Endocrinology and Metabolism*. https://doi.org/10.1210/jc.2003-031830

Liberti, M. V., & Locasale, J. W. (2016). The Warburg Effect: How Does it Benefit Cancer Cells? In *Trends in Biochemical Sciences*. https://doi.org/10.1016/j.tibs.2015.12.001

Linnekamp, J. F., Van Hooff, S. R., Prasetyanti, P. R., Kandimalla, R., Buikhuisen, J. Y., Fessler, E., Ramesh, P., Lee, K. A. S. T., Bochove, G. G. W., De Jong, J. H., Cameron, K., Van Leersum, R., Rodermond, H. M., Franitza, M., Nürnberg, P., Mangiapane, L. R., Wang, X., Clevers, H., Vermeulen, L., … Medema, J. P. (2018). Consensus molecular subtypes of colorectal cancer are recapitulated in in vitro and in vivo models. *Cell Death and Differentiation*. https://doi.org/10.1038/s41418-017-0011-5

Liou, G. Y., & Storz, P. (2010). Reactive oxygen species in cancer. In *Free Radical Research*. https://doi.org/10.3109/10715761003667554

Love, M. I., Huber, W., & Anders, S. (2014). Moderated estimation of fold change and dispersion for RNA-seq data with DESeq2. *Genome Biology*. https://doi.org/10.1186/s13059-014-0550-8

Luthman, M., & Holmgren, A. (1982). Rat Liver Thioredoxin and Thioredoxin Reductase: Purification and Characterization. *Biochemistry*. https://doi.org/10.1021/bi00269a003

Madhukar, N. S., Warmoes, M. O., & Locasale, J. W. (2015). Organization of enzyme concentration across the metabolic network in cancer cells. *PLoS ONE*. https://doi.org/10.1371/journal.pone.0117131

Magaway, C., Kim, E., & Jacinto, E. (2019). Targeting mTOR and Metabolism in Cancer: Lessons and Innovations. In *Cells*. https://doi.org/10.3390/cells8121584

Majumder, P. K., Febbo, P. G., Bikoff, R., Berger, R., Xue, Q., McMahon, L. M., Manolal, J., Brugarolas, J., J McDonnell, T., Golub, T. R., Loda, M., Lane, H. A., & Sellers, W. R. (2004). mTOR inhibition reverses Akt-dependent prostate intraepithelial neoplasia through regulation of apoptotic and HIF-1-dependent pathways. *Nature Medicine*. https://doi.org/10.1038/nm1052

Mindnich, R. D., & Penning, T. M. (2009). Aldo-keto reductase (AKR) superfamily: genomics and annotation. In *Human genomics*. https://doi.org/10.1186/1479-7364-3-4-362

Mitschke, L., Parthier, C., Schröder-Tittmann, K., Coy, J., Lüdtke, S., & Tittmann, K. (2010). The crystal structure of human transketolase and new insights into its mode of action. *Journal of Biological Chemistry*. https://doi.org/10.1074/jbc.M110.149955

Mouradov, D., Sloggett, C., Jorissen, R. N., Love, C. G., Li, S., Burgess, A. W., Arango, D., Strausberg, R. L., Buchanan, D., Wormald, S., O'Connor, L., Wilding, J. L., Bicknell, D., Tomlinson, I. P. M., Bodmer, W. F., Mariadason, J. M., & Sieber, O. M. (2014). Colorectal cancer cell lines are representative models of the main molecular subtypes of primary cancer. *Cancer Research*. https://doi.org/10.1158/0008-5472.CAN-14-0013

Ohashi, T., Idogawa, M., Sasaki, Y., Suzuki, H., & Tokino, T. (2013). AKR1B10, a transcriptional target of p53, is downregulated in colorectal cancers associated with poor prognosis. *Molecular Cancer Research*. https://doi.org/10.1158/1541-7786.MCR-13-0330-T

Osthus, R. C., Shim, H., Kim, S., Li, Q., Reddy, R., Mukherjee, M., Xu, Y., Wonsey, D., Lee, L. A., & Dang, C. V. (2000). Deregulation of glucose transporter 1 and glycolytic gene expression by c-Myc. *Journal of Biological Chemistry*. https://doi.org/10.1074/jbc.C000023200

Pai, E. F., & Schulz, G. E. (1983). The catalytic mechanism of glutathione reductase as derived from x-ray diffraction analyses of reaction intermediates. *Journal of Biological Chemistry*. https://doi.org/10.1016/S0021-9258(18)33050-3

Penning, T. M. (2005). AKR1B10: A new diagnostic marker of non-small cell lung carcinoma in smokers. In *Clinical Cancer Research*. https://doi.org/10.1158/1078-0432.CCR-05-0071

Penning, T. M. (2015). The aldo-keto reductases (AKRs): Overview. *Chemico-Biological Interactions*. https://doi.org/10.1016/j.cbi.2014.09.024

Penning, T. M., & Lerman, C. (2008). Genomics of smoking exposure and cessation: Lessons for cancer prevention and treatment. In *Cancer Prevention Research*. https://doi.org/10.1158/1940-6207.CAPR-08-0047

Perl, A. (2007). The pathogenesis of transaldolase deficiency. In *IUBMB Life*. https://doi.org/10.1080/15216540701387188

Pinto, B., Henriques, A. C., Silva, P. M. A., & Bousbaa, H. (2020). Three-dimensional spheroids as in vitro preclinical models for cancer research. In *Pharmaceutics*. https://doi.org/10.3390/pharmaceutics12121186

Poole, R. C., & Halestrap, A. P. (1993). Transport of lactate and other monocarboxylates across mammalian plasma membranes. In *American Journal of Physiology - Cell Physiology*. https://doi.org/10.1152/ajpcell.1993.264.4.c761

Ramana, K. V. (2011). Aldose reductase: New insights for an old enzyme. In *Biomolecular Concepts*. https://doi.org/10.1515/bmc.2011.002

Reuter, S., Gupta, S. C., Chaturvedi, M. M., & Aggarwal, B. B. (2010). Oxidative stress, inflammation, and cancer: How are they linked? In *Free Radical Biology and Medicine*. https://doi.org/10.1016/j.freeradbiomed.2010.09.006

Schwab, A., Siddiqui, A., Vazakidou, M. E., Napoli, F., Bottcher, M., Menchicchi, B., Raza, U., Saatci, O., Krebs, A. M., Ferrazzi, F., Rapa, I., Dettmer-Wilde, K., Waldner, M. J., Ekici, A. B., Rasheed, S. A. K., Mougiakakos, D., Oefner, P. J., Sahin, O., Volante, M., … Ceppi, P. (2018). Polyol pathway links glucose metabolism to the aggressiveness of cancer cells. *Cancer Research*. https://doi.org/10.1158/0008-5472.CAN-17-2834

Semenza, G. L., Roth, P. H., Fang, H. M., & Wang, G. L. (1994). Transcriptional regulation of genes encoding glycolytic enzymes by hypoxia-inducible factor 1. *Journal of Biological Chemistry*. https://doi.org/10.1016/S0021-9258(17)31580-6

Srivastava, S. K., Yadav, U. C. S., Reddy, A. B. M., Saxena, A., Tammali, R., Shoeb, M., Ansari, N. H., Bhatnagar, A., Petrash, M. J., Srivastava, S., & Ramana, K. V. (2011). Aldose reductase inhibition suppresses oxidative stress-induced inflammatory disorders. *Chemico-Biological Interactions*. https://doi.org/10.1016/j.cbi.2011.02.023

Storz, P. (2005). Reactive oxygen species in tumor progression. In *Frontiers in Bioscience*. https://doi.org/10.2741/1667

Tammali, R., Ramana, K. V., & Srivastava, S. K. (2007). Aldose reductase regulates TNF-α-induced PGE2 production in human colon cancer cells. *Cancer Letters*. https://doi.org/10.1016/j.canlet.2007.01.001

Tang, X. H., & Gudas, L. J. (2011). Retinoids, retinoic acid receptors, and cancer. *Annual Review of Pathology: Mechanisms of Disease*. https://doi.org/10.1146/annurev-pathol-011110-130303

Taskoparan, B., Seza, E. G., Demirkol, S., Tuncer, S., Stefek, M., Gure, A. O., & Banerjee, S. (2017). Opposing roles of the aldo-keto reductases AKR1B1 and AKR1B10 in colorectal cancer. *Cellular Oncology*. https://doi.org/10.1007/s13402-017-0351-7

Trivedi, B., & Danforth, W. H. (1966). Effect of pH on the kinetics of frog muscle phosphofructokinase. *Journal of Biological Chemistry*. https://doi.org/10.1016/S0021-9258(18)99819-4

Tunçer, S., Tunçay Çağatay, S., Keşküş, A. G., Çolakoğlu, M., Konu, & Banerjee, S. (2016). Interplay between 15-lipoxygenase-1 and metastasis-associated antigen 1 in the metastatic potential of colorectal cancer. *Cell Proliferation*. https://doi.org/10.1111/cpr.12267

VanLinden, M. R., Skoge, R. H., & Ziegler, M. (2015). Discovery, metabolism and functions of NAD and NADP. *Biochemist*. https://doi.org/10.1042/bio03701009

Wakil, S. J. (1989). Fatty Acid Synthase, A Proficient Multifunctional Enzyme. *Biochemistry*. https://doi.org/10.1021/bi00437a001

Warburg, O. (1956). On the origin of cancer cells. *Science*. https://doi.org/10.1126/science.123.3191.309

Wsol, V., Szotakova, B., Martin, H. J., & Maser, E. (2007). Aldo-keto reductases (AKR) from the AKR1C subfamily catalyze the carbonyl reduction of the novel anticancer drug oracin in man. *Toxicology*. https://doi.org/10.1016/j.tox.2007.05.021

Yan, R., Zu, X., Ma, J., Liu, Z., Adeyanju, M., & Cao, D. (2007). Aldo-keto reductase family 1 B10 gene silencing results in growth inhibition of colorectal cancer cells: Implication for cancer intervention. *International Journal of Cancer*. https://doi.org/10.1002/ijc.22933

Yang, B., Hodgkinson, A. D., Oates, P. J., Hyug, M. K., Millward, B. A., & Demaine, A. G. (2006). Elevated activity of transcription factor nuclear factor of activated T-cells 5 (NFAT5) and diabetic nephropathy. *Diabetes*. https://doi.org/10.2337/db05-1260

Zhang, S. Q., Yung, K. L. K., Chung, S. K., & Chung, S. M. S. (2018). Aldo-keto reductases-mediated cytotoxicity of 2-deoxyglucose: A novel anticancer mechanism. *Cancer Science*. https://doi.org/10.1111/cas.13604

Zhou, Z., Zhao, Y., Gu, L., Niu, X., & Lu, S. (2018). Inhibiting proliferation and migration of lung cancer using small interfering RNA targeting on Aldo-keto reductase family 1 member B10. *Molecular Medicine Reports*. https://doi.org/10.3892/mmr.2017.8173

APPENDICES

A. MAPS OF VECTORS USED IN THIS STUDY

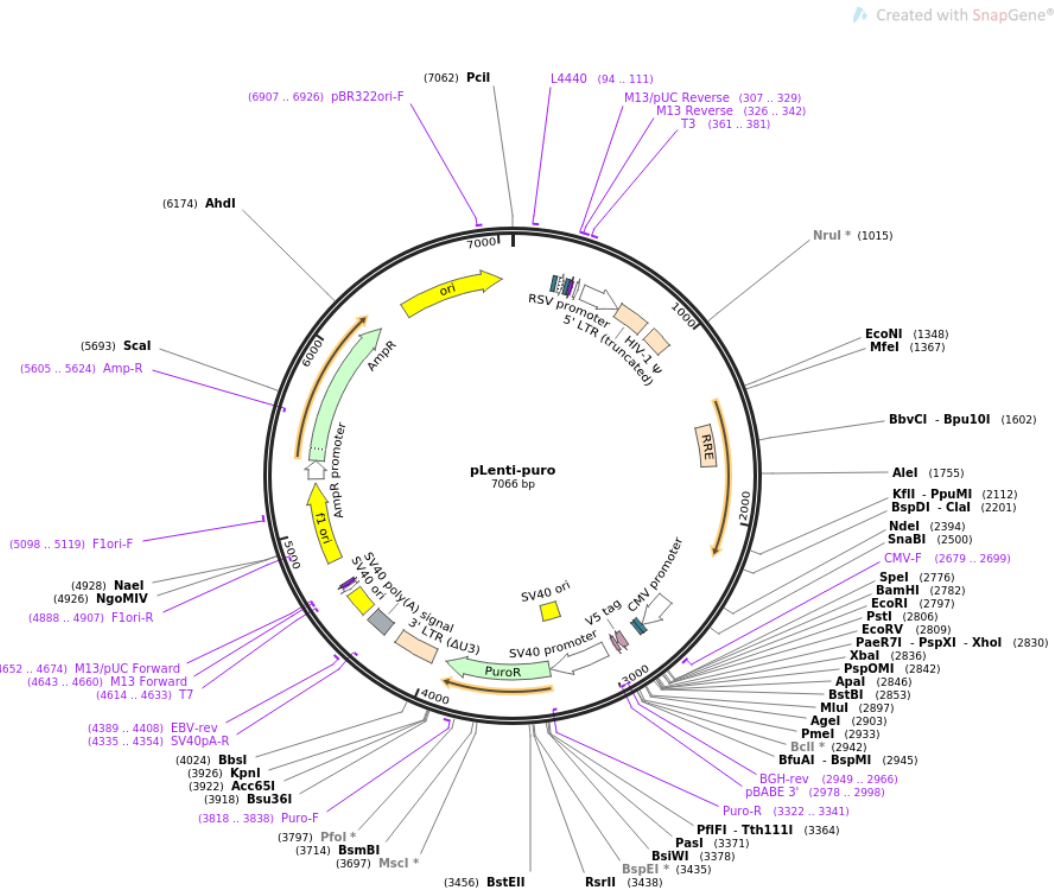

Figure A.1 The vector map of pLenti-puro (Addgene plasmid #39481) third-generation lentiviral transfer plasmid. The cDNA sequences of AKR1B1 and AKR1B10 were cloned into this plasmid.

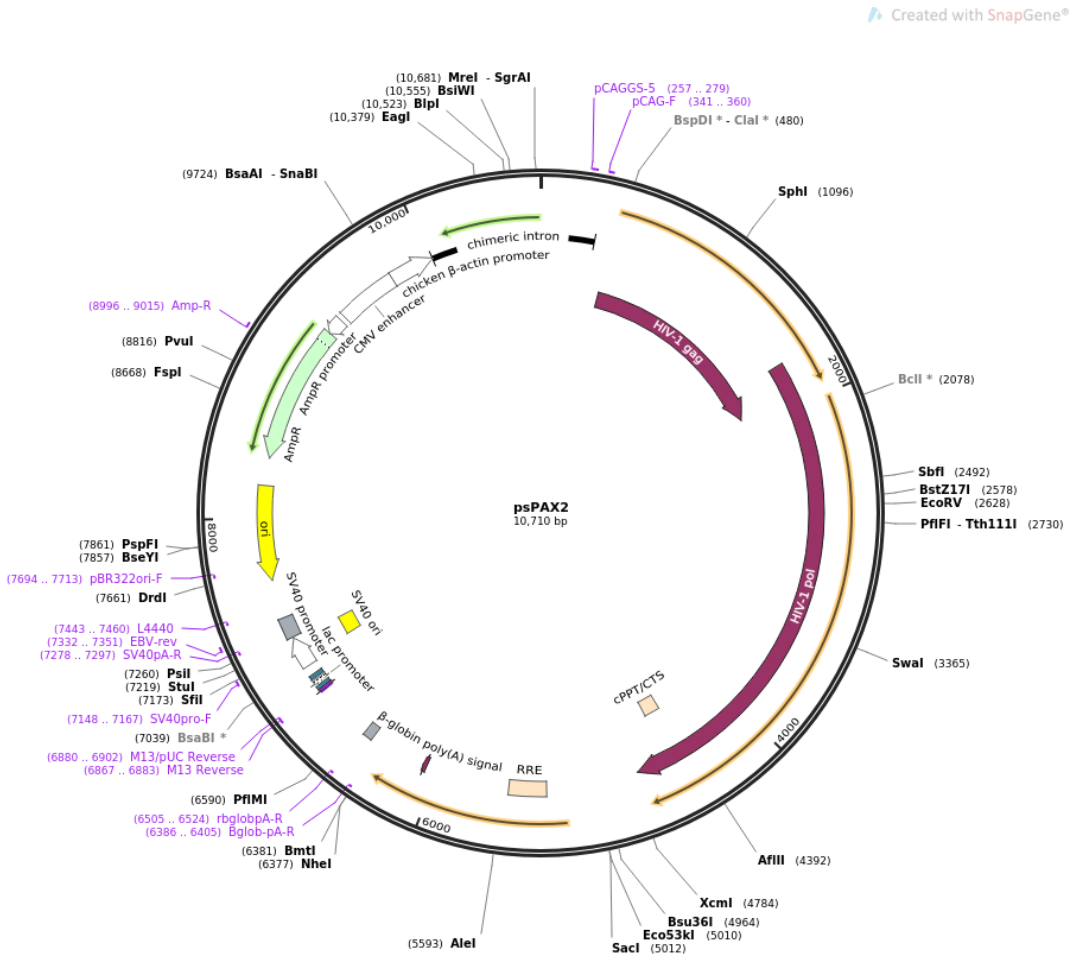

Figure A.2 The vector map of psPax2 (Addgene plasmid #39481) second-generation lentiviral packaging plasmid.

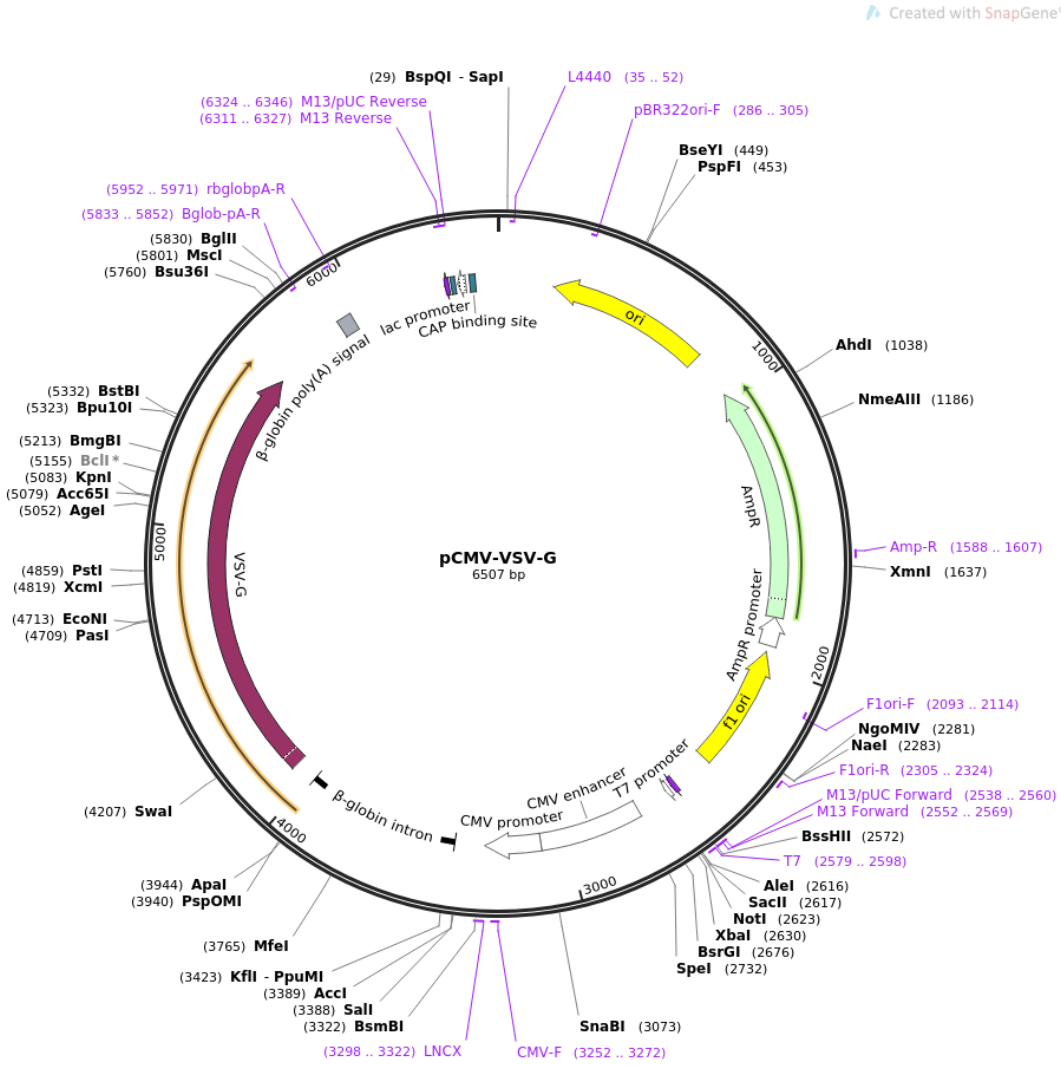

Figure A.3 The vector map of pCMV-VSV-G (Addgene plasmid #39481) lentiviral/retroviral envelope plasmid.

B. COMPOSITIONS OF THE BUFFERS USED IN THIS STUDY

6X SDS-PAGE SAMPLE LOADING DYE

12%	SDS
30%	β-mercaptoethanol
30%	Glycerol
0.012%	Bromophenol blue
0.375 M	Tris-HCl, pH adjusted to 6.8

10X SDS-PAGE RUNNING BUFFER

30.3 g	Tris base
144.4 g	Glycine
10 g	SDS

Dissolved in 1 L of distilled H_2O (dH_2O), diluted to 1X during regular use with 900 mL of dH_2O in a new bottle.

10% SDS-PAGE SEPARATING GEL MIXTURE

4.1 mL	dH_2O
3.33 mL	30% Acrylamide/Bisacrylamide solution
2.5 mL	1.5 M Tris-HCl, pH adjusted to 8.8
100 µL	APS
10 µL	TEMED

12% SDS-PAGE SEPARATING GEL MIXTURE

3.4 mL	dH_2O
4 mL	30% Acrylamide/Bisacrylamide solution
2.5 mL	1.5 M Tris-HCl, pH adjusted to 8.8
100 µL	APS
10 µL	TEMED

4% SDS-PAGE STACKING GEL MIXTURE

3.1 mL	dH_2O
650 µL	30% Acrylamide/Bisacrylamide solution
1.25 mL	0.5 M Tris-HCl, pH adjusted to 6.8
50 µL	APS
5 µL	TEMED

10X WET TRANSFER BUFFER

0.25 M	Tris base
1.92 M	Glycine
1 L	dH_2O, pH adjusted to 8.3

1X WET TRANSFER BUFFER

700 mL	dH_2O
200 mL	Methanol
100 mL	10X Wet transfer buffer

TBS(T)

50 mM	Tris-HCl, pH = 7.4
150 mM	NaCl

The prepared solution was autoclaved and stored as stock TBS. For TBS-T, 0.1% Tween-20 was added before each usage.

MILD STRIPPING BUFFER

15 g	Glycine
1 g	SDS
10 mL	Tween-20
1 L	dH_2O, pH adjusted to 2.2

C. TARGETS OF PRIMERS USED IN THIS STUDY

Table C.1 NCBI accession numbers for targets of the primers used in this study

Primer Target Gene	NCBI Accession Number
AKR1B1	NM_001628.4
AKR1B10	NM_020299.5
G6PD	NM_001042351.3, NM_001360016.2, NM_000402.4
β-actin	NM_001101.5, NM_001199954.3, NM_001614.5, NM_001613.4, NM_001141945.2, NM_001320855.1, NM_001083538.3, NM_001371926.1, NM_001277083.2, NM_001277406.2, NM_001099771.2, NM_005159.5, NM_001100.4, NM_001145442.1, NM_001017992.4
TALDO	NM_006755.2
TKT	NM_001258028.2, NM_001135055.3, NM_001064.4

D. PUROMYCIN KILL CURVES OF RKO AND SW480 CELLS

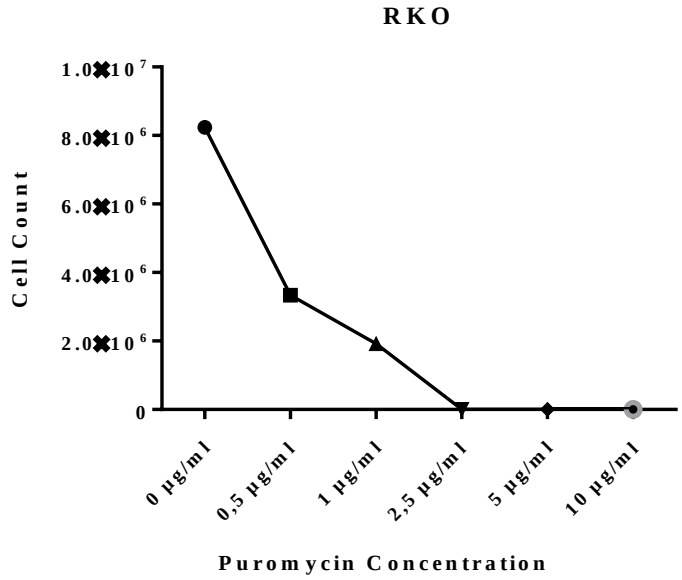

Figure D.1 Puromycin kill curve of RKO cells

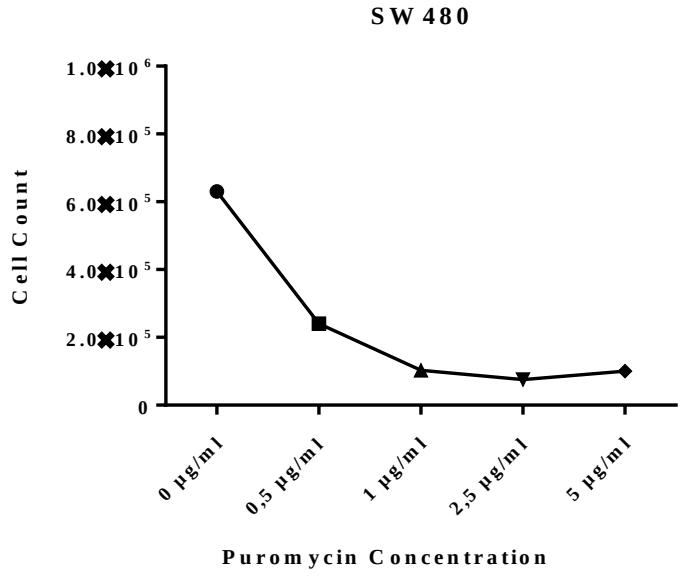

Figure D.1 Puromycin kill curve of SW480 cells

E. DETAILS OF IMAGEJ MACROS USED IN THIS STUDY

```
run("Find Edges");
run("Sharpen");
run("8-bit");
setAutoThreshold("Default");
//run("Threshold...");
call("ij.plugin.frame.ThresholdAdjuster.setMode", "B&W");
setThreshold(0, 56);
setOption("BlackBackground", false);
run("Convert to Mask");
run("Find Edges");
run("Analyze Particles...", "size=4000-Infinity show=Outlines display clear");
```

Figure E.1 The ImageJ macro used to analyze spheroids in this study

```
run("Sharpen");
run("8-bit");
setAutoThreshold("Default");
//run("Threshold...");
call("ij.plugin.frame.ThresholdAdjuster.setMode", "B&W");
setThreshold(0, 190);
setOption("BlackBackground", false);
run("Convert to Mask");
run("Invert LUT");
run("Analyze Particles...", "size=20-Infinity pixel circularity=0.30-1.00
show=Outlines display exclude clear include");
```

Figure E.2 The ImageJ macro used to analyze colony formation assay in this study

```
run("Find Edges");
run("Sharpen");
run("8-bit");
setAutoThreshold("Default");
//run("Threshold...");
call("ij.plugin.frame.ThresholdAdjuster.setMode", "B&W");
setThreshold(0, 56);
setOption("BlackBackground", false);
run("Convert to Mask");
run("Find Edges");
run("Invert LUT");
run("Analyze Particles...", "size=40000-Infinity show=Outlines display clear");
```

Figure E.3 The ImageJ macro used to analyze scratch assays in this study

F. QUALITY CONTROL OF RNA-SEQ SAMPLES

Table F.1 The integrity of RNA-seq samples

Sample	Concentration (ng/µL)	Volume (µL)	Total Mass (µg)	RIN	28S/18S	Test Result
EV_1	194	43	8.34	10	2.2	Qualified
EV_2	180	43	7.74	10	2.2	Qualified
EV_3	188	43	8.08	10	2.1	Qualified
B1_1	316	43	13.59	10	2.3	Qualified
B1_2	168	43	7.22	10	2.6	Qualified
B1_3	131	43	5.63	10	2.3	Qualified
B10_1	271	43	11.65	10	2.4	Qualified
B10_2	156	43	6.71	10	2.4	Qualified
B10_3	187	43	8.04	10	2.7	Qualified

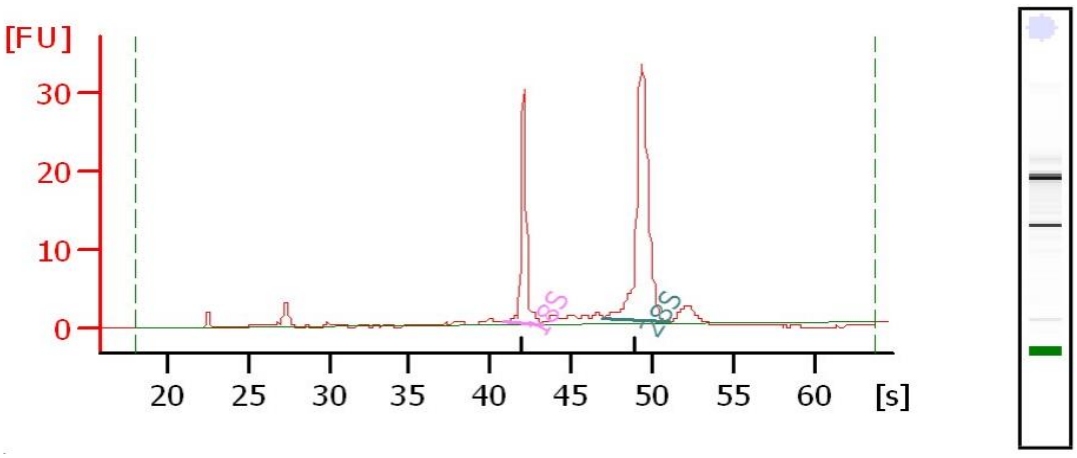

Figure F.1 Electropherogram of sample EV_1

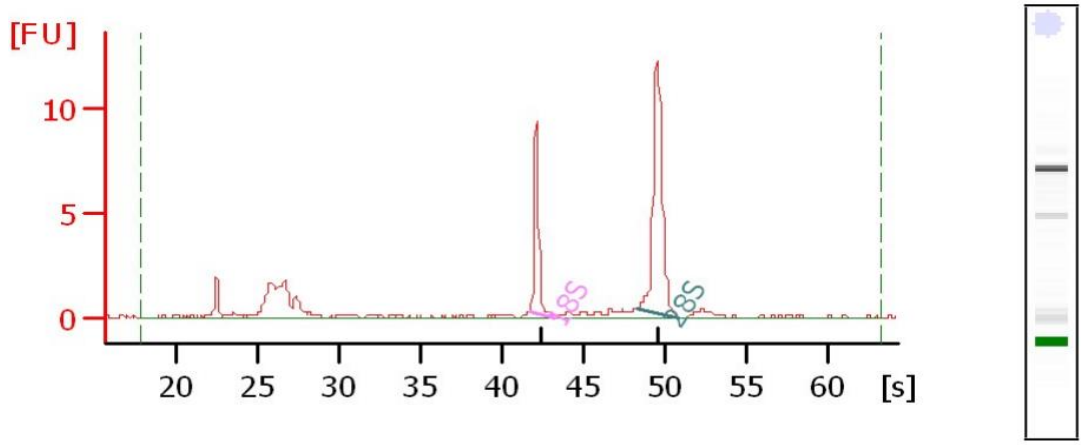

Figure F.2 Electropherogram of sample EV_2

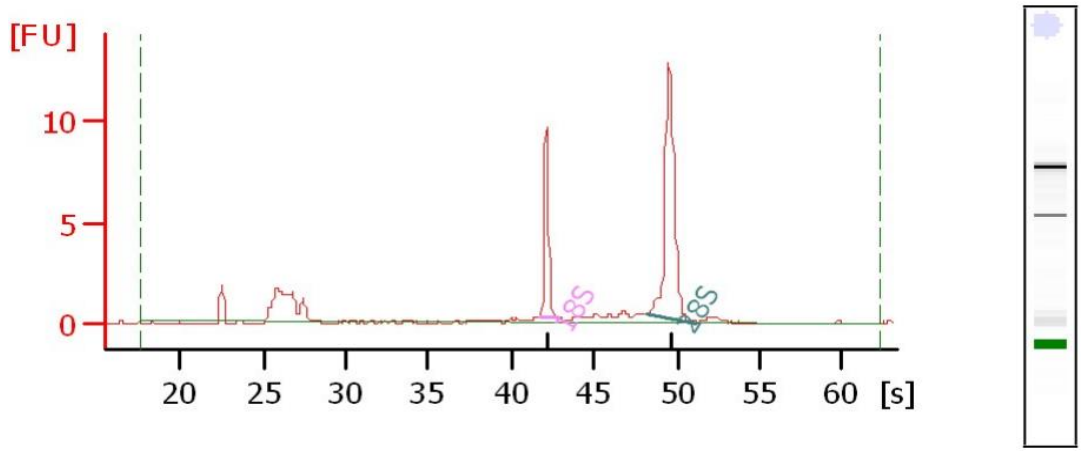

Figure F.3 Electropherogram of sample EV_3

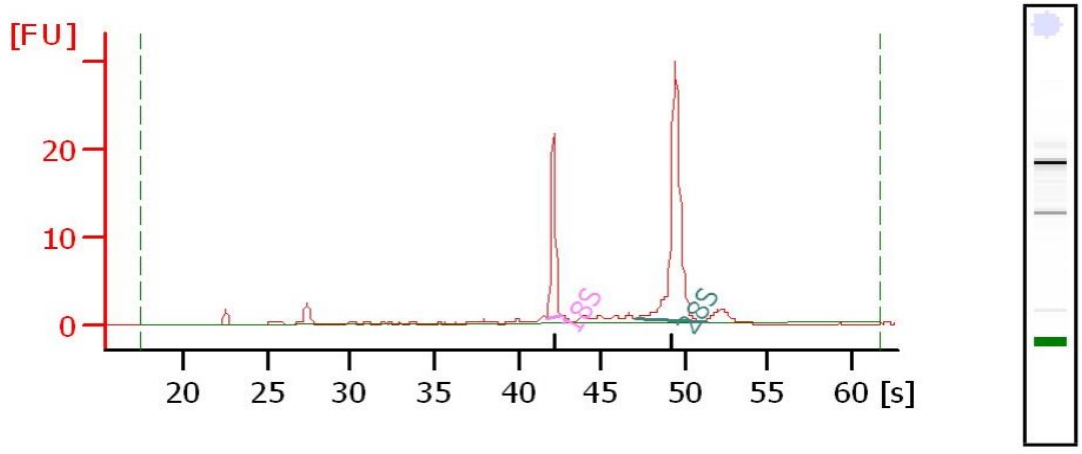

Figure F.4 Electropherogram of sample B1_1

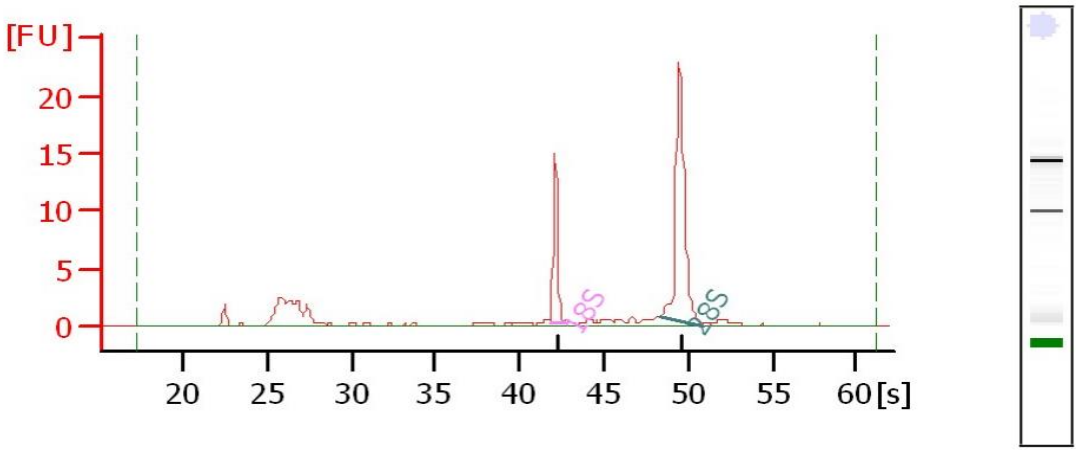

Figure F.5 Electropherogram of sample B1_2

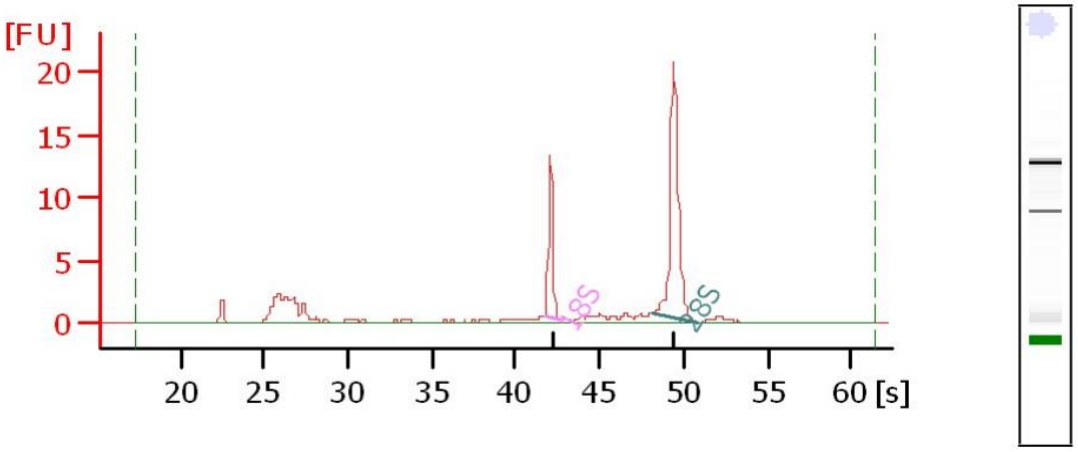

Figure F.6 Electropherogram of sample B1_3

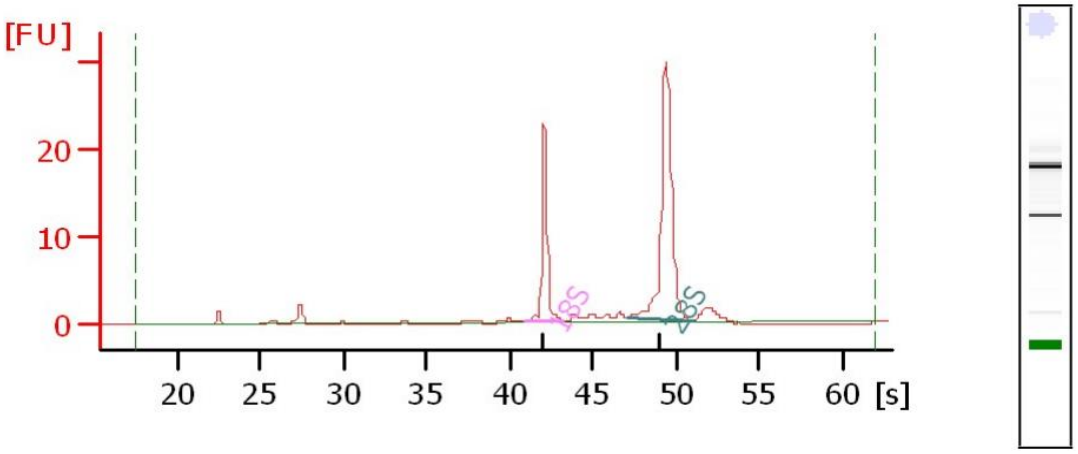

Figure F.7 Electropherogram of sample B10_1

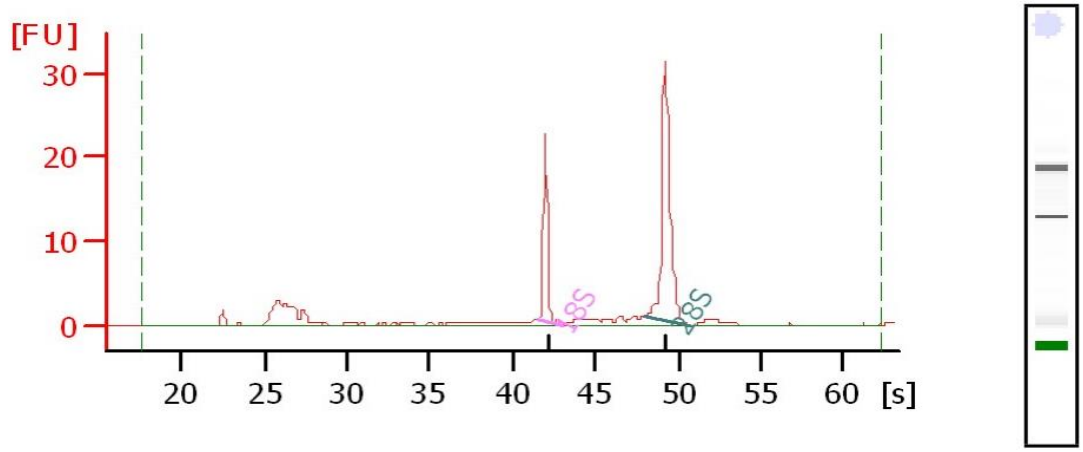

Figure F.8 Electropherogram of sample B10_2

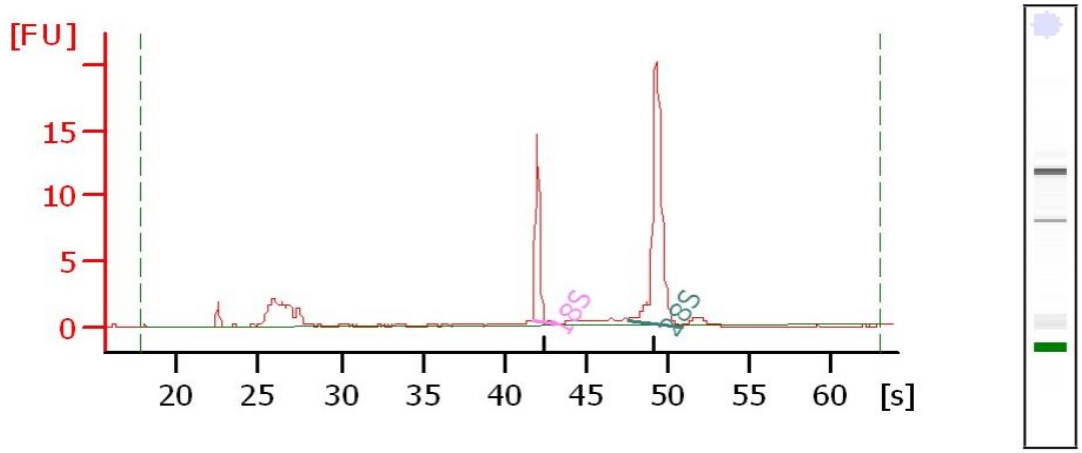

Figure F.9 Electropherogram of sample B10_3

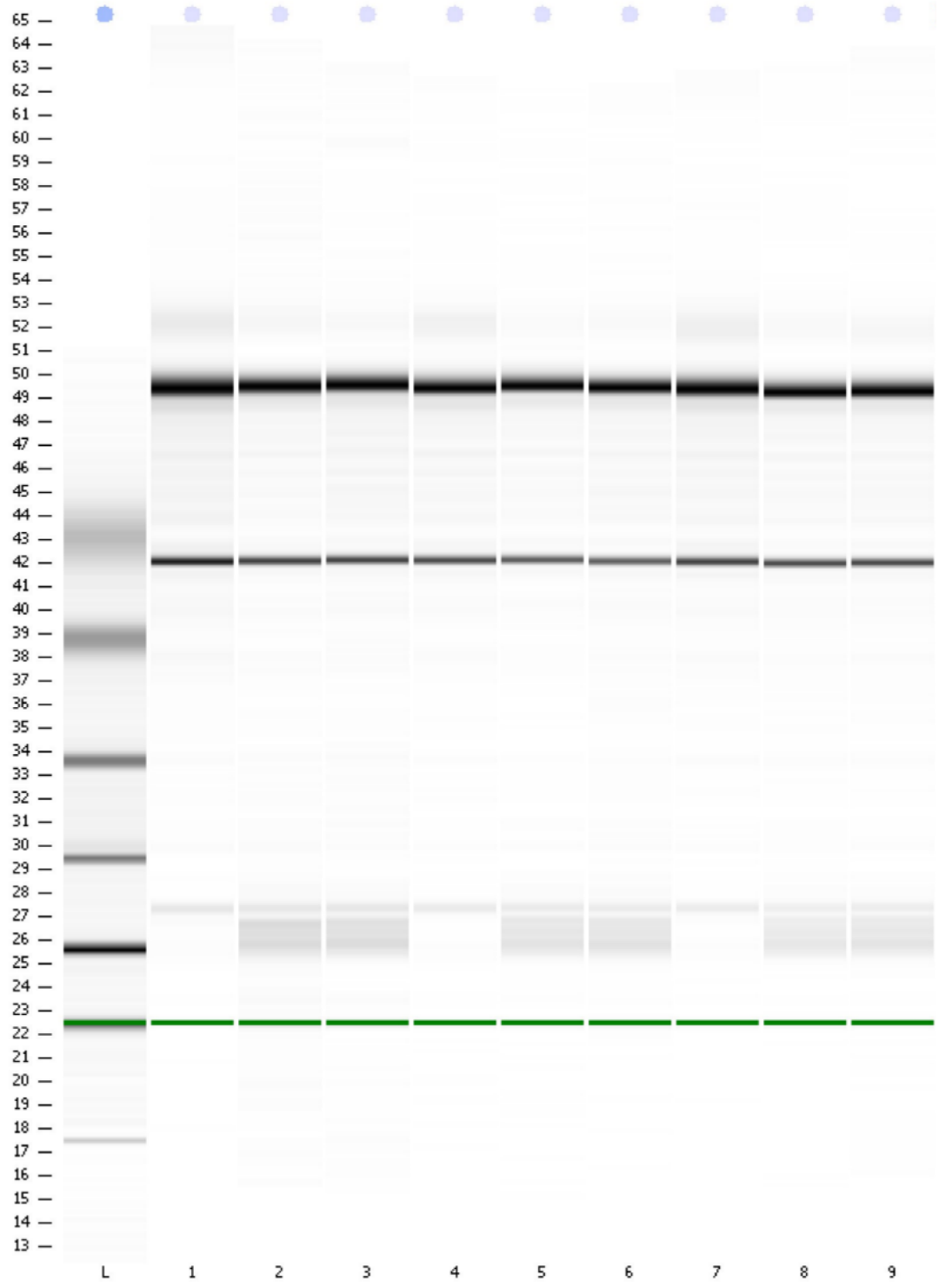

Figure F.10 Bioanalyzer gel image of the samples (L, Ladder; 1, EV_1; 2, EV_2; 3, EV_3; 4, B1_1; 5, B1_2; 6, B1_3; 7, B10_1; 8, B10_2; 9, B10_3)

G. PIPELINE AND QUALITY CONTROL OF RNA-SEQ ANALYSIS

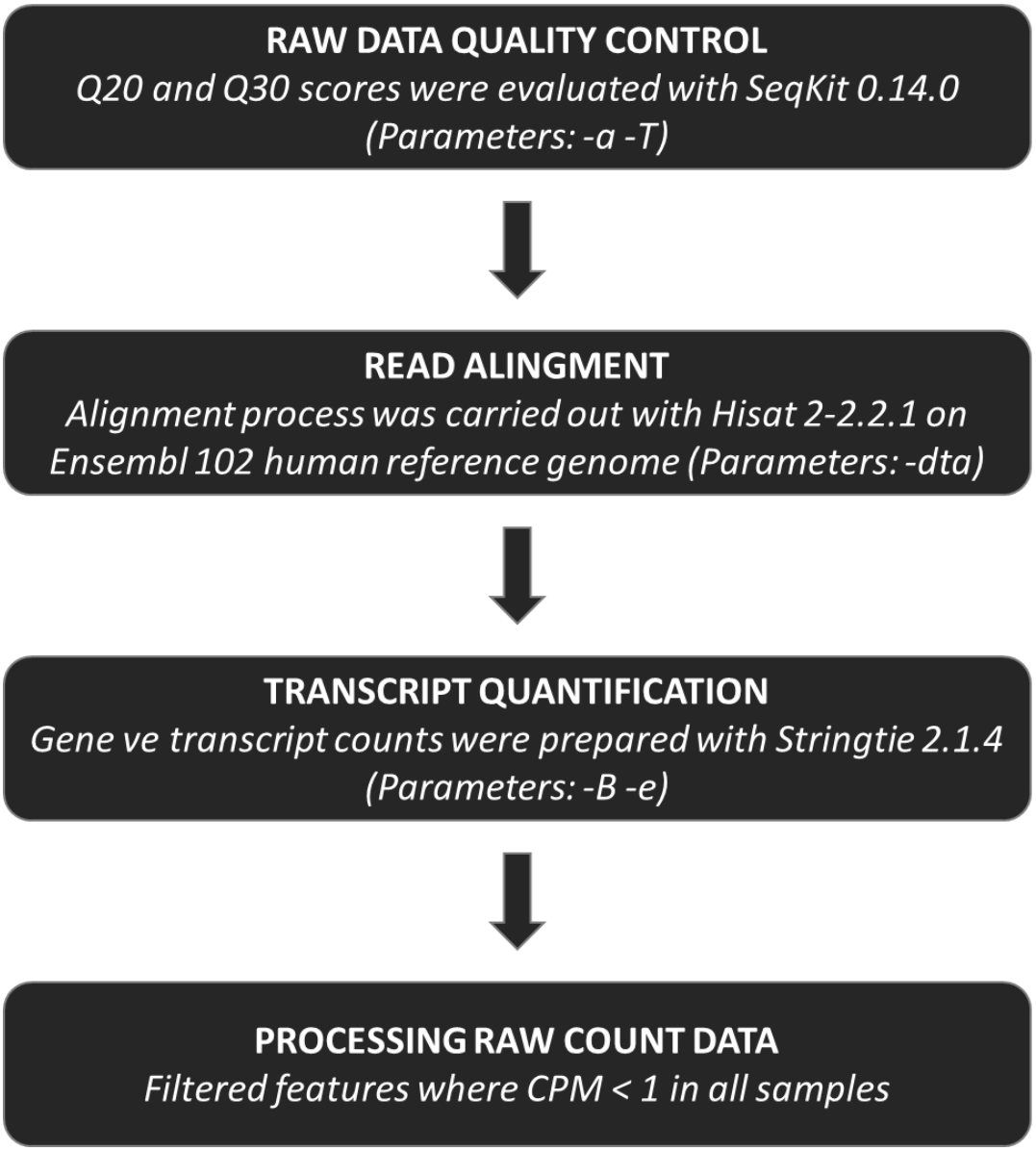

Figure G.1 Pipeline of the RNA-seq analysis carried out by Genoks

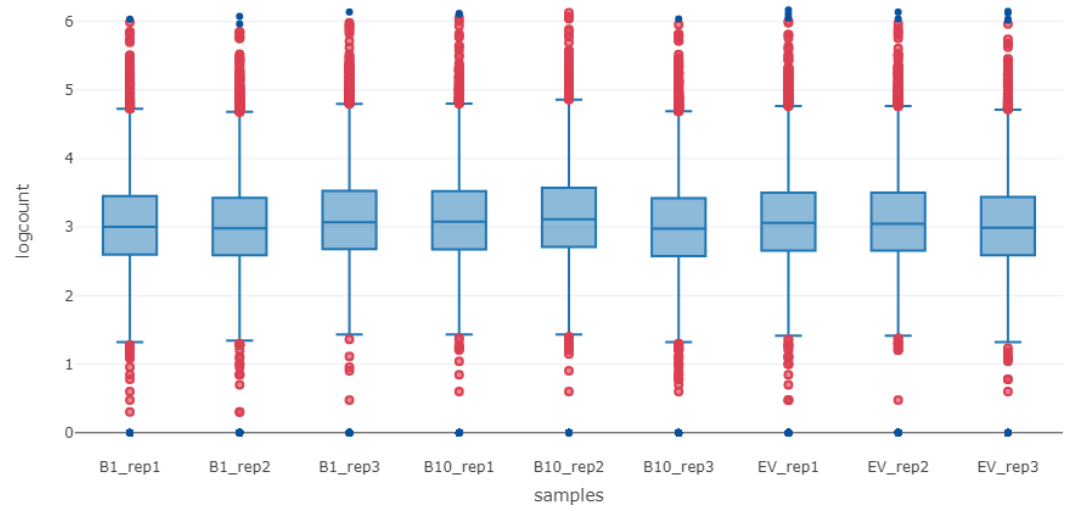

Figure G.2 Interquartile range (IQR) plot of the samples after filtering and batch correction

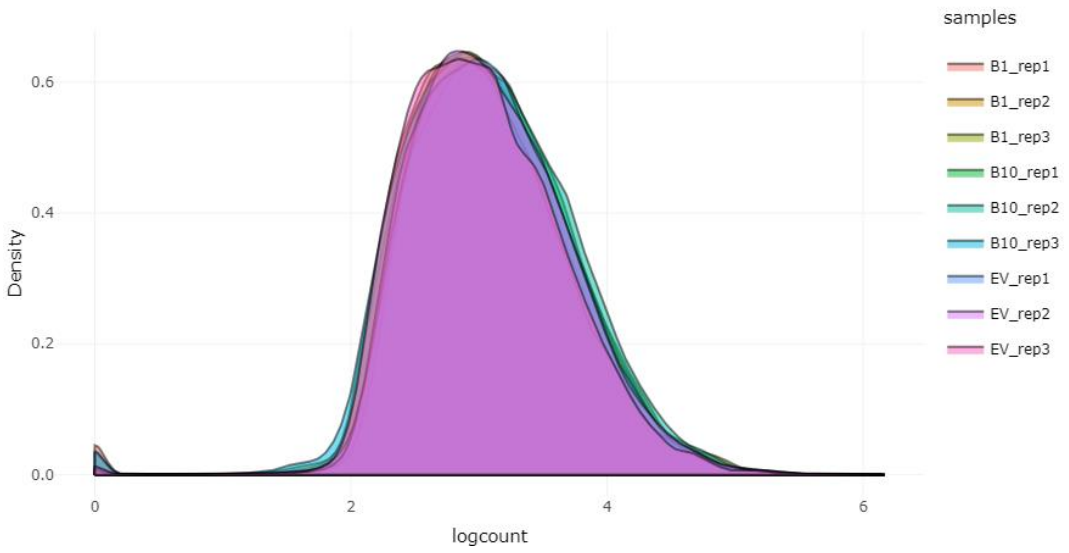

Figure G.3 Density plot of the samples after filtering and batch correction

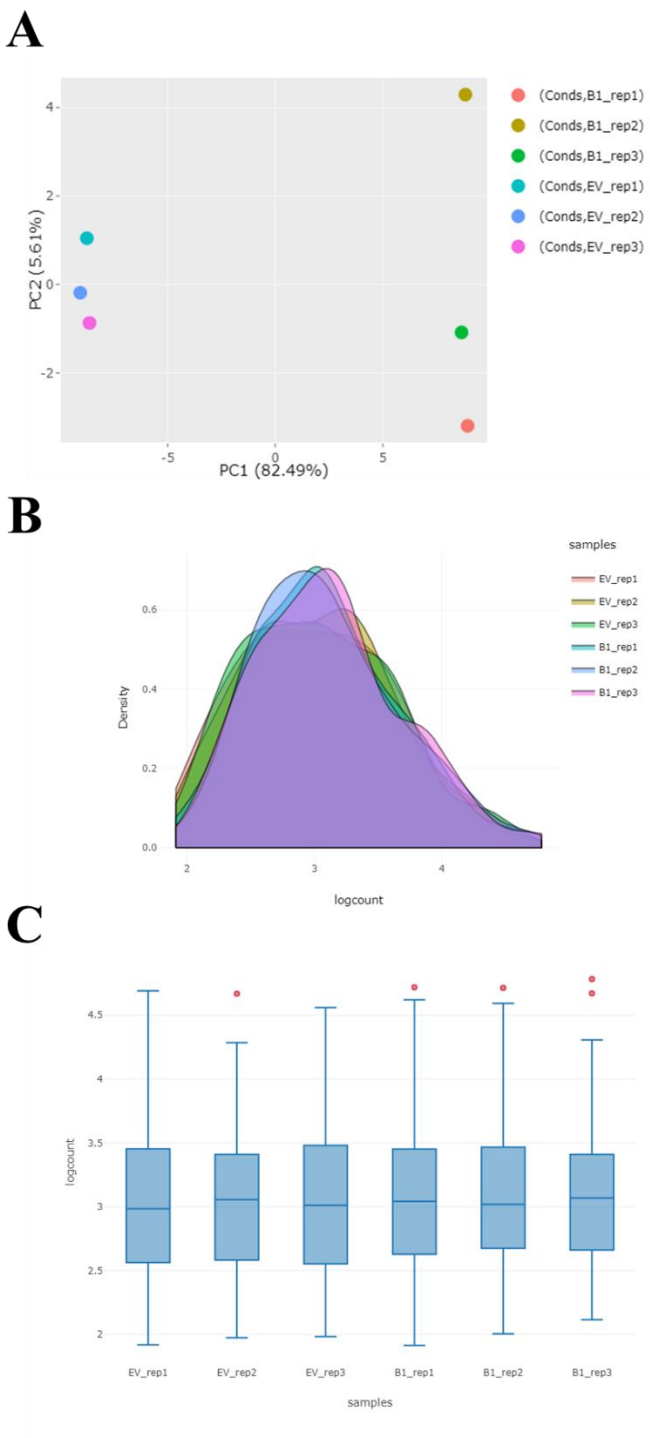

Figure G.3 Quality control plots of the EV vs. AKR1B1 comparison group

(A) Principal component analysis (PCA) plot, (B) density plot, (C) interquartile range (IQR) plot.

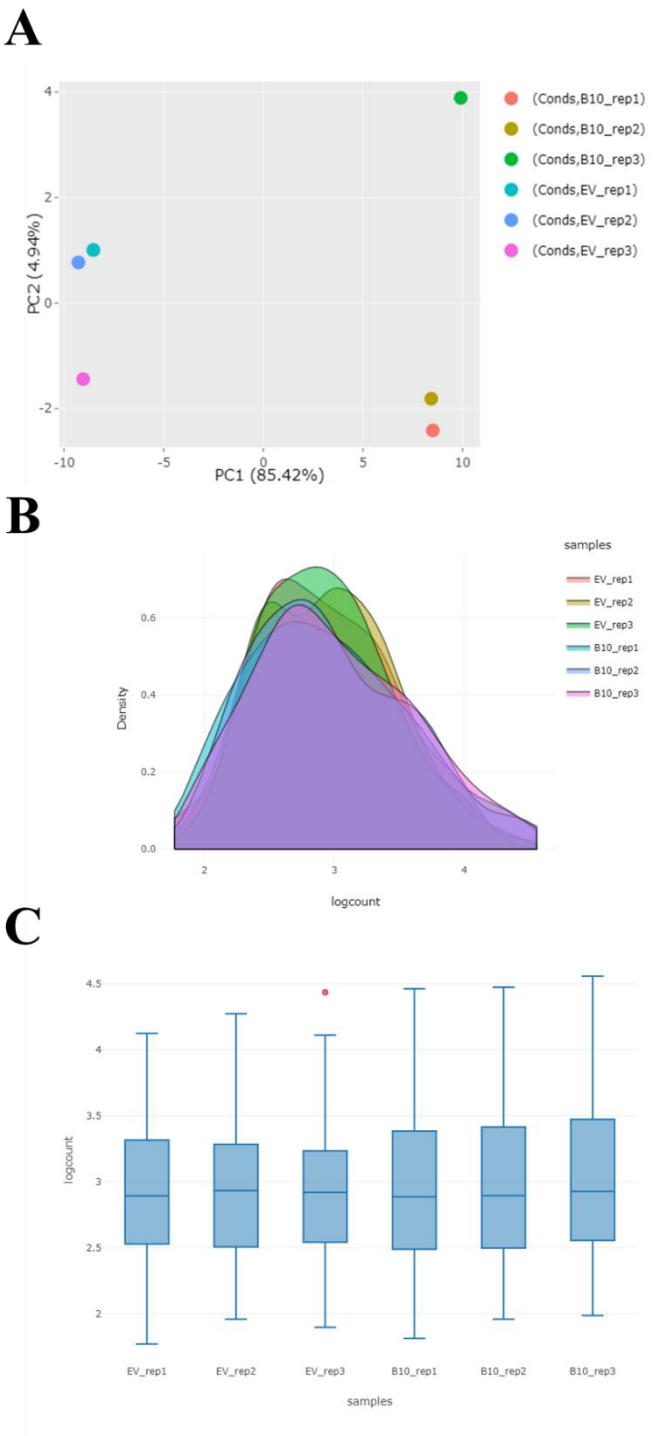

Figure G.3 Quality control plots of the EV vs. AKR1B10 comparison group

(A) Principal component analysis (PCA) plot, (B) density plot, (C) interquartile range (IQR) plot.